Duarte Nuno Rodrigues da Silva

Licenciatura em Ciências da Engenharia

Image processing methodology for assessment of drilling induced damage in CFRP

Dissertação para obtenção do Grau de Mestre em Engenharia Mecânica

Orientador : Jorge Joaquim Pamies Teixeira, Prof. Catedrático, FCT-UNL

Co-orientadora : Carla Maria Moreira Machado, Prof. Auxiliar, FCT-UNL

Júri:

Presidente: Prof. Doutora Rosa Maria Mendes Miranda

Arguente: Prof. Doutor Telmo Jorge Gomes dos Santos

Vogais: Prof. Doutor Jorge Joaquim Pamies Teixeira
Prof. Doutora Carla Maria Moreira Machado

FACULDADE DE CIÊNCIAS E TECNOLOGIA
UNIVERSIDADE NOVA DE LISBOA

Março, 2013

Image processing methodology for assessment of drilling induced damage in CFRP

To my parents

Acknowledgements

It is with immense gratitude that I acknowledge the support and help of my adviser Professor Jorge Pamies Teixeira in achieving another goal in my academic career. Not only this thesis is the result of his scientific curiosity but also because, throughout many years in many different classes, he was able to teach me his ethic values and some of his immensely vast knowledge.

I cannot find words to express my gratitude to my tireless co-adviser Professor Carla Machado, who was closer than anyone in the preparation of this thesis and therefore made an invaluable contribute to this work.

I would like to thank Professor Telmo Santos for the encouragement and support given and to Professor João Lourenço whose help came in a critical time.

A special reference has to be made to Eng. João Gonzalez whose availability, willingness to help and advice allowed me to overcome many obstacles.

I am indebted to my friends and colleagues Júlio Balagões, Henrique Costa, Jorge Martins and Vasco Sobral and everyone else at the Industrial Technology Section that one way or another supported me every day and helped me in this journey.

I wish to thank Mr. António Campos and Mr. Paulo Gonçalves for their contribution to this work.

Finally, I wish to thank my family for the opportunity they have given me to pursue my dreams. To all my friends but specially to those I have lived with in Sweden that are today a big part of me.

Abstract

Composite material components are produced in a near final shape. Machining operations such as drilling are often indispensable, namely for joining of structures. This process introduces damage along the periphery of the hole. Different methods to reduce this induced damage were developed. However, difficulties arise when comparing them since delamination is irregular in shape and in size. The delamination factor and the adjusted delamination factor quantify the damage but none achieved full acceptance since no international standards have been set. The aim of this work is to develop an image processing methodology associated with digital radiography that is capable of assessing the drilling induced damage in CFRP, being easily reproducible and allowing comparison of different drilling approaches. The subtraction of pre and post drill radiographies defined the target image to reach. In the image processing the threshold was found to be the most influential variable causing significant changes to the delamination factors. A new approach to the delamination factor is proposed in order to characterize the drilling induced damage. This approach allows the minimization of the quantified damage for the most irregular delamination shapes while equalling the current delamination factors for regular (crown like) damages.

Keywords: Carbon Fibre Reinforced Plastics, Delamination, NDT, X-Radiography, Image Processing, Threshold

Resumo

Operações de maquinagem, tal como a furação, introduzem dano em componentes fabricados em materiais compósitos. Estes, apesar de serem produzidos numa forma quase final, exigem frequentemente este tipo de operação. Têm vindo a ser desenvolvidos diferentes métodos de redução de dano induzido. No entanto, existem dificuldades na comparação dos mesmos pois a delaminação é irregular na forma e no tamanho. O factor de delaminação e o factor de delaminação ajustado quantificam o dano mas nenhum alcançou plena aceitação e não existe estandardização internacional para o efeito. O objectivo deste trabalho é desenvolver uma metodologia de processamento de imagem associada a radiografia digital capaz de avaliar o dano de furação em CFRP, facilmente reprodutível e que permita a comparação do dano obtido através de diferentes técnicas de furação. A subtracção de radiografias pré e pós furação definiu a imagem a obter. No processamento de imagem, verificou-se que o *Threshold* é a variável mais importante causando variações significativas nos factores de delaminação. Neste trabalho é proposto um novo modelo de quantificação do dano causado pela furação. O factor de delaminação assim obtido permite minimizar o dano quantificado para as formas mais irregulares de delaminação e iguala os actuais factores de delaminação nas formas regulares.

Palavras-chave: Fibra de carbono, Delaminação, END, Raio-X, Processamento de image, *Threshold*,

Contents

List of Figures

List of Tables

List of Symbols and Abbreviations

ANOVA Analysis of Variance.

CER Cutting Edge Rounding.

CFRP Carbon Fibre Reinforced Plastics.

CMC Ceramic Matrix Composites.

FRP Fibre Reinforced Plastics.

GFRP Glass Fibre Reinforced Plastics.

HSD High Speed Drilling.

HSS High Speed Steel.

MMC Metal Matrix Composites.

NDT Non-Destructive Testing.

OGMA Oficinas Gerais de Material Aeronáutico.

PMC Polymer Matrix Composites.

ROI Region of Interest.

1

Introduction

1.1 Motivations

Drilling induced damage causes many composite drilled parts to be rejected in industries where close tolerance is needed and even if the required tolerance is met the part may be structurally compromised due to a reduction of the bearing strength or fatigue resistance.

The state of the art shows a number of damage quantification based methods that are currently used by researchers to better understand the effects of both drilling techniques and their variables. All of these methods start with the acquisition of an image of the damage however, their description is not detailed enough to allow reproducibility and be considered as a potential damage comparative unit. Furthermore, the mathematical quantification of the damage is in itself a point of discussion since no standard on what damage quantification method should be used has been set. In addition, no definition on what constitutes an acceptable drilling induced damage as a function of at least the predicted loading or application of the component has been established.

The work presented on this thesis was motivated by the need to compare the composite drilling induced damage between different composite drilling techniques and equipment to allow the inspection of each method's and tool's qualities.

1.2 Objectives

The main objectives of this thesis are:

- Development of an image processing methodology, based on digital radiographic imaging, that is capable of assessing the drilling induced damage in Carbon Fibre

Reinforced Plastics (CFRP), easily reproducible and allows the comparison of different drilling approaches.

- Re-think the premises of the delamination factor concept.

Complementary objectives are:

- Evaluate the influence of the threshold value on the end results.
- Compare the pre existing damage with post drilling induced damage

1.3 Structure

This thesis comprises 5 chapters: Introduction, Literature Review, Experimental Procedure, Results and Discussion and Conclusions and Future Work.

The Introduction focuses on presenting the motivations and the objectives that constitute the reasoning behind this study. Afterwards, the Literature Review consists of the essential conceptual knowledge that lays the ground work for the tasks here discussed. The State of the Art section contained in this chapter features the latest contributions in the Non-Destructive Testing (NDT) field that are relevant for this work with special focus on the drilling induced damage and damage assessment topics.

The Experimental Procedure chapter presents the materials used as well as the selected equipment and describes the experimental techniques. Both the radiographic procedure and the image processing methodologies are thoroughly depicted in this chapter in order to carefully explain the choices made and emphasize the influence of each step in each procedure such as the image segmentation step.

In chapter 4, the results of the application of the methodologies introduced in chapter 3 are presented and discussed. The variation of the image segmentation is investigated and an analysis is conducted on the delamination quantification leading to a definition of a new approach to the delamination factor.

Finally, chapter 5 presents the conclusions as well as proposals for future work developments.

2

Literature Review

2.1 Background

Composite materials are formed by combining two or more materials that differ in form or composition on a macro scale and have quite different properties, giving the resulting material a unique set of properties. In this mixture at least one of the components acts as a structural reinforcing element and the other(s) as a supporting matrix. Although the constituents or phases work together to improve the properties upon their original states, they do not merge into one another and have to remain identifiable and mechanically separable macroscopically.

Messler [1] categorized composites by their matrix material or phase:

- Polymer Matrix Composites (PMC): organic- or polymer-matrix composites with either thermosetting or thermoplastic matrices and polymeric, ceramic, glass, or metallic reinforcements;
- Metal Matrix Composites (MMC): metal-matrix composites with polymeric, ceramic, intermetallic, or metallic reinforcements;
- Ceramic Matrix Composites (CMC): ceramic-matrix composites with ceramic, glass, metallic, intermetallic, or polymeric reinforcements;

In general, composite materials are very durable, with the right composite being able to withstand heat, corrosion and cyclic loading. In fact, virtually any property can be improved or intentionally modified to satisfy certain requirements through the choice of the right structural and matrix elements, creating the concept of tailor made materials. Another advantage is that composites can be moulded into complex shapes, and designers

can reduce the number of small parts in a system by combining several small parts into one larger composite component. The main drawbacks are the production cost, harder NDT when compared to its metal counterparts and complex manufacturing process.

The lowering production costs and the industry's recognition of their performance capabilities have allowed composite materials to become available to a much wider array of applications such as aerospace, military and automotive industries who found in PMC, the combination of high performance fibres and resin matrices, the perfect choice for a structural component. This composite, often referred to as Fibre Reinforced Plastics (FRP), benefits from high strength and stiffness and provides an opportunity to improve performance when replacing a metallic part through weight reduction.

Prepregs, composite fibres that are pre impregnated with a resin matrix in very precise quantities, are widely used as the starting point to a composite component. They can be shaped as particulate reinforcements, whisker reinforcements, continuous fibre laminated reinforcements or woven composites. A requirement of the prepregs is the appliance of pressure or heat (or both) to consolidate and cure the composite. From here, a variety of processes can be done to meld the fibres with the matrix and achieve the desired final shape such as hand lay-up, vacuum bag moulding, autoclave moulding, resin transfer moulding, etc. The choice of the process should account for variables like the size and shape of the component, application, production volume and the materials involved since both quality and costs vary significantly across the processes, with the appeal on out of autoclave techniques due to possible quality improvements and cost reductions.

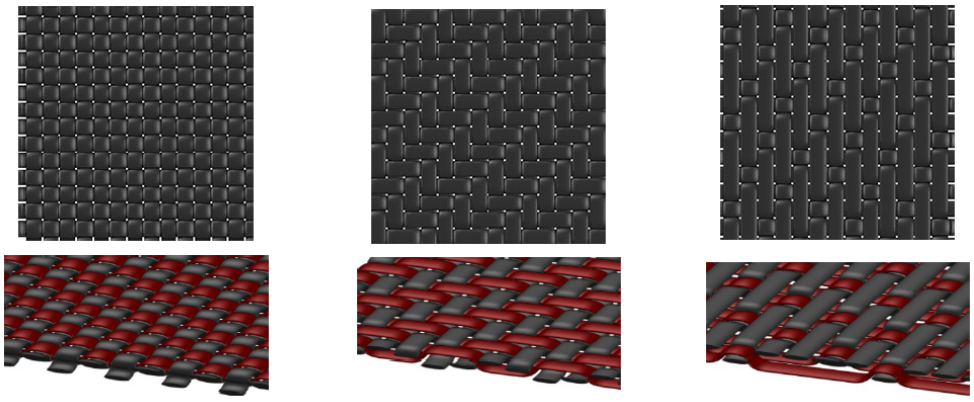

a) b) c)

Figure 2.1 Different types of weaving: a) Plain weave; b) Twill weave; c) Satin weave. Adapted from [2].

In the aerospace industry, composite materials may account for up to 50% of an aircraft (Figure: 2.2). The continuous pursuit of lower operating costs lead to a carbon fibre reinforced plastic fuselage in the Airbus A350XWB resulting in lower fuel burn, easier maintenance and increased resistance to corrosion [3].

In the same way, Boeing has equipped the 787 Dreamliner with 50 per cent composite by weight (Figure 2.4) which allowed for the change in fuselage manufacture where the

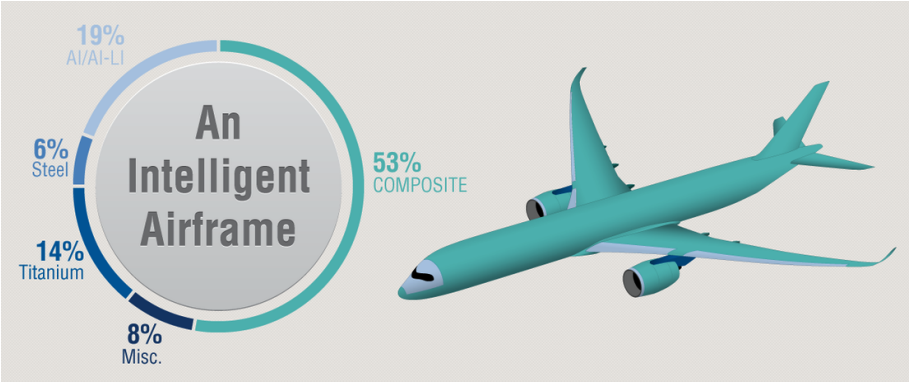

Figure 2.2 Airbus A350XWB airframe composition [3]

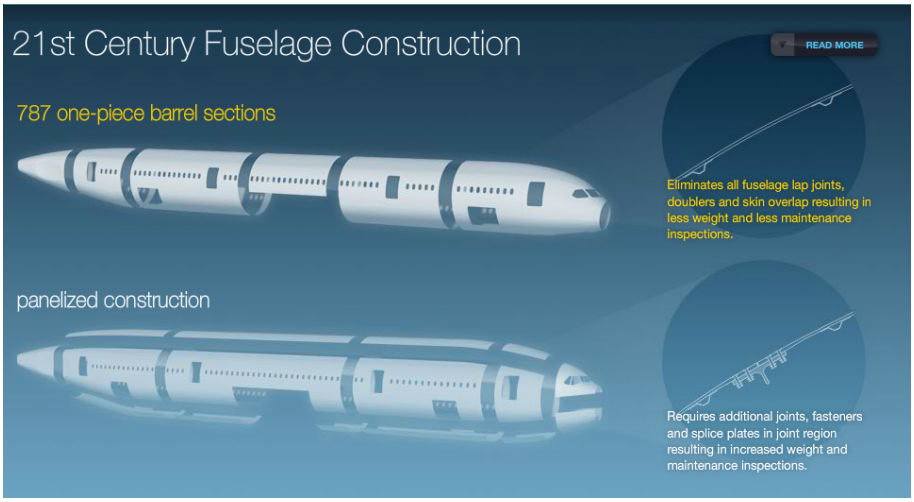

Figure 2.3 Boeing 787 Dreamliner: New and old fuselage construction methods [4]

panelized construction has been replaced by one-piece barrel sections assembly (Figure: 2.3).

Despite replacing metals in many applications, composite materials must be seen as a completely different entity when considering NDT methods. The heterogeneous structure allows multiple defect geometries to occur making the metals' damage assessment criteria, crack growth, inadmissible for composites because no single failure model can adequately describe the critical point when damage becomes significant.

Tool Wear

Unique wear characteristics result from the anisotropy of FRPs and the low thermal conductivity of composite laminates, when compared to that of metals, which leads to a fluctuating load acting on the tool's cutting edge. The hard and abrasive fibres provoke excessive tool wear and frictional heat while a soft and sticky matrix clogs the tool, dulling its edge [6].

Rawat and Attia [7] studied tool wear when drilling CFRP at high speeds using a

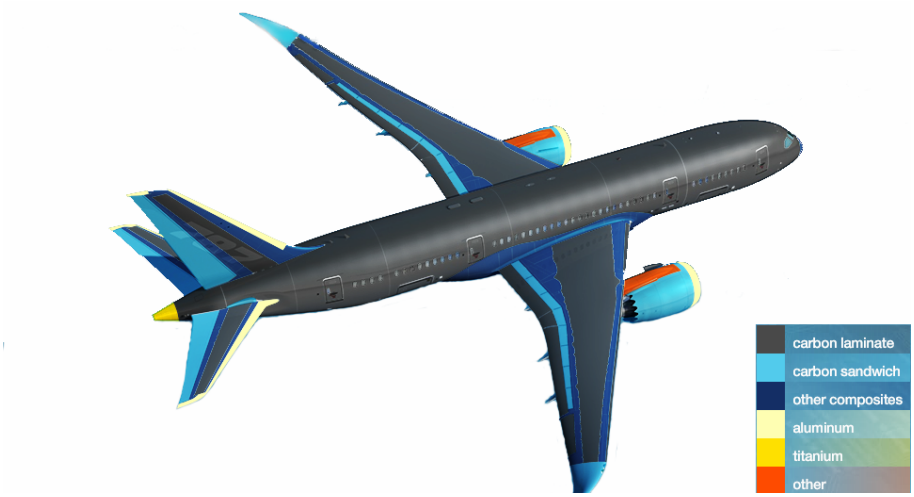

Figure 2.4 Boeing 787 Dreamliner: Structural materials distribution [5]

tungsten carbide drill bit. They state that the progression in the flank wear is not uniform and can be divided into three distinct wear regions:

1. *Initial Wear Region* – at the start of drilling in which the new cutting edge has sharp corner radius that carry cutting forces over a small chip contact area resulting in a heavily loaded system as explained by Teti [8] with a high wear rate with the occurrence of chipping and micro-cracking;

2. *Steady Wear Region* – After cutting edge rounding in the *Initial Wear Region* the increase in contact area between tool and workpiece lowers contact stresses reducing the wear rate;

3. *Severe Wear Region* – Here the flank wear reaches a second critical value causing a rapid increase in cutting force and temperature due to the thermal softening of both tool and workpiece causing an increase in applied contact pressure becoming again an highly loaded system with high wear rate.

Furthermore, tool wear is both affecting and being affected by the cutting parameters. While cutting forces and temperature control the mechanism and the kinetics of the wear process, the latter in turn alters the tool geometry, deteriorates the cutting capability of the tool and thus ultimately dictates the hole quality of the laminate. Figure 2.5 shows that both thrust force and cutting force increase with the increase in flank wear which in turn leads to an increase in delamination [7].

2.1.1 Non-Destructive Testing

Composite materials require specific processing operations because of their unique microstructure and geometry. A variety of defects with different dimensions may be formed during the manufacturing process in a composite. Typical defects include delaminations,

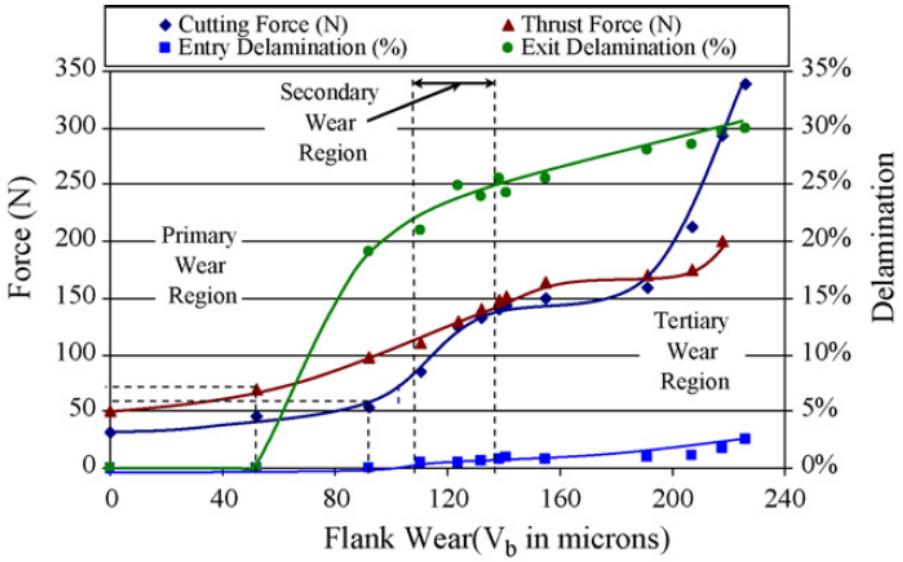

Figure 2.5 Effect of flank wear on thrust force, cutting force, entry and exit delamination at spindle speed of 15000 rpm and feed rate of 100 µm/rev. After [7]

fibre breaks, microcracks, matrix pores and fibre-matrix detachment. Many of these defects or micro structural variations result in changes of the composite properties which can lead to high rejection rates when compared to conventional materials. These prevent the full exploitation of these materials and lead to the development of NDT techniques for the manufacturing quality control where variables such as porosity, fibre/matrix distributions and fibre volume fractions are observed.

When considering on duty composites NDT methods search for damage and degradation like impact damage, delaminations, disbonds, heat damage and stress rupture which have the potential for catastrophic failure. Operations such as milling and drilling can cause this type of damage and if so make the component useless.

2.2 State of the Art

2.2.1 Drilling Composite Materials

The mechanism of material removal is another aspect of divergence between metals and composites due to the heterogeneity of the composites structure [8]. Several machining operations can be employed to composite drilling however most literature is dedicated to conventional drilling.

Comprehensive experiments have been conducted with this drilling method providing extensive data on the influence of input variables such as feed rate, spindle speed, drill bit geometry and materials and tool wear, on output variables such as delamination and thrust force.

Having concluded how the input variables influence the output many authors have searched ways to minimize or achieve delamination free holes.

In the pursuit of better results, experiments on other drilling methods such as Grinding Drilling [9], Vibration Assisted Drilling [10], and High Speed Drilling (HSD) have been performed. Although HSD requires specific machinery it somehow became a widely used technology due to the inherent capacity of achieving higher production rates. The main expectation from the application of HSD was reduced delamination through the lessening of thrust forces. A variety of drill geometries (Figure 2.6) and materials has been used in composite drilling with the twist drill in the spotlight. Due to the abrasive nature of the reinforcements the drill bit material dictates tool wear which causes severe degradation in hole quality. Numerous authors support that the drill bit geometry plays an important role in hole quality so many special drill bits have been developed such as straight flute [11], step drill [12], core drills [13] and step-core drills [14]. In general, special drill bits allow the use of higher feed rates without delamination when comparing to twist drills [15]. Other delamination reduction techniques include the drill of pilot holes [16] and the use of support plates to minimize delamination at hole exit [17].

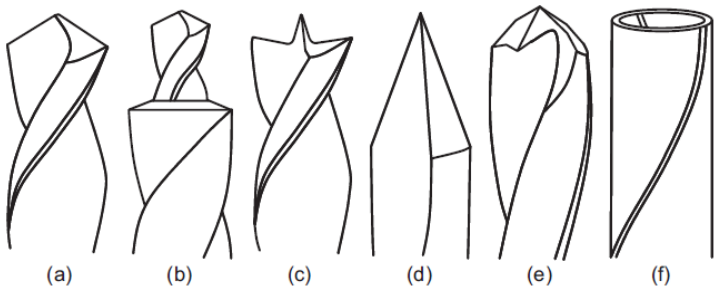

Figure 2.6 Schematic of special drill bit geometries: a) standard twist drill; b) step drill; c) W-shape drill; d) straight flute drill; e) multifaceted drill; f) core drill. After [18]

Drilling Induced Damage

Damage produced while drilling can lead to mechanical failure of a component or assembly as well as cause a component to be rejected because of a nonconformity in the hole tolerance. The most common types of damage referred in literature are delamination, microcracks, fibre-matrix debonding, matrix cratering and thermal damage [19]. None of which is as important as delamination, an inter-ply failure phenomenon that reduces assembly tolerances and bearing strength and as the potential for long term deterioration under fatigue load.

Delamination consists in the separation of individual plies within the laminate. It is often categorized in literature as "Peel up" or "Push-out" because different causes have similar consequences (Figures 2.7a and 2.7b respectively). Peel up delamination occurs at hole entrance due to a peeling force that pulls the first plies separating them from each other while push out happens at hole exit because of the force exerted by the drill bit in the last few uncut plies deforming and separating them. Experimentation has showed that push-out delamination is worse than peel up.

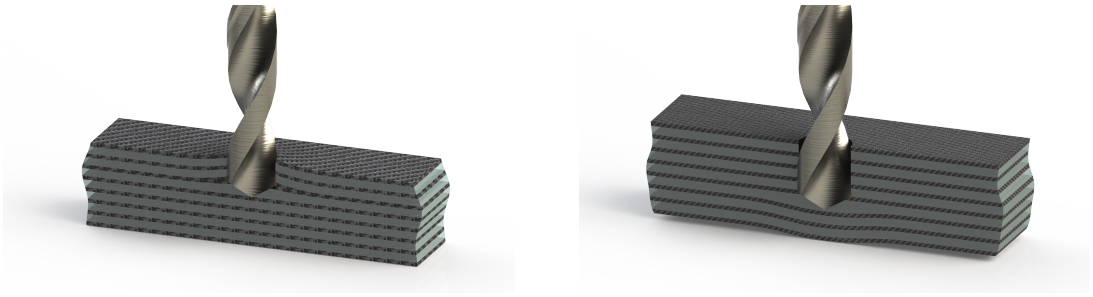

a) b)

Figure 2.7 Delamination mechanisms: a) Peel up at entrance; b) Push-out at exit. Adapted from [20].

Chen [6] used X-ray non-destructive inspection to investigate the damage zone in unidirectional and multi-directional CFRP laminates. The laminates were drilled with a 5.0 mm carbide drill and High Speed Steel (HSS) drill. This method required the hole edge to be coated with Tetrabromoethane to single out x-ray absorption of the damaged areas. To enable the comparison between different cutting conditions, the delamination degree was defined as the ratio between the maximum diameter of the damage zone and the predicted hole diameter (Equation 2.1). Chen's main conclusions were that the delamination varied linearly with average thrust force for both drills. Additionally, he presented the relation between flank wear and delamination factor with the number of drilled holes showing that this causes an increase of the delamination as a consequence of the increase in thrust force. Also the laminate properties had significant influence on the delamination factor with the multi-directional CFRP achieving better results.

Davim and Reis [21] used a Mitutoyo TM 500 optical microscope with 30x magnification and 1 µm together with a statistical study based on the Taguchi method and Analysis of Variance (ANOVA) to investigate cutting parameters selection for "Straight Shank" and "Brad & Spur" drills. The "Straight Shank" presents less specific cutting pressure and specific power than the "Brad & Spur" drill. They concluded that the feed rate was the most significant factor on power and specific cutting force for either drill bit. Delamination increases with both cutting parameters with feed rate being the most significant factor on entry delamination whereas for exit delamination it is the cutting velocity that has the highest influence.

Avdelidis, Almond, Dobbinson, *et al.* [22] made use of transient thermal NDT to assess aircraft composites. This method accomplished the visualization of notches and simulated delamination in carbon and boron epoxy composites with good agreement between the measured damaged area and the real defective area. The overall quality is dependent on defect depth and size thus restricting its application to near-surface defect imaging.

Tsao and Hocheng [23] observed that the quality of the hole and delamination are reduced using W-shaped drill and saw drill geometries when compared to twist drill geometry.

Hocheng and Tsao [15] compared the effects of five different HSS drill bits, namely twist drill, saw drill, W-shape drill, core drill and step drill, on the onset of delamination. They found that the special geometries can be operated at larger feed rate without delamination damage when compared to the twist drill.

Hamdoun, Guillaumat, and Lataillade [24] researched the fatigue resistance of drilled composites at 60% of compression notched strength. Two sets of drilling parameters were employed producing two types of samples, one "defect free" and another with intentionally introduced defects. X-ray and optical microscopy analysis were used to observe the damage. The samples were impregnated with Zinc Iodide to enhance contrast. Defect free samples showed a narrow dark band around the hole where the Zinc Iodide did not penetrate due to fibre wrenching during the drilling process. Besides the damage seen in defect free samples, severe drilling conditions caused larger delamination areas which emerged in the x-rays as two different scales of damage, a dark narrow band and a larger lighter area where detachment of the last layers occurred. Longitudinal cracks were the main visible fatigue damage.

Campos Rubio, Abrão, Faria, *et al.* [25] chose an optical toolmaker's microscope at 30x magnification and $1\,\mu m$ (Mitutoyo TM 500) to evaluate the effect of delamination in HSD of Glass Fibre Reinforced Plastics (GFRP) with three K20 cemented carbide drills: two $5\,mm$ diameter twist drills with different point angle and one "Brad & Spur" drill. They found that both increasing spindle speed and decreasing feed rate causes delamination to decrease for spindle speeds up to $8000\,rpm$. The Brad & Spur" produced less delamination than both twist drills. Feed rate was seen to loose influence on delamination for higher spindle speeds ($40000\,rpm$). The use of such spindle speeds yields higher material removal rates and minimal delamination.

Rawat and Attia [7] used the machinability maps approach to study the effects of cutting conditions on the quality attributes of high speed drilled holes of woven graphite epoxy composites with $5\,mm$ and 118° tungsten carbide drills. Delamination was analysed using the Olympus Model GZX 12 optical microscope with hole circularity and diameter error measured on a Mitutoyo-Mach 806 coordinate measuring machine. The observations showed that the effect of thrust force is significant on tool wear and quality of the final hole, and the delamination increases with increased tool wear. From the machinability maps presented in figure 2.8, they concluded that the optimal cutting conditions for minimum damage and maximum productivity are $8500\,rpm$ and $100\,\mu m/rev$.

Faraz, Biermann, and Weinert [27] introduced the idea of Cutting Edge Rounding (CER) and studied its evolution on various carbide drills (with four different geometries) during drilling of CFRP using firstly a constant set of cutting conditions and analysed the progression of CER with respect to thrust and torque and the resulting effect on hole damage. Delamination was examined through image processing (AnalySIS – pixel count based software) in conjunction with stereomicroscopy (Wild Type M3C Microscope with an integrated Canon camera). Very good correlations were observed between mechanical loads and CER as well as delamination results and CER while its measurement is much

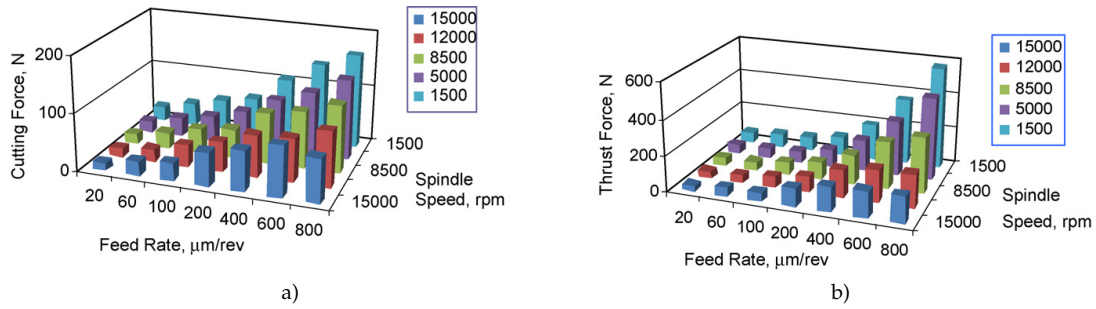

a) b)

Figure 2.8 Effect of spindle speed and feed rate on the thrust and cutting forces: a) Cutting Force; b) Thrust Force. After [26]

easier than conventional flank wear.

Torres Marques, Durão, Magalhães, *et al.* [28] analysed the selection of cutting parameters and the delamination of CFRP drilled with a four different drill geometries by enhanced radiography with diiodomethane contrasting fluid and image post processing. The processing sequence comprised a manual selection of the interest zone, a noise reducing filter, automatic binarization, erosion and dilation morphologic filters for noise reduction and finally a measuring algorithm. A correct selection of cutting parameters was found to have the potential to reduce delamination between 4 and 5%. Moreover, a selection of a dedicated tool further improves the end results, particularly with a pilot hole associated with a twist drill allowing an additional improvement of 2% when compared to the second best result. A special step drill bit can be useful to reduce delamination however the tested tool does not yet show a significant advantage when compared to the commercial tools available. The enhanced radiography method was found capable of determining and quantifying the damage caused by drilling.

Shyha, Aspinwall, Soo, *et al.* [29] applied the Taguchi method with ANOVA to study the influence of process parameters on tool life and workpiece damage when drilling 3 mm thick CFRP with TiN-coated and uncoated step and twist drills ($\phi = 1.5$ mm). A Joel 6060 Scanning Electron Microscope was used to acquire digital image of the workpiece plates which were afterwards processed in Omnimet software. The measurements were performed with a DEA coordinate measuring machine equipped with a 1 mm ruby ball stylus and a Renishaw head. Drill geometry and feed rate were the most significant parameters on measured outputs. Cutting speed and feed rate had the greater effect on torque. The combination of stepped drill geometry, higher feed rates and the use of uncoated tools maximized tool life in terms of number of drilled holes while the worst results were found for the TiN-coated conventional twist drill.

Curnick [30] investigated drilling of CFRP and GFRP. A series of parameters were employed to an HSS twist drill and a multifaceted carbide drill with the results being inspected through optical microscopy (Leica L2) and evaluated by the delamination factor. Drill exit damage was greater than entry point damage while delamination was found to increase with feed rate and lessen with increasing spindle speed. The multifaceted drill yielded less damage than the twist drill.

Tsao and Chiu [31] found that using compound core-special drills is more advantageous when drilling CFRP, since a reduction of thrust force, delamination, chip clogging occurs with higher chip removal.

Machado [2] characterized the high speed drilling damage in CFRP, with three drill geometries (straight flute, W-shape and twist drills), through the development of empirical models that correlate the output response (thrust force, torque and delamination factor) with the process variables (spindle speed, feed rate, drill diameter, workpiece thickness) using a design of experiments together with Response Surface Methodology (RSM) and minimize the occurrence of drilling induced damage. A *Kodak RVG 5100* associated with a *Kodak RX 2100* unit was used to perform digital radiographic analysis on di-iodomethane immersed samples while image processing resulted from the combination of *Photoshop*, *Matrox* and *Solidworks* software in order to measure the extent of the damage caused by the drilling operation. The input variables that influence most the thrust force and torque responses are the workpiece thickness, the tool diameter and the feed per tooth whereas the spindle speed is the factor which least affects the response. The tool diameter and workpiece thickness are the most significant factors with regard to the delamination factor and adjusted delamination factor responses. Analysis by digital radiography demonstrated to be a good option for measuring the delamination damage despite the compulsory use of a contrast medium.

Durão, Tavares, Albuquerque, *et al.* [32] drilled a batch of CFRP plates with different drills and measured the resultant delamination extension from digitally enhanced radiographies, with a contrast agent, using computational techniques of image processing. The concept of circularity is combined with the delamination factor in the evaluation of the damage so that the shape of the damaged is taken into account. The results confirmed that higher feed rates correspond to higher delamination extensions regardless of the criterion used. Circularity was found to decrease with the increase of feed rate.

2.2.2 Delamination Assessment

The drilling damage is often evaluated by the delamination factor (F_d) presented by Chen, which encloses the damage in a circle concentric with the drill hole. It is defined as:

$$F_d = \frac{D_{max}}{D} \tag{2.1}$$

where F_d is the delamination factor, D_{max} is the maximum diameter of the damage zone and D is the hole diameter. This hypothesis may represent the damage inadequately when just a few fibres or fibres bundles are peeled up or pushed down thus creating a significant damaged width, will never represent truly the extend of the damage across the entire hole periphery. Therefore Faraz, Biermann, and Weinert [27] propose a different delamination factor F_a (Equation 2.2):

$$F_a = \left(\frac{A_{del} - A_{nom}}{A_{nom}} \right) \% \tag{2.2}$$

where A_{del} is the delamination damage area and A_{nom} is the nominal area of the hole.

Davim, Rubio, and Abrão [33] propose a different approach in order to better assess the damage patterns shown in figure 2.9: a digital analysis methodology together with an adjusted delamination factor F_{da}. The first part of equation 2.3 accounts for the size of the crack, which is Chen's delamination factor, and the second part accounts for the occupation rate of the maximum diameter of the damage zone where A_d is the damaged area, A_{max} is the area corresponding to D_{max} and A_0 is the area of the nominal hole.

$$F_{da} = \alpha \frac{D_{max}}{D_0} + \beta \frac{A_{max}}{A_0} \tag{2.3}$$

The parameters α and β are used as weights with β being considered as the ratio of the damage area to the area corresponding to the area of the delamination zone minus the nominal hole area and α being a complement of β:

$$\alpha = 1 - \beta \tag{2.4}$$

$$\beta = \frac{A_d}{A_{max} - A_0} \tag{2.5}$$

Equation 2.3 can be rewritten by substituting equations 2.4 and 2.5 thus obtaining equation 2.6:

$$F_{da} = F_d + \frac{A_d}{A_{max} - A_0}(F_d^2 - F_d) \tag{2.6}$$

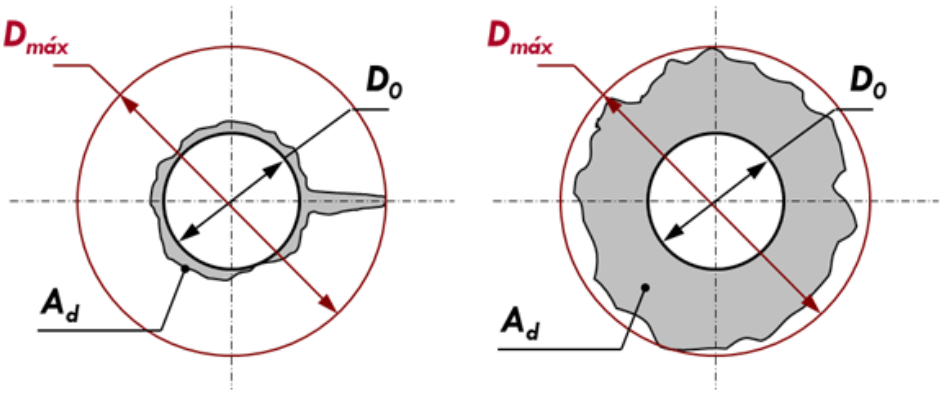

Figure 2.9 Delamination patterns: a) fine cracks b) uniform damage area. After [33]

Durão, Tavares, Albuquerque, *et al.* [32] conjecture that the shape of the damaged area should be considered in the analysis of the delamination factor. This is done through the calculation of the shape's circularity (i.e. the shape's compactness compared to a circle of

equal perimeter) using equation 2.7.

$$f = 4\pi \frac{A}{P^2} \tag{2.7}$$

When the damage pattern resembles a circle, the circularity is near 1 at which it becomes a perfect circle. As the value approaches 0 the damage pattern becomes an elongated polygon.

2.2.3 Digital Radiography

This technique involves the use of penetrating gamma or X-radiation to examine parts and products for imperfections. An X-ray machine or radioactive isotope is used as a source of radiation. Radiation is directed through a part and onto film or other media causing shades to appear, called shadowgraph. The resulting shades show the attenuation of the signal while it has passed through the sample [34].

X-rays are attenuated when they interact with energy states of electrons in the atoms in the beam's path resulting in different shades to appear in the shadowgraph. The denser the material is, and the more material there is, the more the x-rays will be attenuated while travelling through the sample. Therefore, different shades mean differences in material density, material thickness or both [35].

X-radiography of composites is slightly different because composites are highly transparent to x-rays requiring low energy x-rays to be used. Otherwise, if energies that are commonly used when scanning other materials were used, such x-rays would go through the composite sample almost as if there was no sample in place, producing merely saturated images. Such defects as delaminations and disbonds are virtually invisible to x-rays because they do not significantly change the composition or total amount of materials through which the x-rays travel. However, it is possible to get delaminations and disbonding visible in x-ray image with radio-opaque absorbent penetrant using chemical fluids like diiodomethane, dibromomethane or zinc iodide which serve as contrast agents, causing the damage to become visible in the x-ray image [35].

The method can detect following defect types:

- matrix cracking
- cracks
- delaminations
- inclusions
- voids
- porosities

Digital radiography differs from conventional radiography by the use of an x-ray digital detector eliminating the need of chemical revelation processes.

For a digital sensor, the notion of resolution is rather different from the resolution of an analogical detector. It is always possible to detect an object which is smaller than an

image element (pixel), if its contrast is important enough. On the other hand, it is not obviously possible to separate two distant objects of less than two pixels. The detectability of a detail is thus connected to two essential notions for the detector: the resolution in contrast and the spatial resolution Berthel, Bonin, Cadilhon, *et al.* [36].

The advantages of the digital sensors with regard to the traditional film are:

- Significant benefits on consumables, safety and environment (screen, chemical supplies), and on maintenance (simpler on a scanner than on a developing machine),
- Use of the same sources of radiation, the same metal screens as the radiography film,
- Wide range of exposure with a linear relation between the luminescence intensity and the received dose,
- Reduction of the exposure time (in certain conditions) and dose debits with regard to the film
- Treatment and filing of the data.
- Real time applications and sharing possibilities.
- A quasi-immediate availability of the image.

Since no chemical revelation is needed, there is no more need to refer the exposure time but rather the integration time. The advantage of digital radiography compared to films is shown in figure 2.10. Note that the integration times used for the digital technique are much smaller in comparison with the exposure times used with traditional films.

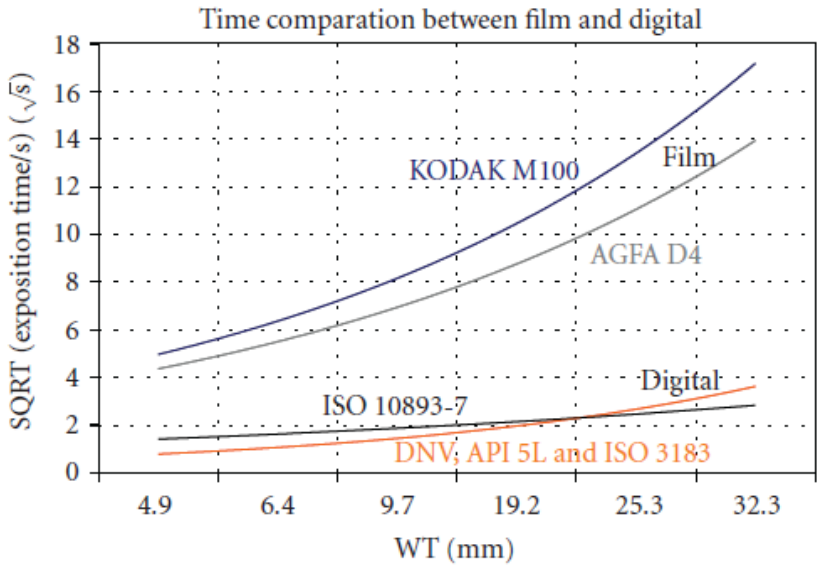

Figure 2.10 Integration time vs Exposure time. After [37]

2.2.4 Image Segmentation

Image processing is used to identify the areas of interest in a given image, in this case the damage in composite materials. The most important step in this process is the segmentation of the image which consists in partitioning the input image into groups of pixels that

share a certain property. The simplest method of image segmentation is the threshold method which transforms a gray-scale image into a binary one, depending solely in the selected threshold value, where the object will be assigned one state and the background another.

If we plot the number of pixels which have a specific grey level versus that value we create the histogram of the image Petrou and Petrou [38]. The grey levels of pixels belonging to the object often are substantially different from the grey levels of the pixels belonging to the background. For a medical x-ray this is particularly useful since the resulting image consists of a dark background and a bright object that translate into the histogram plot as two peaks and a valley in between. The best possible threshold will be the lowest valley point since it represents the highest variation between the object and the background. However CFRP x-rays do not have a similar histogram so the threshold selection is much harder. Instead they feature unimodal distributions as that shown on figure 2.11.

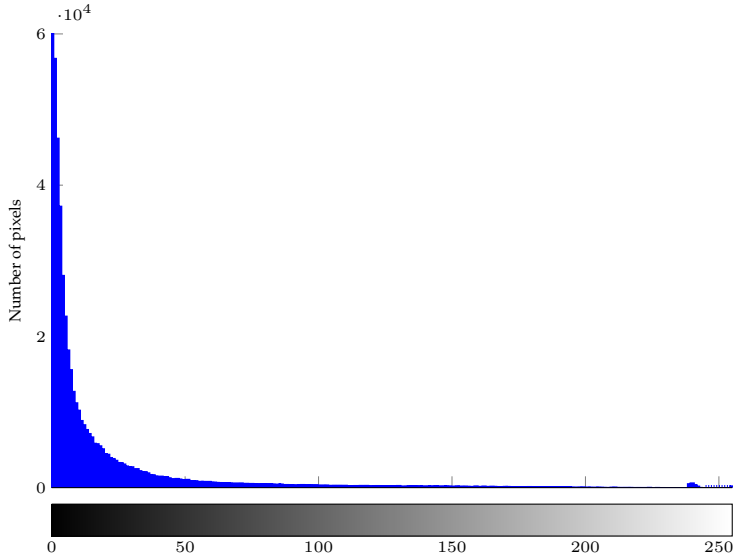

Figure 2.11 Unimodal histogram

Sezgin and Sankur [39] conducted an extensive survey on automated image thresholding techniques and quantitative performance evaluation. The authors categorized the thresholding methods according to the information they are exploiting:

1. histogram shape-based methods, where, for example, the peaks, valleys and curvatures of the smoothed histogram are analysed.

2. clustering-based methods, where the grey-level samples are clustered in two parts as background and foreground (object), or alternately are modelled as a mixture of two Gaussian distributions.

3. entropy-based methods result in algorithms that use the entropy of the foreground

and background regions, the cross-entropy between the original and binarized image, etc.

4. object attribute-based methods search a measure of similarity between the grey-level and the binarized images, such as fuzzy shape similarity, edge coincidence, etc.

5. the spatial methods use higher-order probability distribution and/or correlation between pixels.

6. local methods adapt the threshold value on each pixel to the local image characteristics.

The evaluation followed criteria based the difficulties of each method when facing disproportionate backgrounds and foregrounds and overlapping distributions of grey levels, namely misclassification, edge mismatch, relative foreground area error, modified Hausdorff distance and non-uniform region. The five criteria were then combined into a single factor, the average score, to sort all methods according to their results. Two datasets were organised in groups of 40 images, one built with NDT images and the other with document images. Table 2.1 summarizes the results obtained. The result of each algorithm differs significantly depending on what image type is inputted. For NDT applications, the highest-ranking seven techniques are all from the clustering and entropy category.

Table 2.1 Threshold evaluation according to overall average quality. a) Evaluation of 40 NDT images; b) Evaluation of 40 document images. After [39]

a)			b)		
Rank	Method	Average score (AVE)	Rank	Method	Average score (AVE)
1	Cluster – Kittler	0.256	1	Cluster – Kittler	0.046
2	Entropy – Kapur	0.261	2	Local – Sauvola	0.066
3	Entropy – Sahoo	0.269	3	Local – White	0.080
4	Entropy – Yen	0.289	4	Local – Bernsen	0.090
5	Cluster – Lloyd	0.292	5	Shape – Ramesh	0.093
6	Cluster – Otsu	0.318	6	Attribute – Leung	0.110
7	Cluster – Yanni	0.328	7	Entropy – Li	0.114
8	Local – Yanowitz	0.339	8	Cluster – Ridler	0.136
9	Attribute – Hertz	0.351	9	Entropy – Shanbag	0.144
10	Entropy – Li	0.364	10	Shape – Sezan	0.145

Otsu [40] developed a non parametric and unsupervised method of automatic threshold selection for picture segmentation in which an optimal threshold is selected by discriminant criterion in order to maximize the distinguishable resulting classes in grey levels. The selection is automatic and stable since it is not based on a local property such as the valley but on the integration, a global property of the histogram.

2.2.5 Literature Review Conclusion

From the State of the Art it can be concluded that most authors rely on optical methods to analyse the drilling induced damage. However, this is a surface analysing method while the damage varies along the thickness of the workpiece thus questioning the accuracy of the results. Moreover, no author refers thoroughly the image processing settings used to prepare for the measurements.

The observation of the presented image segmentation techniques shows that a number of automatic methodologies have the potential to be implemented in post processing of NDT radiography however manual thresholding should not be completely set aside as it is always coupled with the observers experience and thus an indispensable tool for verification of automatic methods. Furthermore, the image processing data presented in literature seems to be only capable of analysing continuous damage samples with discontinuous ones being completely disregarded.

In respect to drilling variables, it is clear that they have a significant influence on hole quality with feed rate being the dominant cutting parameter despite losing influence on HSD. This led to the idea that high spindle speeds coupled with high feed rates are capable of minimizing drilling induced damage. Workpiece thickness and diameters larger than 6 mm do not have enough data available for reference.

Regarding the Delamination Assessment, many solutions have been presented however none has attained full consensus between scientific researchers. The lack of independence of the measurement process may be responsible for this fact while also impeding the comparison between different drilling processes.

3

Experimental Procedure

3.1 Introduction

The assessment of drilling induced damage in CFRP is strongly dependent on the methods used for this purpose. Table 3.1 provides a general overview of all available methods and focus on each methods' capacity of identifying different types of damage. In here, radiography imaging is seen as a capable technique having qualitative evaluations similar to destructive methods such as de-ply and fractography.

Several researchers [2], [32] successfully made use of this technique to quantify delamination and benefited from the conversion to digital radiography which allowed this technique to become an even more proficient tool in detecting damage in CFRP, despite still requing the application of a contrast agent. Afterwords, image processing is employed in order to quantitatively assess the registered damage.

Two image processing methodologies based on image segmentation are presented: the first, an observer guided method, and a second, an automatic algorithm. Experiments were conducted with these methodologies to investigate the influence of the variables present in image acquisition and processing on the measure of delamination in CFRP. Image subtraction was performed with pre-drilling and the post-drilling radiographies. Although this technique is highly impractical, it allows the evaluation of the damage without accounting for the previously existing damage. This way, a reference result for the image segmentation was attained.

Table 3.1 Comparison of sensitivity to impact damage in CFRP's between major inspection methods. After [41]

Damage	De-ply	Fractography	Visual Inspection	Ultrasonics	Radiography imaging
Damage type:					
Delaminations	Good	Very good	Good	Good	Fair
Fibre breakage	Fair	Good	Fair	Very poor	Good
Matrix cracks	Fair	Fair	Fair	Very poor	Good
Surface defects	Good	Good	Very good	Poor	None
Damage size:	Good	Good	Fair	Good	Good
Damage location:					
Distance from surface	Good	Very good	Fair	Good	Good

Damage	Thermal imaging	Acoustic emission	Laser-based optical imaging	Microwave	Eddy-current testing
Damage type:					
Delaminations	Fair	Poor	Fair	Very poor	Very poor
Fibre breakage	Poor	Poor	Poor	Poor	Good
Matrix cracks	Poor	Poor	Poor	Poor	Poor
Surface defects	Poor	Very poor	Poor	None	Poor
Damage size:	Fair	Very poor	Poor	Fair	Fair
Damage location:					
Distance from surface	Poor	Very poor	Very poor	Very poor	Poor

3.2 Materials

The CFRP samples shown in figure 3.1, were supplied by OGMA from leftovers of the *NH-90* helicopter construction in the shape of plies with $300\,\text{mm} \times 300\,\text{mm}$. The plies were manufactured using an autoclave and consist of 10 prepreg plies of plain weave 3K yarn with a 50% carbon fibre to epoxy content ratio and a thickness of $0.2\,\text{mm}$ per ply. The plies were then stacked in a $[0_{10}]$ sequence, resulting in a final thickness of $2\,\text{mm}$. They were cut in $250\,\text{mm} \times 20\,\text{mm}$ samples and since different thicknesses were needed for this work, they were joined with the same manufacturing technique to build samples with thicknesses of $4\,\text{mm}$ and $8\,\text{mm}$. This joining procedure is common in industry and does not cause significant changes in the behaviour of the samples.

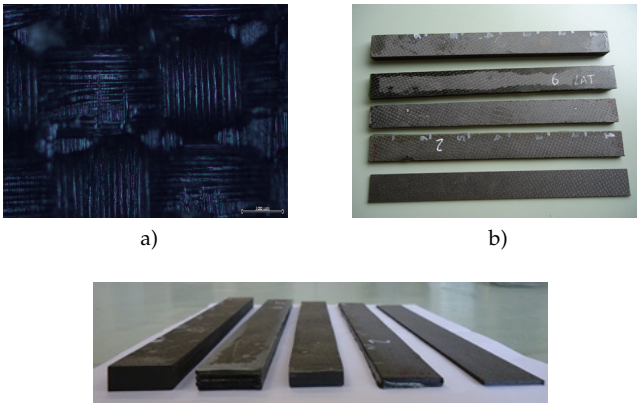

a) b)

c)

Figure 3.1 CFRP samples: a) Plain weave detail; b) Test samples; c) Different thickness samples.

3.3 Equipment

The drilling tests were performed in a LEADWELL VMC-15 vertical machining centre coupled with a NIKKEN BT30-NX5-153 spindle speeder as presented in figure 3.2, which allows a maximum rotation of 20000 rpm

a) b)

Figure 3.2 Drilling equipment: a) CNC machining centre – LEADWELL VMC-15; b) Spindle speeder – NIKKEN BT30-NX5-153.

The samples were drilled using the cutting parameters shown in table 3.2. The individual information of each test can be found in appendix A. Tungsten Carbide K20 drills were used with two diameters, 5 mm and 9 mm and three different drill geometries, a twist drill with 120° point angle, a straight flute drill and a W-shape drill (recommended by DORMER). Figure 3.3 presents the tool geometries used used.

The combination of the cutting parameters with the drilling diameter and the workpiece thickness resulted in a set of 32 different tests. A preliminary set of experiments was performed, using the straight flute drill and the Twist drill, for the analysis of the image processing implementation totalling 64 drilled holes. Then, after the development of the image processing methodology, another set of experiments was conducted, this time using the W-shaped drill and the Twist drill with the last being combined with a

a) b) c)

Figure 3.3 Tool geometries used on the experimental work: a) Twist drill; b) Straight flute drill; c) W-shaped drill.

new clamping fixture that compresses the CFRP sample as presented in [2]. All tests were conducted with new unused drills.

Table 3.2 Test data summary. After [2]

Spindle Speed	8000 rpm, 12000 rpm, 16000 rpm and 18000 rpm
Feed Rate	0.3250 mm/tooth, 0.05500 mm/tooth, 0.7750 mm/tooth and 0.08875 mm/tooth
Tool Geometry	Twist, Straight flute and W-shaped
Tool Diameter	5 mm and 9 mm
Workpiece Thickness	4 mm and 8 mm

The new clamping fixture is composed of two aluminium plates with two guide pins and a central concentric hole. The compression is attained through the bolted connection. A specific tightening of the screws provides a certain pressure exerted to the CFRP sample that are placed in between the plates. The central hole diameter is the same diameter as the tool being used to drill the CFRP sample so that the clearance is as small as possible to avoid edge bending and fracturing.

The radiographic analysis was performed using a combination of a KODAK 2100 RX unit and a KODAK RVG 5100 digital radiography system. The RX unit is a high frequency DC X-ray generator with a tube voltage of 60 kV working at 7 mA with a 23 mm $\times$ 35 mm collimator and a maximum focal distance of 200 mm This system features a spatial resolution of 18.5 µm and an active sensor area of 22 mm $\times$ 30 mm and a maximum integration time of 620 ms.

X-radiography alone does not suffice to evaluate the delamination extension so a contrast enhancing agent needs to be used. Diiodomethane, a radio-opaque penetrant, was the contrast fluid used in this work.

3.4 Experimental Methodology

3.4.1 Radiography Stage

The specimens were radiographed perpendicularly to the radiation source, 50 mm below the collimator and with an integration time of 160 ms inside a lead box for radiation

containment after being immersed for at least an hour in diiodomethane.

Radiographies covering the entire sample area were taken prior to the drilling operation to allow the comparison of the magnitude of the formation damage on the post drilling radiographies. All images were saved in high resolution tiff format files with 1200 pixels $\times$ 1600 pixels.

3.4.2 Image Processing Stage

There are many tools available to conduct image processing tasks. In this section, the procedures associated to an observer based methodology coupled with image processing software and an automatic algorithm developed with tools from MATLAB's Image Processing Toolbox are analysed. The basic principles are shared by both methodologies and consist in:

1. Selecting the Region of Interest (ROI);
2. Differentiating the contents of the ROI;
3. Segmenting its contents;
4. Collecting data for delamination assessment.

The points of divergence lie in the criteria used in each step to make certain decisions in the path to the delamination quantization. The observer based methodology, as the name indicates is under control of the user or observer and depends entirely on the experience of the observer. Therefore this methodology can virtually use any image processing software since it is only present as a tool for the observer and the commands required come as standard in most commercial software, like ADOBE PHOTOSHOP, or free software, such as IMAGEJ.

Task 1, the selection of the ROI, is simply the cropping of an adequate area of the original radiography, that encloses the drilled hole and should encompass the two farthest points in terms of x-ray reception so that the linearization of two different images is close enough to allow a precise comparison between them. This means that the image should have, besides the drilled hole, at least one pixel receiving the full amount of incident radiation and another receiving no radiation whatsoever. If these two points always exist in the images then, for that equipment, accurate comparison can be performed for different images. Having a radiation sensor bigger than the test samples should help in achieving this result. The influence of the size of the cropped area, that contains the ROI, over the threshold result has not been established.

Task 2 consists in choosing, using a "Magic Wand" tool, the damage caused by the drilling process and separating it from the damage prior to the drilling stage. This is the most critical step to the observer and it is here that the experience has its most significant role. A bad decision in this task may lead to a delamination factor that is completely misleading. Although the formation process damage has not been quantified in this work it is substantially smaller than the drilling induced damage ergo the regions can be separated according to their area with the smallest being excluded from the image thereby

leaving just the drilling induced damaged areas.

Image segmentation, task 3, is one of the main topics of this thesis. Many researchers [2], [28], [32], [33] have employed thresholds to process their radiographs but none have addressed this tool as a source of either error or room for improvement despite using different image segmentation techniques. Section 2.2.4 presented an overview on the principles of applying a threshold to an image and the different types of techniques available. From this it can be concluded that the results can vary significantly depending on what technique is employed however, relying on the experience, the observer can supersede this question and manually adjust the threshold value according to the specific image under analysis and its parent radiography without any consideration for the image histogram. In addition, the histograms of all radiographs taken were always very close to being unimodal which was expected as it is a hallmark of radiographic images.

This choice should bear some thought because by defining individual thresholds per image the assurance that two thresholded images are comparable decreases significantly especially if the selected threshold values differ considerably.

Finally, in task 4 the data needed to quantify the damage is retrieved from the selection previously made in task 2 and evidenced numerically through the segmentation in task 3. Choosing the inside of the resulting areas, that now possess the same value due to the threshold operation, allows for the determination of an approximation to the drilling centre. From here the smallest circle that encloses the resulting areas can be drawn. This circle defines the total affected area and its diameter features both in Chen's delamination factor and Davim's adjusted delamination factor.

The application of MATLAB's Image Processing Toolbox is nothing more than the evolution of the observer's interpretations with the laying out of some of the criteria discussed above and an attempt to remove the issue of the definition of individual threshold values.

As such, task 1 should be performed in the same manner to build the input for the MATLAB scripts. This input is then translated into numerical pixel values according to its intensity in a grey scale. The visual information the observer relied on to identify the region of interest is not something that the algorithm can execute. For this reason, the image segmentation is performed beforehand so that the resulting finite boundaries can be used for the identification of each area.

For comparison with the values obtained through the observer methodology, ten sequential values between 30 and 120 were picked from the 0 to 255 grey scale for the manual segmentation to represent the majority of the pixel intensities under analysis. The usage of an algorithm permits the introduction of the automatic segmentation methods referred to in section 2.2.4. Three threshold algorithms were chosen according to their ease of application as well as their performance in evaluating NDT images as shown in table 2.1. Consequently Kittler [42] and Kapur [43], the top two methods, were selected together with Otsu's method because it is a built in MATLAB function and also thoroughly reviewed and referenced in literature.

The use of automatic segmentation algorithms improves the comparability of the end results since more image data is taken into account. In addition, if the images feature the two farthest points in terms of x-ray reception they will have similar linearizations and hence the algorithms will respond with similar threshold values despite whatever cutting variables are employed. Preliminary tests with the algorithm and the observer method showed that the use of a manually set threshold of constant value had the potential to become a standardized method. However, this constant value is a function of at least the sensor covered area which has an effect on the linearization of the highest and lowest radiation points.

After the segmentation is executed, the regions can be sorted according to their areas. Again, since the formation process damage is smaller than the drilling induced damage, the smaller areas are deleted from the image leaving only the drilling induced damaged areas.

After removing the irrelevant areas, the data collection can begin. Firstly, the drilling centre and drill radius are estimated from the unsegmented image through the application of a Hough transform. Secondly, a manually adjusted filter is applied to the segmented image. This is performed in order to remove all damage that is not considered to be drilling induced. Afterwards, the convex polygon with the least number of sides that circumscribes the segmented image is computed. From the vertices of this polygon the minimum enclosing circle can be determined. Finally, the shape's external boundary is traced and the distances between the latter and both the drill centre and the minimum enclosing circle centre are calculated.

Image subtraction

In order to have a realistic target for the image processing methodologies based on the threshold application, an image subtraction technique was conducted. Image subtraction is a process that makes use of the digital conversion of an image to perform a subtraction of the pixel values between two different images. This is often used in astrophotography for asteroid detection since static bodies such as stars do not move and consequently the pixels that represent them maintain their intensity values whereas moving bodies do change position and a change in pixel intensity occurs. The subtraction of such images features only the moving pixels in a dark background. Other applications include the detection of flaws and defects in production lines through the comparison of a "Golden Template", an image of a correctly manufactured product.

The application of this technique in drilling induced damaged specimens requires two images to be acquired, one portraying the specimen prior to the drilling and another portraying the drilled hole. The quality of the subtraction is evaluated by the registration, or alignment, of the images. This is especially troublesome in this work since the radiographic images do not supply enough details for an automatic registration to succeed, which imposes the need to carry out a manual registration of the images. For an accurate

manual registration notches up to 5 mm long were cut on one side of the specimens.

This technique can be implemented in a variety of image processing software just as the observer based methodology for threshold application. The layer registration is obtained through the visual alignment of the notches using the transparent feature of the different layers. After attaining a satisfactory registration the subtraction can be performed. Figure 3.4 illustrates the subtraction process. Some software uses another variable to correct the brightness of the resulting image called *Offset*. In this work an *Offset* of -50 was found adequate.

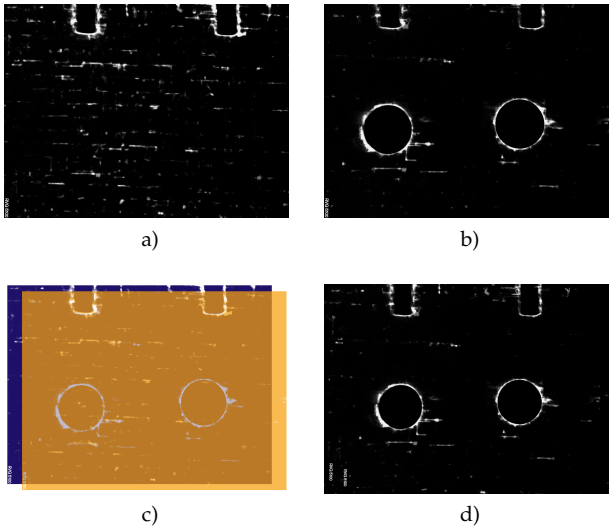

Figure 3.4 Image subtraction process example – Tests V01 and V05 performed with the twist drill.a) Pre drill radiography; b) Post drill radiography; c) Manual image registration; d) Subtraction results.

4

Results and Discussion

A preliminary set of experiments using two drill geometries, straight flute and twist drill, was conducted for the development of the methodologies' implementation procedure which were compared to the image subtraction results.

These tests featured a variety of cutting parameters as well as two workpiece thicknesses so that a representative sample of drilling damage could be achieved in order to investigate the influence of the segmentation of the image on the damage assessment.

4.1 Threshold Investigation

For a selection of relevant tests performed with the straight flute and twist drill, the influence of the threshold on the affected area, delamination factor and adjusted delamination factor is presented in the following figures. The corresponding drilling variables can be found in appendices A.1 and A.3 for the twist drill and the straight flute drill, respectively.

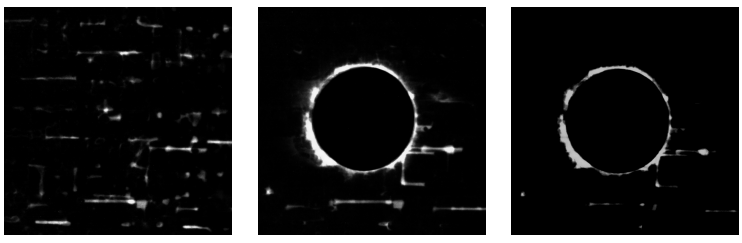

a) b) c)

Figure 4.1 Image subtraction for the twist drill test V01: a) Pre Drill; b) Post Drill; c) Image subtraction.

The image subtraction method is shown in figure 4.1 for the twist drill and figures 4.2 for the straight flute drill. In these, damage isolation is almost perfect despite the manual alignment of the pre drill (figures 4.2a and 4.1a) and post drill (figures 4.2b and 4.1b) radiographies.

a) b) c)

Figure 4.2 Image subtraction for the straight flute drill test V01: a) Pre Drill; b) Post Drill; c) Image subtraction.

Manual thresholding is illustrated in figures 4.3 and 4.4. The evolution of the affected area with the increase of the threshold value for both drills is visible. A threshold value that is too small will cause formation damage to appear connected to the drilling induced damage. On the other hand, a threshold value too high will neglect some drilling induced damage, leading to the thinning or even disconnecting of some areas.

The penetrability of the contrasting fluid is a factor that is inseparable of the application of x-radiography to composite materials. The variability of the drilling induced damage in shape, in size and in depth, causes differences in the penetration of the diiodomethane thus affecting the radiographic process with obvious consequences. This indicates that the threshold value should be a consequence of the properties of the radiography of each drilled hole and not a constant predetermined value.

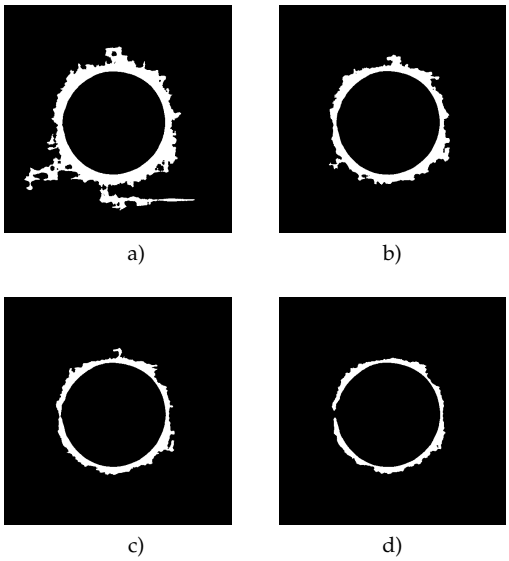

a) b)

c) d)

Figure 4.3 Manually thresholded images for the straight flute drill: a) Threshold = 30; b) Threshold = 60; c) Threshold = 90; d) Threshold = 120.

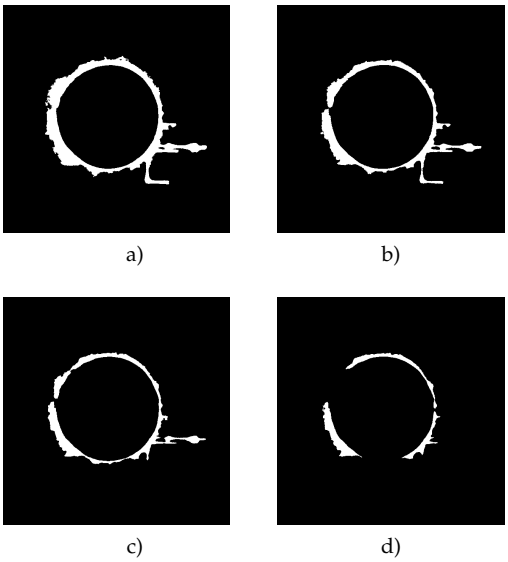

Figure 4.4 Manually thresholded images for the twist drill: a) Threshold = 30; b) Threshold = 60; c) Threshold = 90; d) Threshold = 120.

Comparison with the image subtraction results confirms that the targeted result is contained in the selected threshold interval. The 60 to 90 threshold interval seems to be the closest interval that contains all image subtraction results.

Using the output of all manual thresholds, the affected area, the delamination factor and the adjusted delamination factor were determined. The following figures contain a selection of six tests that represent the majority of the findings. The full set of results can be found in appendix A. In figures 4.5 through 4.7, the data appears connected with lines however this is merely indicative and serves no other purpose than to facilitate the comparison between tests.

The results for the affected area are depicted in figures 4.5a and 4.5b. An exponential decay of the affected area with increasing threshold level for both drills can be observed. This decay is most significant until the threshold reaches 60. Looking at the damage produced by both drill geometries, it can be seen that the spade drill geometry achieved better results with the 9 mm diameter whereas the twist drill geometry performed better with the 5 mm diameter. The fact that the spade drill performed better with a larger hole diameter was expected since it possesses a tapered leading edge in its design. The leading edge allows for a progressive removal of material until the desired full diameter is attained, therefore reducing the rate of material removal when compared to the other drilling geometries. Moreover, the damage created on drill entry is irrelevant since the damaged area caused by the first contact of the drill is chipped away. This leads to a somewhat more linear correlation between hole area and affected area for larger holes which is evidenced by the *compactness* of the tests with the spade drill when compared to the twist drill that shows a higher *dispersion* of the tests.

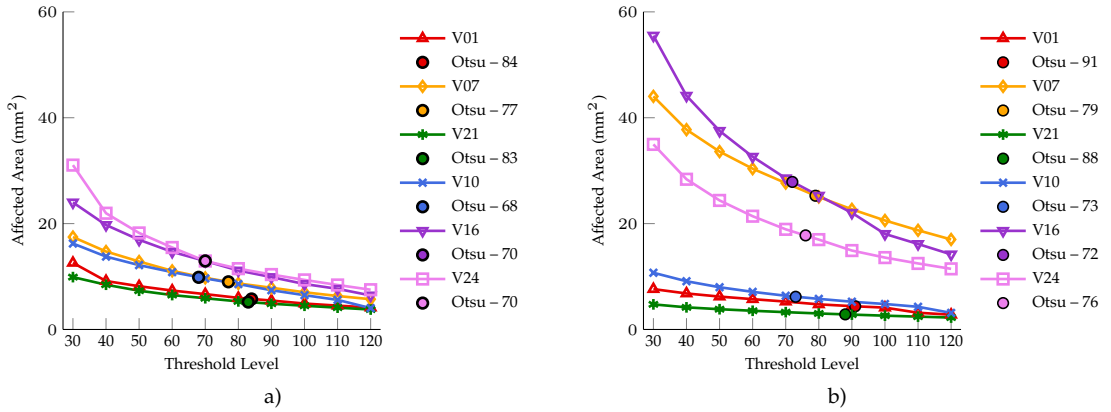

Figure 4.5 Affected Area: a) Straight flute drill; b) Twist drill.

The delamination factor as defined by Chen, shown in figure 4.6, is not influenced as much as the affected area by the increase in the threshold value. To a lower extent the delamination factor displays a similar decay. However a step-like behaviour occurred for some tests with a significant change in both delamination factors. This is a consequence of the thinning of some shapes in one direction in spite of an equiaxed contraction of the shapes' dimensions. Therefore, in some of the tests, the farthest damaged points from the theoretical drilling centre remain connected to the larger damaged areas as well as almost unchanged in size for a certain range of threshold values.

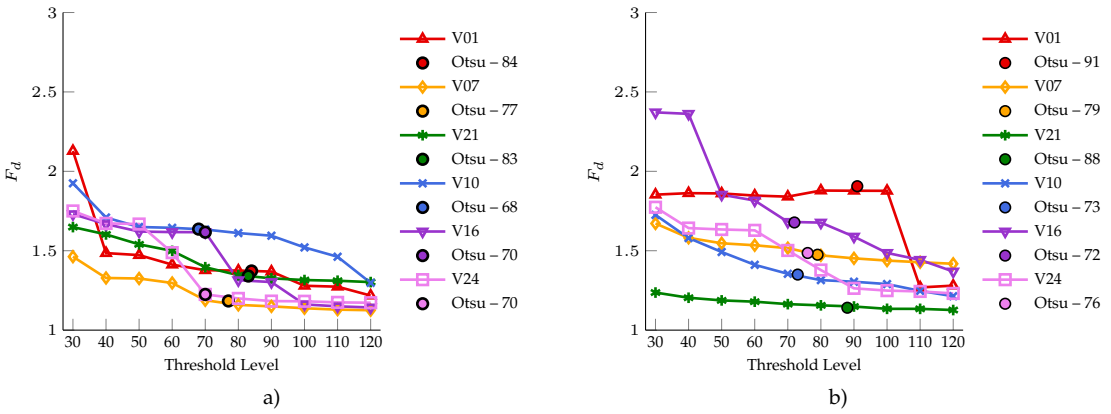

Figure 4.6 Delamination Factor: a) Straight flute drill; b) Twist drill.

The adjusted delamination factor variation with the threshold value is displayed in figure 4.7. In the same manner as the delamination factor a decrease of the adjusted delamination factor can be seen with the increase of the threshold value, although it should be noted that the threshold value has a greater impact in the adjusted delamination factor. This result was anticipated because the formulation of the adjusted delamination factor accounts directly for the affected area. The step like behaviour previously referred for the delamination factor is also clear for the adjusted delamination factor.

The lower sensitivity of Chen's delamination factor when compared to the adjusted

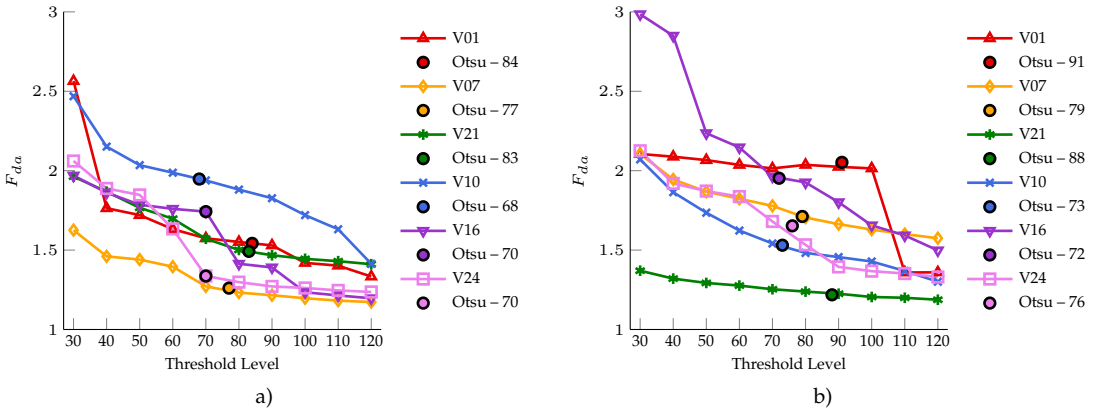

Figure 4.7 Adjusted delamination factor: a) Straight flute drill; b) Twist drill.

delamination factor is because of the diluted effect of the affected area in the formulation of the delamination factor. The affected area is contained in the maximum area (Eq. 4.1) which is represented by the maximum diameter in Chen's formula (Eq. 2.1). This equation can then be developed into equation 4.2 evidencing the presence of the square root of the maximum damaged area unlike the adjusted delamination factor which explicitly features the affected area in its formulation.

$$A_{affected} \subset A_{max} \tag{4.1}$$

$$F_d = \frac{D_{max}}{D_0} = \frac{2 \cdot \sqrt{\frac{A_{max}}{\pi}}}{D_0} \tag{4.2}$$

The automatic thresholding algorithms vary significantly in quality. The different effects of each thresholding method are displayed in figure 4.8 and 4.9 for the spade drill and the twist drill, respectively.

a) b) c)

Figure 4.8 Automatic thresholding methods for the straight flute drill: a) Otsu; b) Kapur; c) Kittler.

a) b) c)

Figure 4.9 Automatic thresholding methods for the twist drill: a) Otsu; b) Kapur; c) Kittler.

While Kapur's and Otsu's algorithms yielded similar results to the image subtraction method, Kittler's algorithm proved inadequate despite achieving the best average score in Sezgin and Sankur's [39] work. Figure 4.10 clearly marks how much Kittler's algorithm deviated from an acceptable result.

For the straight flute drill both Kapur and Otsu provided similar threshold values with even similar averages and standard deviations however, with the twist drill Kapur's method increased significantly the standard deviation although the average result remained comparable to Otsu's algorithm. Consequently Kapur's suggested thresholds for tests V01, V16 and V21 significantly deviate from the image subtraction results.

Unlike Kapur's algorithm, Otsu's method performed well for the entire test range with its output always in the 60 to 90 threshold interval as can be seen in figure 4.10. Its results are also plotted as coloured points on figures 4.5, 4.6 and 4.7 for each selected test with the exact threshold value displayed in the graph legend.

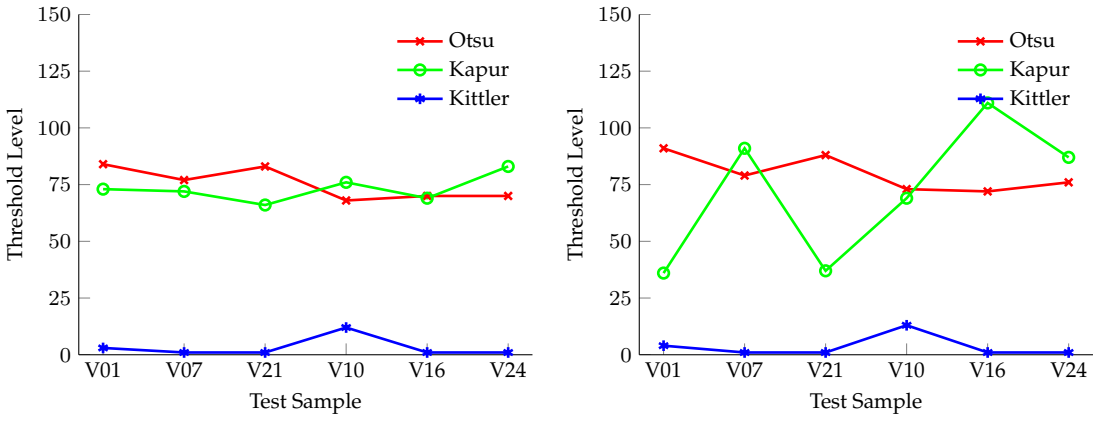

Figure 4.10 Automatic thresholding algorithms: a) Straight flute drill; b) Twist drill.

Comparing these results with the application of manual threshold values shows that the automatic algorithm often concurs with a stabilization of the variation of two consecutive manual threshold values. In figure 4.5, it is clear that the output of the algorithm coincided with a reduction in the decay rate of the exponential behaviour of the affected area. In the case where a step occurs, Otsu's result is immediately before this step (for instance, in tests V01 and V16) thus demonstrating that, for a manual threshold methodology, the threshold choice should fall in an interval where a slight variation of the threshold value does not greatly influence the end results.

4.2 Delamination Quantification

After the investigation on the image processing variables was completed, the test array was increased through the addition of the test sets using the W-shaped drill and the combination of the Twist drill and the new clamping fixture. The delamination factor was determined for every test through the application of Otsu's automatic threshold algorithm.

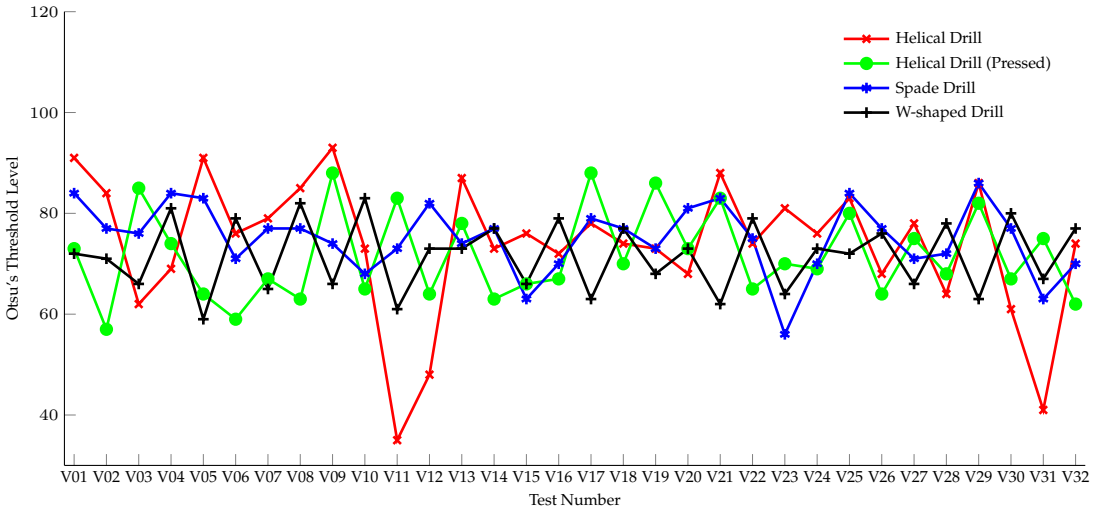

Figure 4.11 Threshold analysis

The threshold values obtained are in conformity with those acquired during the preliminary tests. The results presented in figure 4.11 show that the 60 to 90 threshold range covers the majority of the tests. Nonetheless three tests performed with the twist drill stand out, due to their exceptionally low threshold level with tests V11, V12 and V31 having thresholds below 50.

The cause of this irregularity has two motives. Firstly, the proximity of two sequential

tests where the distance between them is so small that prevents the realization of individual radiographs. Secondly, a significant variation in the drilling induced damage of both tests, consequence of the different drilling variables, in which the damage of one test surmounts the other. In turn, this leads to a different radiation absorption by the x-ray sensor in these areas. The combination of these two factors results in a considerable difference in the grey scale of the radiographies which induces a considerable difference in the white colour intensity of the two damaged areas as depicted in figures 4.12a, 4.12b and 4.12c.

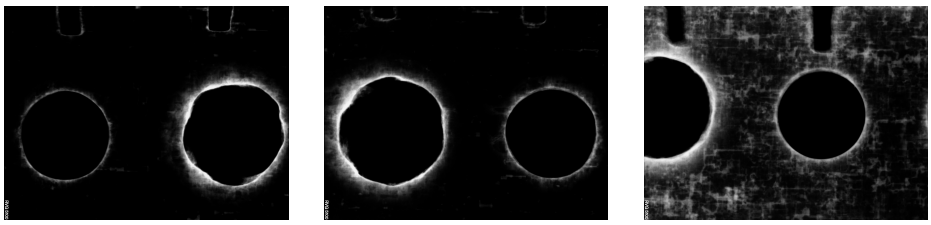

a) b) c)

Figure 4.12 Low threshold images: a) Tests V11 and V15 with the twist drill; b) Tests V27 and V31 with the twist drill; c) Tests V12 and V16 with the twist drill.

In this situation, the application of a constant threshold value would produce an incorrect result. In theory, the constant threshold value would be near the 60 to 90 range considering the minimum, maximum or average of all the samples taken. Regardless of the amount of this value, it would be significantly higher than the result of Otsu's algorithm and it would seem that an almost perfect hole with practically no trace of damage was performed as figure 4.13 illustrates.

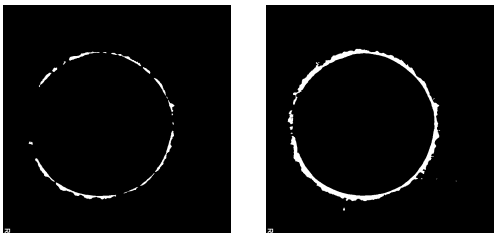

a) b)

Figure 4.13 Low threshold images: a) Constant threshold = 75; b) Otsu's threshold = 35.

Furthermore, twist drill tests V04, V12 and V28 should be discarded due to the drilling induced damage having connected with the notches for the image subtraction as this thwarts the accurate determination of what is the area affected by the drilling process. Additionally, straight flute test V02 should be neglected due to connecting with the damage of an experimental test. The discarded tests are displayed in figure 4.14.

Figures 4.15 through 4.18 show the overall damage quantification results. The effect of the drilling variables on the drilling induced damage can be found in Appendix B with the dominant drilling variables in this work being the tool diameter and the tool

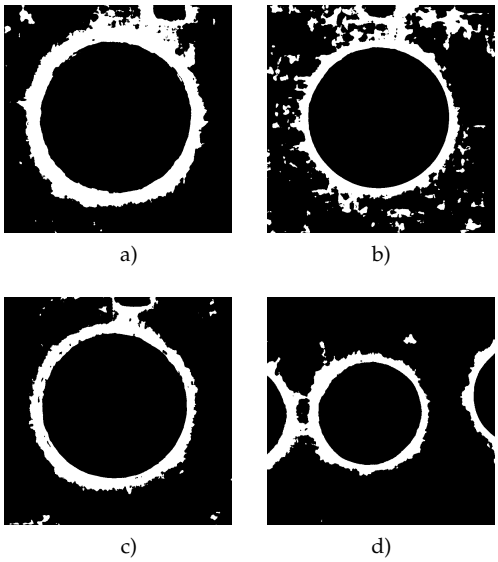

Figure 4.14 Discarded tests: a) Twist drill test V04; b) Twist drill test V12; c) Twist drill test V28; d) Straight Flute drill test V02.

geometry. To allow an easier observation, figures 4.19 through 4.22, the tests are divided according to the tool diameter. The results of the delamination factor, adjusted delamination and the minimum delamination factor, which is discussed in section 4.3, can be compared. The performance observed in the preliminary results remains valid with the twist drill overcoming all others with the 5 mm diameter (figure 4.19a) and the spade drill excelling with the 9 mm diameter (figure 4.20b). As figure 4.21 shows, the W-shaped drill proved inadequate for the cutting parameters used in this work with its best result in the proximity of $F_d = 1.5$.

The application of the compressive force on the vicinity of the hole resulted in a reduction of the damage and consequently the delamination factor as well for some of the tests. Figure 4.22b shows that especially when drilling with higher diameters the application of this methodology may prove beneficial.

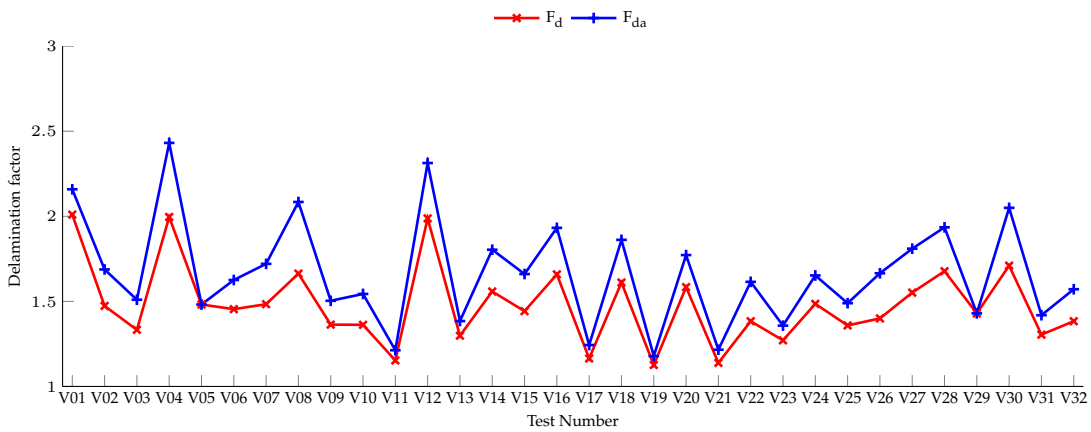

Figure 4.15 Delamination factor obtained with the twist drill

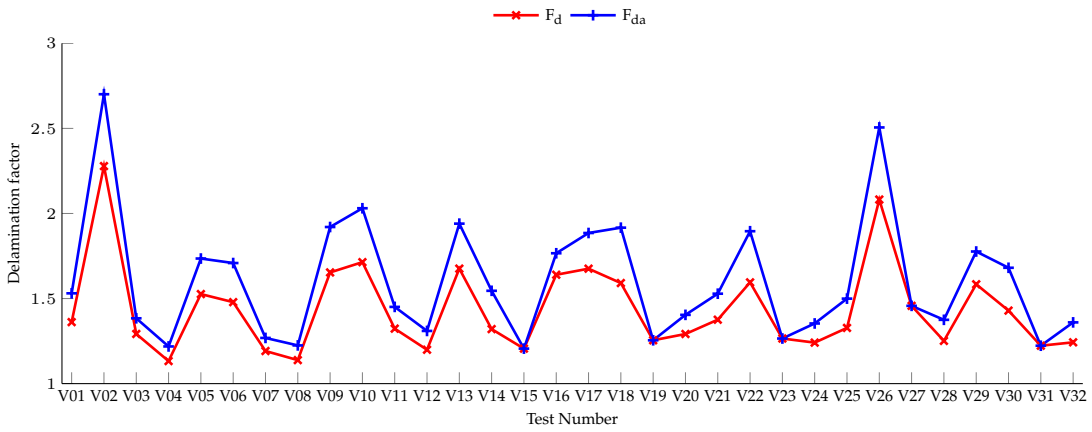

Figure 4.16 Delamination factor obtained with the straight flute drill

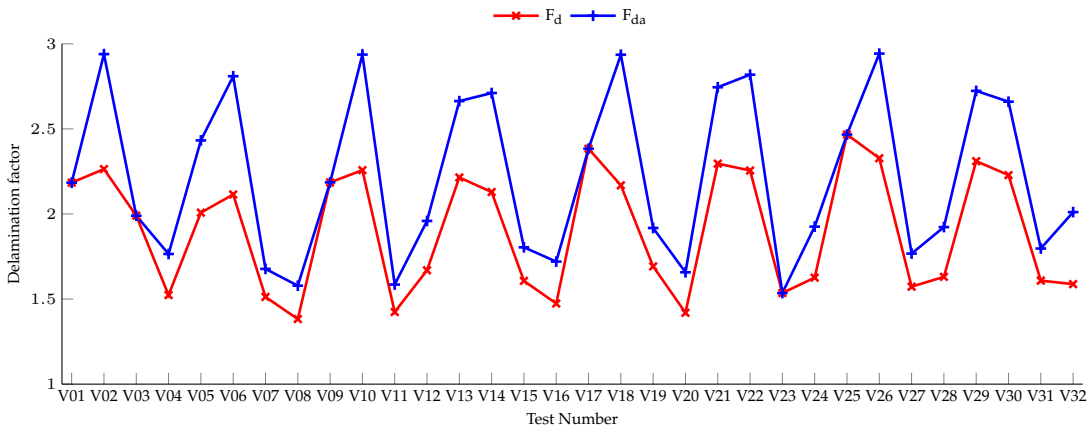

Figure 4.17 Delamination factor obtained with the W-shaped drill

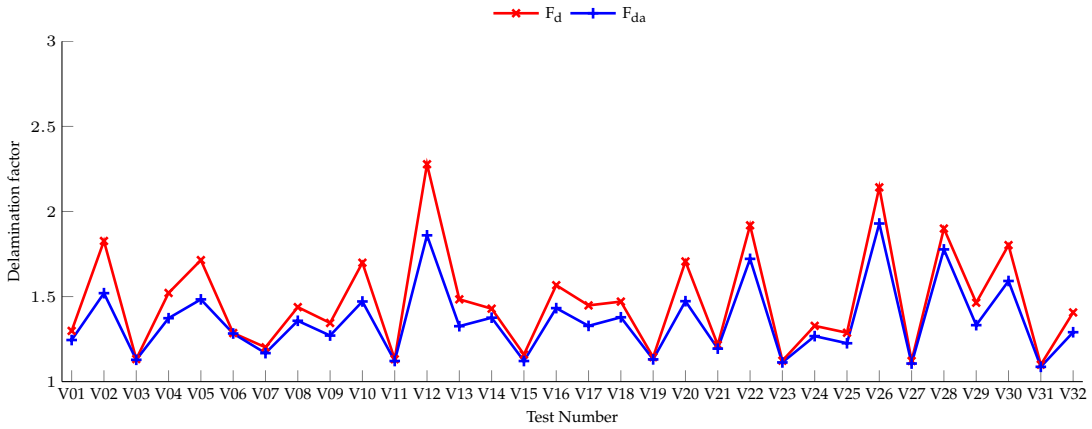

Figure 4.18 Delamination factor obtained with the twist drill pressed setup

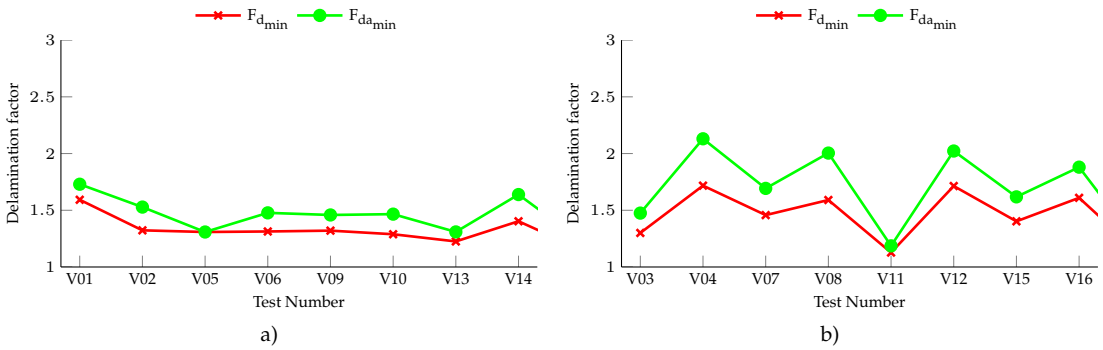

Figure 4.19 Effect of tool diameter on twist drilled tests: a) 5 mm; b) 9 mm.

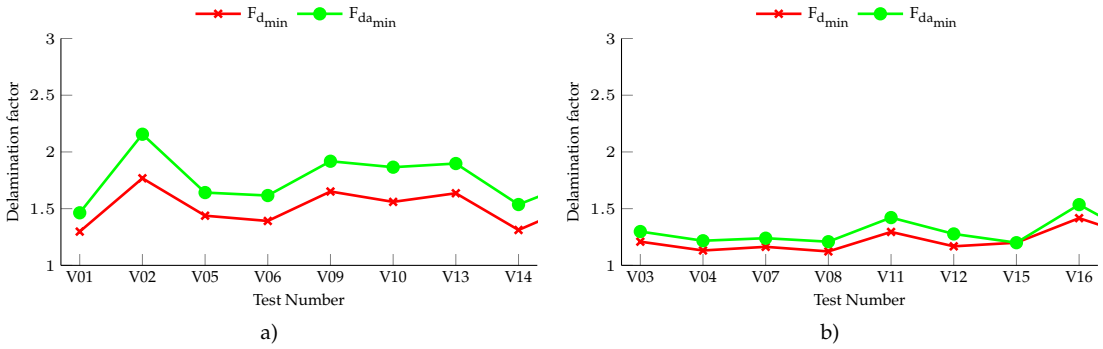

Figure 4.20 Effect of tool diameter on straight flute drilled tests: a) 5 mm; b) 9 mm.

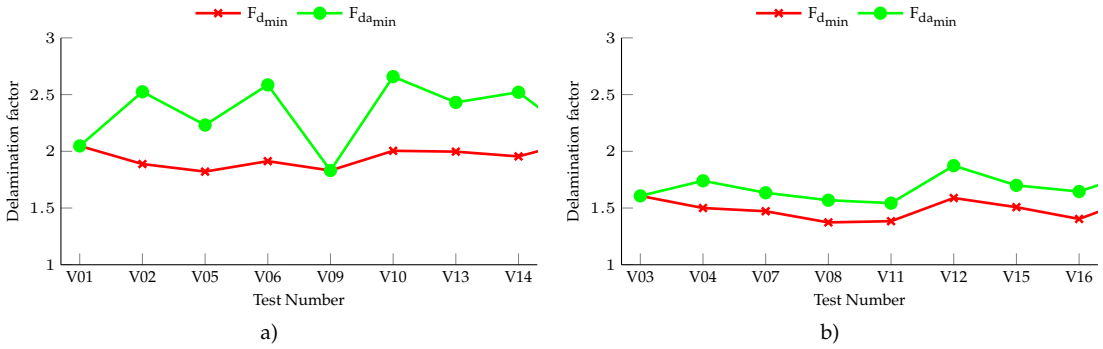

Figure 4.21 Effect of tool diameter on W-shaped drilled tests: a) 5 mm; b) 9 mm.

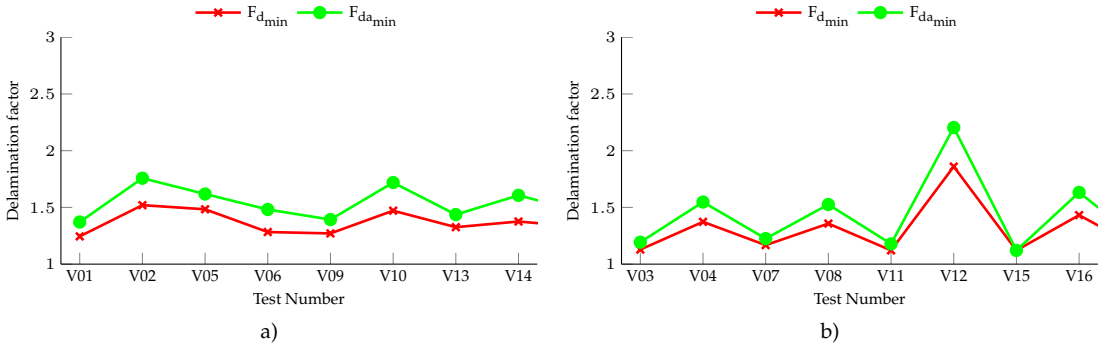

Figure 4.22 Effect of tool diameter on twist drilled pressed tests: a) 5 mm; b) 9 mm.

4.3 Delamination Factor Study

The process of determining the delamination factors raised some questions about its concept. Chen's interpretation of the delamination factor consists in characterizing the irregularly shaped drilling induced damage that surrounds the drilled hole through a dimensionless quantity based on the minimum circle that, while concentric with the drilled hole, circumscribes the affected area. Through this, investigations on the drilling parameters that influenced the mentioned area can be developed thus setting a path to improve the drilling methodologies. As the state of the art points out, several researchers found the results of Chen's formula inadequate because, as Davim, Rubio, and Abrão conjecture, when the damage presents itself as an irregular form containing several breaks and cracks, the quantization through the size of the defect does not correctly depict the magnitude of the damage.

This uneasiness led to several other delamination quantization formulas to be developed. From these, only Davim's formula attained some consensus since it performed well in the extreme cases where Chen's F_d underperformed. Davim, Rubio, and Abrão [33] wanted not only that the adjusted delamination factor performed as well as Chen's delamination factor when the damaged area approached a regular crown like shape but also that it performed better than Chen's when the damaged area became irregular. This was attempted by incorporating the damaged areas in the formulation of the adjusted delamination factor (Equation 2.6). However figures 4.15 through 4.18 suggest that no approximation occurs between both delamination factors when crown like damage is found, so the problem the adjusted delamination factor tried to solve remains open to question.

In this work a novel approach to quantify the drilling induced damage, the minimum delamination factor ($F_{d_{min}}$) is proposed. At the origin of the delamination factor is the need to easily compare the resulting damage between different drilling methodologies. Therefore, if the goal is to evaluate the damage quantity, the damaged shape becomes irrelevant. In other words, the focus of the delamination quantization should be in assessing the smallest area that contains all of the damage that resulted from the drilling process.

This concept is very similar to the one devised by Chen however, as the emphasis is now on minimizing the calculated factor, the concentricity between the drilled hole and the damage enclosing area is eliminated and the enclosing area's centre should coincide with the affected area's centre. From here the $F_{d_{min}}$ can be calculated with Chen's formula as a weighing between the diameter of the minimum enclosing area (D_{min}) and the pretended drill area (D_0):

$$F_{d_{min}} = \frac{D_{min}}{D_0} \tag{4.3}$$

The formulation of the $F_{d_{min}}$ lays out the concept of minimal drilling induced damage and allows a better comparison between different drilling methodologies. Its results do not deviate from Chen's when the damage is a regular crown as the centre of the crown will be very close to the drilling centre and it will improve upon Chen's results for irregular areas.

A comparison between the delamination factor and the minimum delamination factor is introduced in figures 4.23 through 4.33. For each drill a set of three representative tests of the shapes that the delamination factor has the most problems is displayed as well as a plot with a direct comparison between both factors where the variation is calculated through equation 4.4. The same comparison is performed for the adjusted delamination factor and the minimum adjusted delamination factor using equation 4.5

$$Variation = \frac{F_{d_{min}} - F_{d_{Chen}}}{F_{d_{Chen}}} \times 100(\%) \tag{4.4}$$

$$Variation = \frac{F_{da_{min}} - F_{da_{Davim}}}{F_{da_{Davim}}} \times 100(\%) \tag{4.5}$$

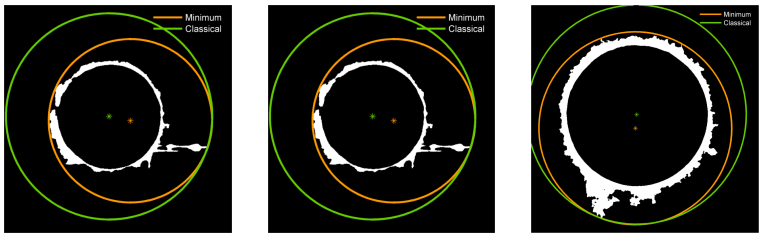

Figure 4.23 Comparison of $F_{d_{min}}$ with $F_{d_{Chen}}$ for the twist drill

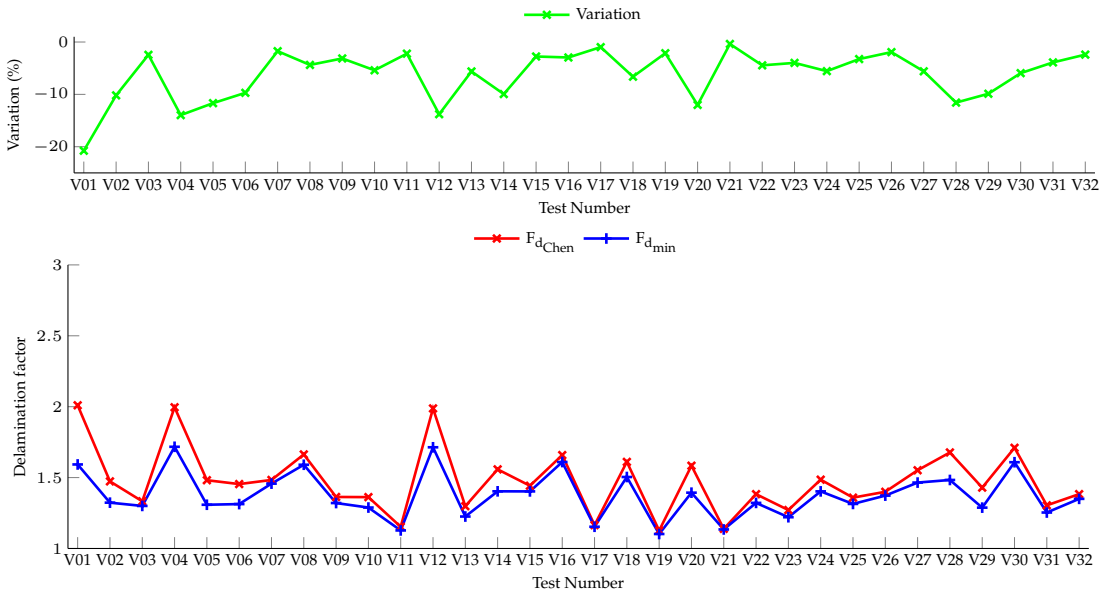

Figure 4.24 Delamination factors plot comparison for twist drill tests

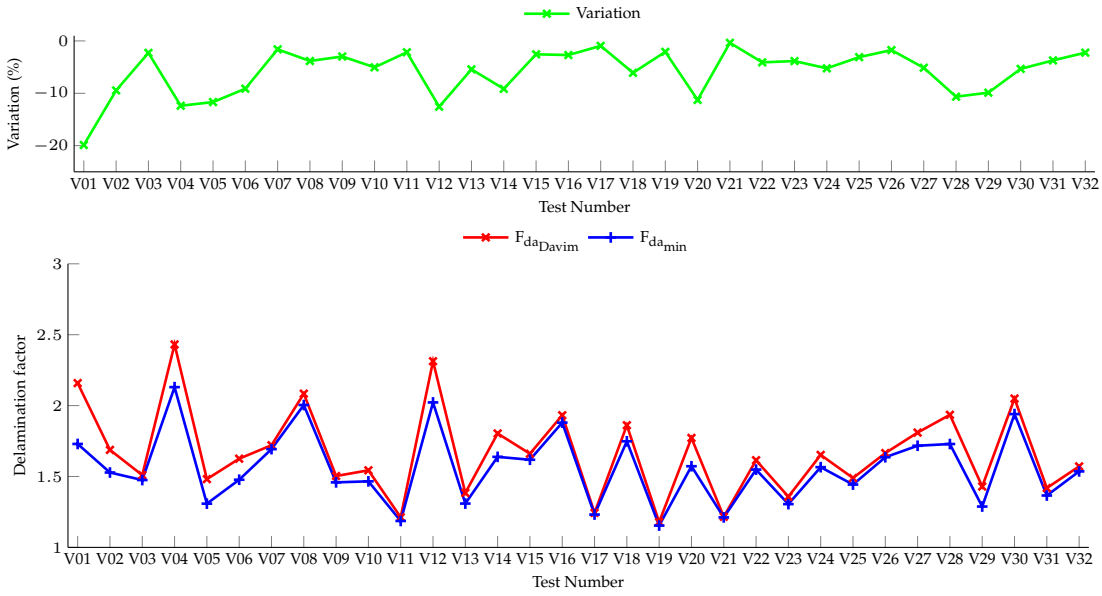

Figure 4.25 Adjusted delamination factors plot comparison for twist drill tests

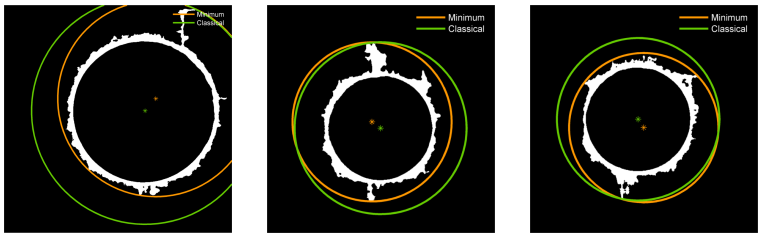

a) b) c)

Figure 4.26 Comparison of $F_{d_{min}}$ with $F_{d_{Chen}}$ for the straight flute drill

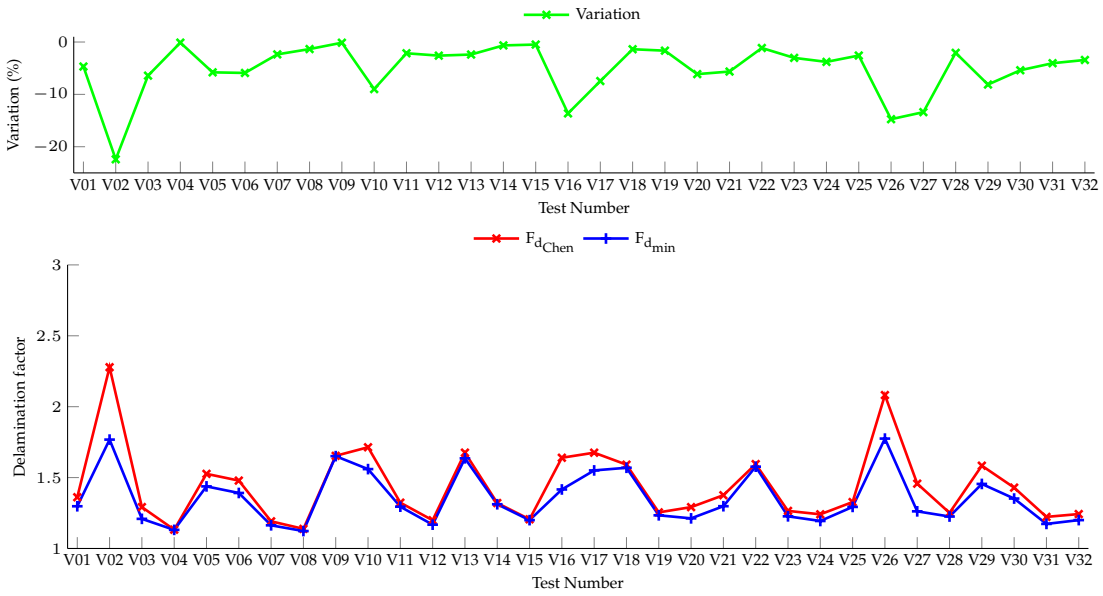

Figure 4.27 Delamination factors plot comparison for straight flute drill tests

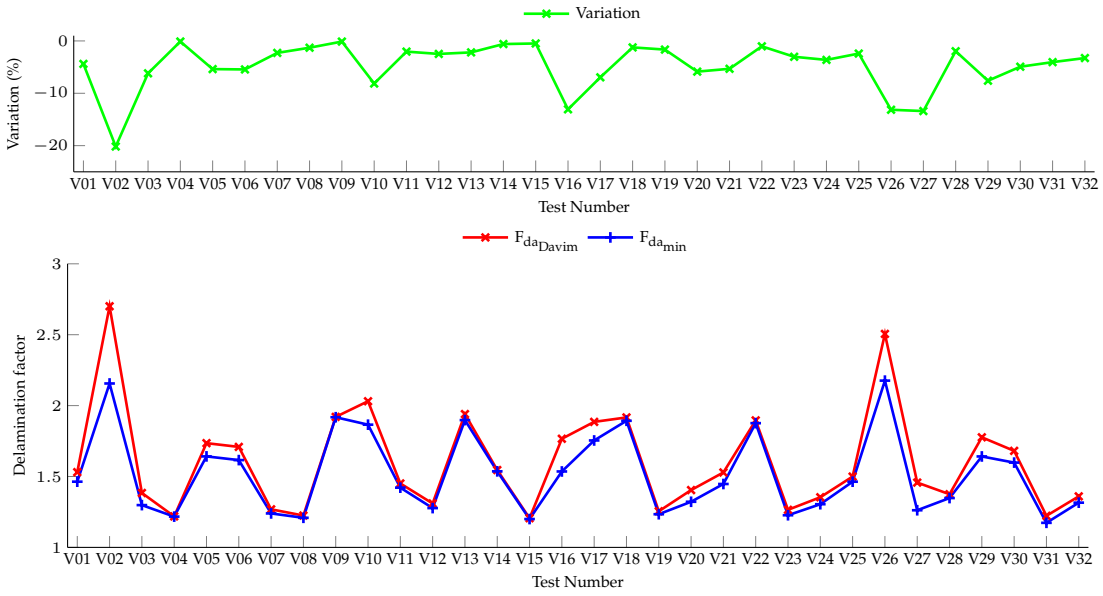

Figure 4.28 Adjusted delamination factors plot comparison for straight flute drill tests

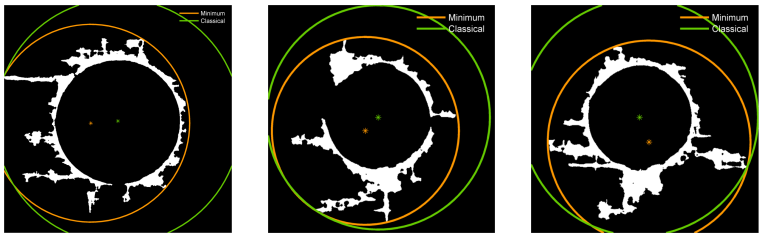

Figure 4.29 Comparison of $F_{d_{min}}$ with $F_{d_{Chen}}$ for the W-shaped drill

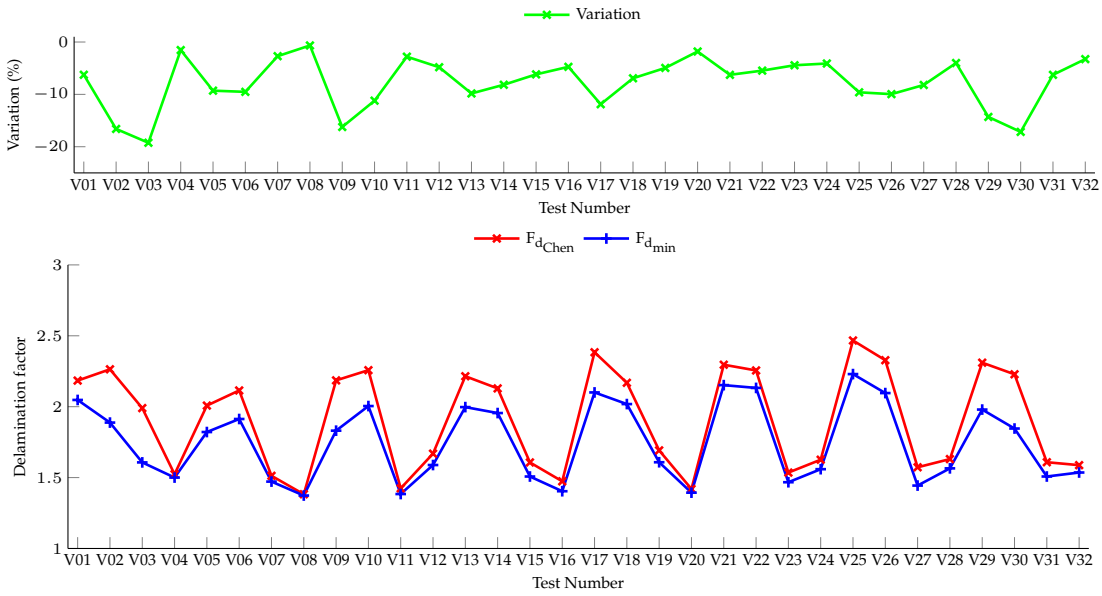

Figure 4.30 Delamination factors plot comparison for W-shaped drill tests

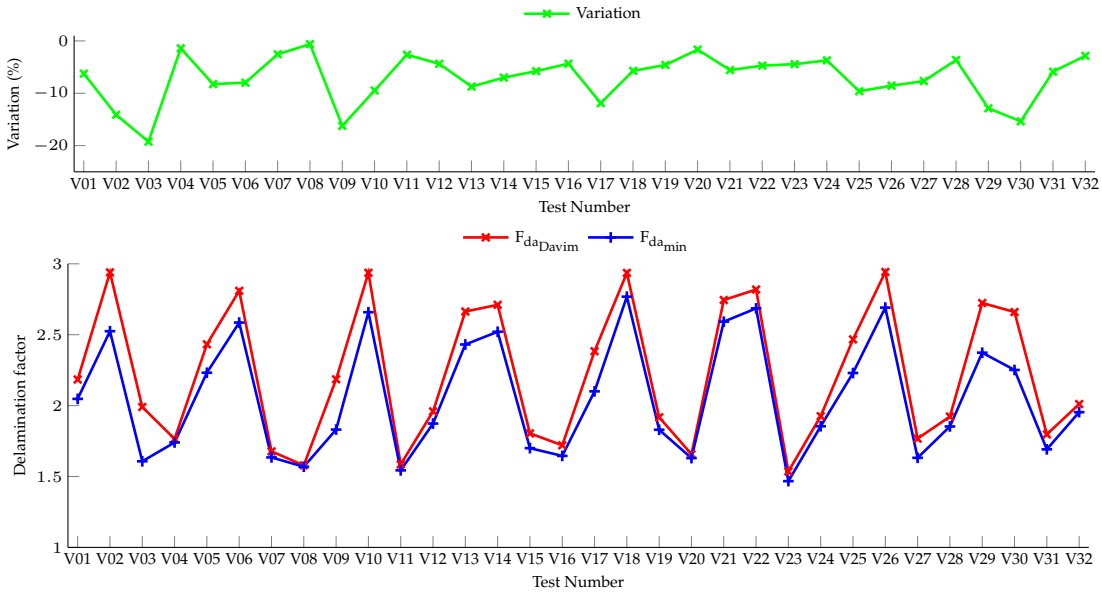

Figure 4.31 Adjusted delamination factors plot comparison for W-drill tests

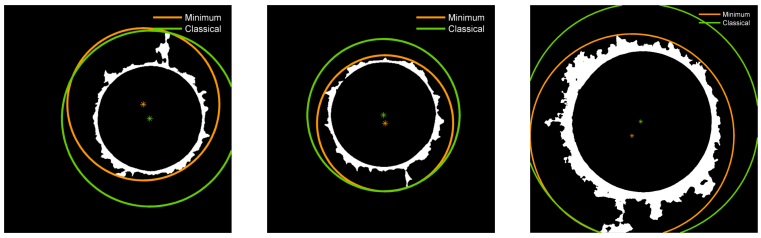

Figure 4.32 Comparison of $F_{d_{min}}$ with $F_{d_{Chen}}$ for the twist drill (pressed)

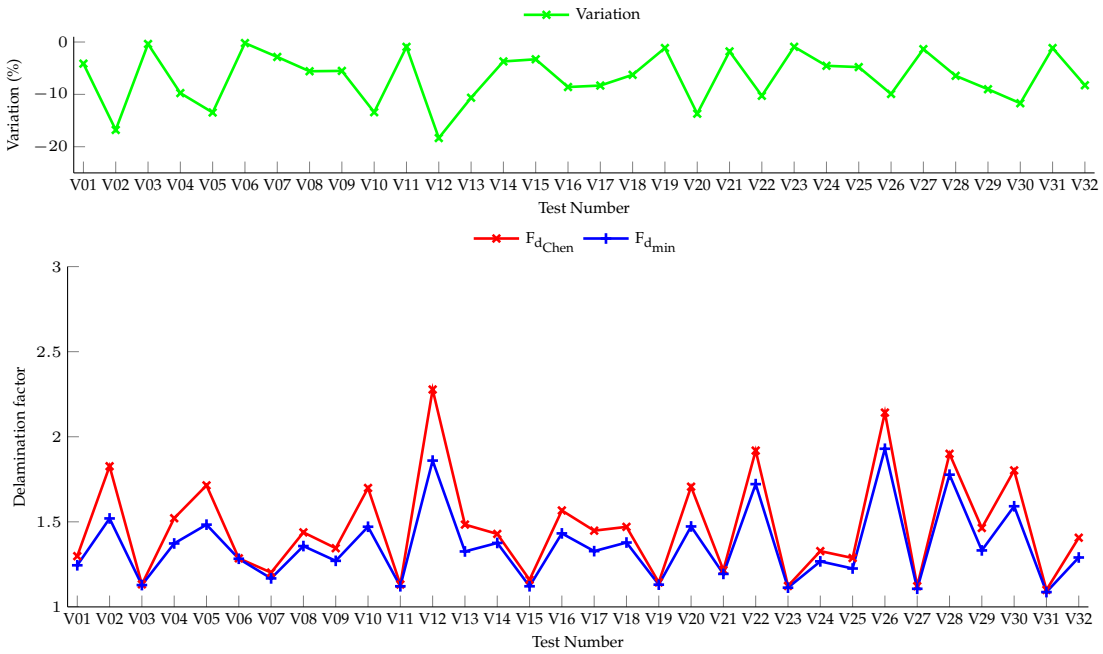

Figure 4.33 Delamination factors plot comparison for twist drill pressed tests

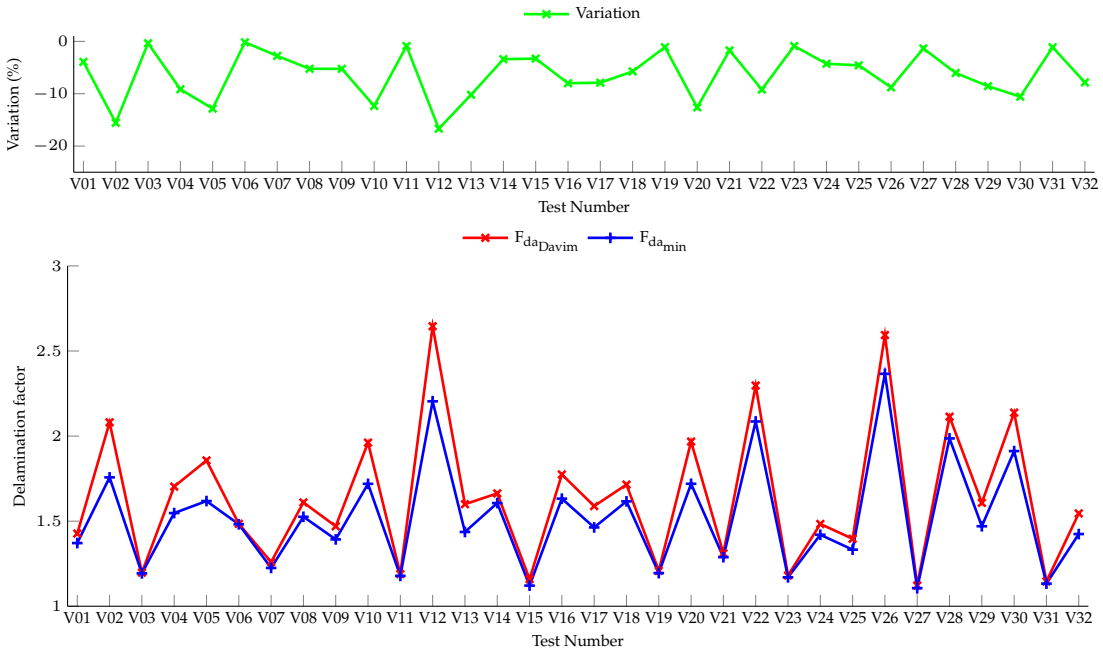

Figure 4.34 Adjusted delamination factors plot comparison for twist drill pressed tests

As expected, the performance of the minimum delamination factor improved the results of the delamination factor but, unlike the adjusted delamination factor, an agreement exists between the compared factors when the damage resembles a crown shape. The relation between the affected area amount and the quantified damaged area is improved with the minimum delamination factor since the circle that encloses the damaged area is smaller thus referring to the fact that less undamaged area is accounted for in this methodology.

5

Conclusions and Future Work

5.1 Conclusions

Image processing analysis was conducted on drilled CFRP samples. The aim was to establish the need to account for and further investigate the image processing variables.

Both automatic and manual thresholds proved to be functional in the analysis of this type of radiographic images.

- The radiographic image acquisition can be performed using a set of parameters that is not dependent on the operator. The use of a contrast agent is however indispensable.
- The delamination factor as well as the adjusted delamination factor were found to be influenced by the threshold value. An increase in the threshold value caused an exponential decay in both factors.
- The image subtraction methodology validated the thresholds applied to all the tests. The adopted strategy of indenting the samples proved inadequate and the development of a different approach could make this method a valid alternative to the threshold application.
- The application of manual thresholds allowed the investigation of its influence and constitutes a good experimental tool of analysis. However, a constant threshold value cannot be defined as a standard due to the dependence on the sensor's covered area and the linearization of the farthest points.
- Otsu's and Kapur's methods were found adequate providing correct identification of the damaged areas. On the other hand, Kittler's method was unable to provide

quality results despite being highly regarded by Sezgin and Sankur. These results are in accordance with those obtained with the image subtraction methodology.

- The influence of the image processing and, in specific, the threshold value on the delamination assessment evidences the need to standardize the image processing methodologies so that different drilling results can be comparable.

Therefore it can be concluded that errors can be made when comparing differently thresholded images and thus no proved methodology exists that allows an effective comparison of the drilling induced damage.

Nonetheless, the comparison of drilling induced samples is not influenced solely by the radiographic and image processing stage. A study into the formulation of the delamination factor was realised with a new method of mathematically expressing the drilling induced damage being proposed. The intent was to limit the analysis of the damage to the actual extent of the damage rather than the difference between the extent and the drilling centre as used by Chen and Davim, Rubio, and Abrão.

The minimal delamination factor in combination with the digital image processing proved to be successful in describing the drilling induced damage.

- In a similar manner to the delamination factor and adjusted delamination factor, also the minimal delamination factor is strongly influenced by the threshold value.
- For crown like damage shapes the agreement between the delamination factor and the minimal delamination factor is very satisfactory.
- For irregular damage shapes the minimal delamination factor is capable of establishing an approximation to the smallest possible enclosing area, thus reducing the delamination factor when compared to other methods.
- The area of the damage enclosing circle with the minimum delamination factor is closer to the affected area than any other delamination factor.
- The use of automatic algorithms, as the one presented, allows to somehow diminish the sensitivity of the operator with clear gains in terms of the comparability of the results.

5.2 Future Work

The radiographic process can be subjected to some improvements. A comparison between the radiographic imaging and other capable NDT methods is needed for the verification of the performance, for instance as a function of the thickness of the materials. The penetrability of the contrast agent should be investigated.

In terms of image processing, more robust and mathematically efficient methods should be pursued. Not only automatic registration algorithms can be devised for implementation of the image subtraction methodology but also in regard to the process of

filtering what constitutes drilling induced damage. The estimation of the centre of the affected area should also be investigated in order to improve the convergence of the algorithm and its accuracy.

More importantly, in order to allow a correct comparison of different techniques, the development of standards on the image processing methodologies and the discussion of what an acceptable damage should be as a function of the drill diameter as well as the application of the composite part should constitute the focus for the upcoming works in this area.

Bibliography

[1] R. W. Messler, "Joining Composite Materials and Structures", in *Joining of Materials and Structures*, Elsevier Butterworth-Heinemann, 2004, ch. 14, pp. 647–696.

[2] C. M. M. Machado, "Empirical Models for Quantification of Machining Damage in Composite Materials", PhD thesis, Universidade Nova de Lisboa, 2012, p. 179.

[3] Airbus. (2012). A350 XWB - Airframe composition, [Online]. Available: `http://www.a350xwb.com/\#sensational/shape/` (visited on Dec. 10, 2012).

[4] Boeing. (2012). 787 Dreamliner: Fuselage Construction, [Online]. Available: `http://www.newairplane.com/787/design\_highlights/\#/visionary-design/composites/one-piece-barrel-construction` (visited on Dec. 10, 2012).

[5] Boeing. (2012). 787 Dreamliner: Structural Materials Distribution, [Online]. Available: `http://www.newairplane.com/787/design\_highlights/\#/visionary-design/composites/advanced-composite-use` (visited on Dec. 10, 2012).

[6] W.-C. Chen, "Some experimental investigations in the drilling of carbon fiber reinforced plastic (CFRP) composite laminates", *International Journal of Machine Tools and Manufacture*, vol. 37, no. 8, pp. 1097–1108, 1997.

[7] S. Rawat and H. Attia, "Wear mechanisms and tool life management of WC–Co drills during dry high speed drilling of woven carbon fibre composites", *Wear*, vol. 267, no. 5-8, pp. 1022–1030, Jun. 2009.

[8] R. Teti, "Machining of Composite Materials", *CIRP Annals - Manufacturing Technology*, vol. 51, no. 2, pp. 611–634, Jan. 2002.

[9] H. Hocheng and C. C. Tsao, "Comprehensive analysis of delamination in drilling of composite materials with various drill bits", *Journal of Materials Processing Technology*, vol. 140, no. 1-3, pp. 335–339, Sep. 2003.

[10] R. Krishnamurthy, J. Ramkumar, S. Aravindan, *et al.*, "An enhancement of the machining performance of GFRP by oscillatory assisted drilling", *The International Journal of Advanced Manufacturing Technology*, vol. 23, no. 3-4, pp. 240–244, Feb. 2004.

[11] M. Fernandes and C. Cook, "Drilling of carbon composites using a one shot drill bit. Part I: Five stage representation of drilling and factors affecting maximum force and torque", *International Journal of Machine Tools and Manufacture*, vol. 46, no. 1, pp. 70–75, Jan. 2006.

[12] L. M. P. Durão, D. J. S. Gonçalves, J. a. M. R. S. Tavares, *et al.*, "Drilling tool geometry evaluation for reinforced composite laminates", *Composite Structures*, vol. 92, no. 7, pp. 1545–1550, Jun. 2010.

[13] C. C. Tsao and H. Hocheng, "Parametric study on thrust force of core drill", *Journal of Materials Processing Technology*, vol. 192-193, pp. 37–40, Oct. 2007.

[14] C. C. Tsao, "Experimental study of drilling composite materials with step-core drill", *Materials and Design*, vol. 29, no. 9, pp. 1740–1744, Oct. 2008.

[15] H. Hocheng and C. C. Tsao, "The path towards delamination-free drilling of composite materials", *Journal of Materials Processing Technology*, vol. 167, no. 2-3, pp. 251–264, Aug. 2005.

[16] C. C. Tsao, "The effect of pilot hole on delamination when core drill drilling composite materials", *International Journal of Machine Tools and Manufacture*, vol. 46, no. 12-13, pp. 1653–1661, Oct. 2006.

[17] E. Capello, "Workpiece damping and its effect on delamination damage in drilling thin composite laminates", *Journal of Materials Processing Technology*, vol. 148, no. 2, pp. 186–195, May 2004.

[18] V. Schulze, C. Becke, K. Weidenmann, *et al.*, "Machining strategies for hole making in composites with minimal workpiece damage by directing the process forces inwards", *Journal of Materials Processing Technology*, vol. 211, no. 3, pp. 329–338, Mar. 2011.

[19] E. Capello, A. Langella, L. Nele, *et al.*, "Drilling Polymeric Matrix Composites", in *Machining*, J. P. Davim, Ed., Springer London, 2008, pp. 167–194.

[20] H. Ho-Cheng and C. K. H. Dharan, "Delamination During Drilling in Composite Laminates", *Journal of Engineering for Industry*, vol. 112, no. 3, p. 236, 1990.

[21] J. P. Davim and P. Reis, "Drilling carbon fiber reinforced plastics manufactured by autoclave—experimental and statistical study", *Materials and Design*, vol. 24, no. 5, pp. 315–324, Aug. 2003.

[22] N. Avdelidis, D. Almond, a. Dobbinson, *et al.*, "Aircraft composites assessment by means of transient thermal NDT", *Progress in Aerospace Sciences*, vol. 40, no. 3, pp. 143–162, Apr. 2004.

[23] C. C. Tsao and H. Hocheng, "Taguchi analysis of delamination associated with various drill bits in drilling of composite material", *International Journal of Machine Tools and Manufacture*, vol. 44, no. 10, pp. 1085–1090, Aug. 2004.

[24] Z. Hamdoun, L. Guillaumat, and J. Lataillade, "Influence of the drilling quality on the fatigue compression behaviour of carbon epoxy laminates", *International Journal of Fatigue*, vol. 28, no. 1, pp. 1–8, Jan. 2006.

[25] J. Campos Rubio, A. M. Abrão, P. Faria, *et al.*, "Effects of high speed in the drilling of glass fibre reinforced plastic: Evaluation of the delamination factor", *International Journal of Machine Tools and Manufacture*, vol. 48, no. 6, pp. 715–720, May 2008.

[26] S. Rawat and H. Attia, "Characterization of the dry high speed drilling process of woven composites using Machinability Maps approach", *CIRP Annals - Manufacturing Technology*, vol. 58, no. 1, pp. 105–108, Jan. 2009.

[27] A. Faraz, D. Biermann, and K. Weinert, "Cutting edge rounding: An innovative tool wear criterion in drilling CFRP composite laminates", *International Journal of Machine Tools and Manufacture*, vol. 49, no. 15, pp. 1185–1196, Dec. 2009.

[28] A. Torres Marques, L. M. P. Durão, A. G. Magalhães, *et al.*, "Delamination analysis of carbon fibre reinforced laminates: Evaluation of a special step drill", *Composites Science and Technology*, vol. 69, no. 14, pp. 2376–2382, Nov. 2009.

[29] I. Shyha, D. Aspinwall, S. Soo, *et al.*, "Drill geometry and operating effects when cutting small diameter holes in CFRP", *International Journal of Machine Tools and Manufacture*, vol. 49, no. 12-13, pp. 1008–1014, Oct. 2009.

[30] P Curnick, "An investigation into the drilling of fibre-reinforced polymer composites using the optical microscopy inspection method", *Insight - Non-Destructive Testing and Condition Monitoring*, vol. 53, no. 5, pp. 248–252, May 2011.

[31] C. C. Tsao and Y. C. Chiu, "Evaluation of drilling parameters on thrust force in drilling carbon fiber reinforced plastic (CFRP) composite laminates using compound core-special drills", *International Journal of Machine Tools and Manufacture*, vol. 51, no. 9, pp. 740–744, Sep. 2011.

[32] L. M. P. Durão, J. a. M. R. S. Tavares, V. H. C. de Albuquerque, *et al.*, "Damage evaluation of drilled carbon/epoxy laminates based on area assessment methods", *Composite Structures*, vol. 96, pp. 576–583, Feb. 2013.

[33] J. P. Davim, J. C. Rubio, and A. M. Abrão, "A novel approach based on digital image analysis to evaluate the delamination factor after drilling composite laminates", *Composites Science and Technology*, vol. 67, no. 9, pp. 1939–1945, Jul. 2007.

[34] A. Handbook, "Nondestructive evaluation and quality control - Volume 17", *ASM International, Metals Park, OH*, 1989.

[35] netcomposites. (2013). Interactive Knowledge Base on NDE of Composites, [Online]. Available: http://www.netcomposites.com/ikb/browse/default.asp?ST=1\&SC=1\&S=13 (visited on Jan. 21, 2013).

[36] A. Berthel, T. Bonin, S. Cadilhon, *et al.*, "Digital Radiography : Description and User ' s Guide 1 Introduction Seeing and measuring inside substance thanks to radiography allows to obtain basic", in *International Symposium on Digital industrial Radiology and Computed Tomography*, Lyon, 2007.

[37] E. Moreira, J. Barbosa Rabello, M. Pereira, *et al.*, "Digital Radiography using digital detector arrays fulfills critical applications for offshore pipelines", *EURASIP Journal on Advances in Signal Processing*, vol. 2010, no. 1, 2010.

[38] M. Petrou and C. Petrou, *Image Processing: The Fundamentals*, 2nd ed. Chichester, UK: John Wiley & Sons, Ltd, Apr. 2010, p. 818.

[39] M. Sezgin and B. Sankur, "Survey over image thresholding techniques and quantitative performance evaluation", *Journal of Electronic Imaging*, vol. 13, no. 1, pp. 146–165, 2004.

[40] N. Otsu, "A Threshold Selection Method from Gray-Level Histograms", *IEEE Transactions on Systems, Man, and Cybernetics*, vol. 9, no. 1, pp. 62–66, 1979.

[41] S.-L. Gao and J.-K. Kim, "Scanning acoustic microscopy as a tool for quantitative characterisation of damage in CFRPs", *Composites Science and Technology*, vol. 59, no. 3, pp. 345–354, Feb. 1999.

[42] J Kittler and J Illingworth, "Minimum error thresholding", *Pattern Recognition*, vol. 19, no. 1, pp. 41–47, Jan. 1986.

[43] J. Kapur, P. Sahoo, and A. Wong, "A new method for gray-level picture thresholding using the entropy of the histogram", *Computer Vision, Graphics, and Image Processing*, vol. 29, no. 3, pp. 273–285, Mar. 1985.

Appendix A

Test data

Table A.1 Manual threshold application – Twist drill: Delamination factor. Cutting variables after [2]

Test	Spindle Speed	Feed per tooth	Tool ϕ	Thickness	Delamination Factor F_d									
	rpm	mm/tooth	mm	mm	30	40	50	60	70	80	90	100	110	120
V01	12000	0.03250	5	4	1.853	1.863	1.861	1.847	1.841	1.879	1.878	1.877	1.269	1.280
V02	12000	0.03250	5	8	1.596	1.511	1.426	1.394	1.381	1.371	1.368	1.240	1.229	1.220
V03	12000	0.03250	9	4	1.427	1.379	1.353	1.339	1.317	1.297	1.286	1.266	1.259	1.247
V04	12000	0.03250	9	8	2.757	2.048	2.022	2.004	1.992	1.977	1.938	1.945	1.928	1.398
V05	18000	0.03250	5	4	1.706	1.704	1.693	1.681	1.454	1.432	1.432	1.421	1.414	1.410
V06	18000	0.03250	5	8	1.965	1.574	1.587	1.412	1.401	1.391	1.244	1.229	1.213	1.202
V07	18000	0.03250	9	4	1.672	1.581	1.547	1.534	1.516	1.471	1.452	1.438	1.427	1.418
V08	18000	0.03250	9	8	1.930	1.959	1.802	1.706	1.664	1.662	1.621	1.570	1.564	1.531
V09	12000	0.07750	5	4	1.553	1.504	1.491	1.461	1.354	1.354	1.348	1.348	1.343	1.341
V10	12000	0.07750	5	8	1.726	1.580	1.492	1.411	1.355	1.315	1.305	1.290	1.247	1.214
V11	12000	0.07750	9	4	1.146	1.120	1.112	1.107	1.104	1.092	2.072	2.070	2.440	0.568
V12	12000	0.07750	9	8	2.252	2.129	1.985	1.718	1.710	1.318	1.232	1.215	1.144	1.128
V13	18000	0.07750	5	4	1.385	1.359	1.346	1.340	1.330	1.317	1.310	1.301	1.285	1.278
V14	18000	0.07750	5	8	1.704	1.584	1.555	1.464	1.441	1.375	1.319	1.291	1.279	1.267
V15	18000	0.07750	9	4	1.590	1.568	1.545	1.463	1.448	1.434	1.399	1.382	1.371	1.354
V16	18000	0.07750	9	8	2.371	2.362	1.853	1.816	1.682	1.677	1.589	1.486	1.442	1.369
V17	8000	0.05500	5	4	1.462	1.225	1.209	1.172	1.159	1.150	1.143	1.141	1.137	1.138
V18	8000	0.05500	5	8	2.037	2.071	1.735	1.636	1.620	1.377	1.337	1.287	1.260	1.232
V19	8000	0.05500	9	4	1.236	1.164	1.151	1.140	1.109	1.103	1.098	1.095	1.091	1.090
V20	8000	0.05500	9	8	2.132	2.132	2.060	2.061	1.571	1.561	1.558	1.446	1.317	1.299
V21	8000	0.08875	5	4	1.237	1.204	1.187	1.179	1.164	1.156	1.149	1.134	1.134	1.127
V22	8000	0.08875	5	8	1.798	1.550	1.450	1.420	1.367	1.339	1.267	1.259	1.238	1.224
V23	8000	0.08875	9	4	1.358	1.353	1.320	1.313	1.317	1.277	1.264	1.262	1.196	1.190
V24	8000	0.08875	9	8	1.774	1.643	1.634	1.628	1.502	1.378	1.263	1.249	1.244	1.231
V25	16000	0.05500	5	4	1.666	1.521	1.466	1.439	1.411	1.391	1.311	1.256	1.274	1.268
V26	16000	0.05500	5	8	2.983	1.783	1.526	1.493	1.408	1.364	1.312	1.281	1.258	1.212
V27	16000	0.05500	9	4	1.643	1.621	1.575	1.560	1.549	1.517	1.496	1.474	1.450	1.447
V28	16000	0.05500	9	8	1.684	1.678	1.677	1.672	1.670	1.683	1.678	1.628	1.506	1.282
V29	16000	0.08875	5	4	1.469	1.465	1.463	1.458	1.456	1.436	1.426	1.420	1.295	1.261
V30	16000	0.08875	5	8	3.538	2.257	1.760	1.735	1.692	1.540	1.509	1.456	1.452	1.456
V31	16000	0.08875	9	4	1.305	1.289	1.278	1.223	1.225	1.221	1.216	1.120	1.119	1.111
V32	16000	0.08875	9	8	1.933	1.851	1.452	1.440	1.416	1.337	1.342	1.321	1.236	1.231

Table A.2 Manual threshold application – Twist drill: Adjusted delamination factor. Cutting variables after [2]

Test	Spindle Speed	Feed per tooth	Tool ϕ	Thickness	Delamination Factor F_d									
	rpm	mm/tooth	mm	mm	30	40	50	60	70	80	90	100	110	120
V01	12000	0.03250	5	4	2.105	2.088	2.067	2.037	2.014	2.037	2.024	2.014	1.359	1.360
V02	12000	0.03250	5	8	2.008	1.859	1.723	1.660	1.620	1.588	1.565	1.407	1.380	1.357
V03	12000	0.03250	9	4	1.705	1.617	1.560	1.520	1.476	1.437	1.408	1.373	1.351	1.327
V04	12000	0.03250	9	8	3.597	2.662	2.562	2.488	2.422	2.356	2.267	2.229	2.175	1.576
V05	18000	0.03250	5	4	1.885	1.865	1.841	1.817	1.569	1.531	1.524	1.506	1.494	1.485
V06	18000	0.03250	5	8	2.315	1.840	1.821	1.609	1.580	1.554	1.381	1.353	1.325	1.303
V07	18000	0.03250	9	4	2.105	1.945	1.868	1.823	1.778	1.705	1.663	1.629	1.601	1.575
V08	18000	0.03250	9	8	2.752	2.696	2.425	2.253	2.155	2.103	2.017	1.927	1.887	1.819
V09	12000	0.07750	5	4	1.824	1.735	1.698	1.647	1.517	1.506	1.490	1.482	1.469	1.459
V10	12000	0.07750	5	8	2.071	1.864	1.735	1.623	1.541	1.482	1.456	1.428	1.368	1.301
V11	12000	0.07750	9	4	1.213	1.173	1.153	1.136	1.122	1.104	2.084	2.077	2.444	0.569
V12	12000	0.07750	9	8	2.817	2.538	2.296	1.928	1.883	1.432	1.325	1.293	1.194	1.161
V13	18000	0.07750	5	4	1.534	1.491	1.463	1.446	1.428	1.408	1.394	1.374	1.352	1.329
V14	18000	0.07750	5	8	2.124	1.926	1.864	1.735	1.686	1.592	1.513	1.465	1.433	1.403
V15	18000	0.07750	9	4	1.952	1.887	1.833	1.719	1.680	1.643	1.585	1.548	1.518	1.484
V16	18000	0.07750	9	8	2.985	2.850	2.236	2.147	1.963	1.926	1.801	1.656	1.592	1.498
V17	8000	0.05500	5	4	1.622	1.349	1.319	1.270	1.244	1.227	1.214	1.206	1.195	1.184
V18	8000	0.05500	5	8	2.615	2.549	2.101	1.944	1.886	1.595	1.530	1.458	1.409	1.353
V19	8000	0.05500	9	4	1.336	1.248	1.226	1.206	1.163	1.151	1.142	1.130	1.123	1.115
V20	8000	0.05500	9	8	2.703	2.597	2.444	2.377	1.755	1.726	1.700	1.570	1.423	1.394
V21	8000	0.08875	5	4	1.370	1.320	1.293	1.276	1.253	1.239	1.225	1.205	1.200	1.187
V22	8000	0.08875	5	8	2.246	1.898	1.752	1.691	1.608	1.549	1.450	1.425	1.386	1.358
V23	8000	0.08875	9	4	1.507	1.485	1.437	1.419	1.415	1.365	1.344	1.335	1.260	1.250
V24	8000	0.08875	9	8	2.125	1.920	1.872	1.837	1.680	1.533	1.394	1.367	1.352	1.330
V25	16000	0.05500	5	4	1.914	1.733	1.654	1.605	1.562	1.527	1.432	1.344	1.353	1.344
V26	16000	0.05500	5	8	3.857	2.195	1.861	1.791	1.668	1.592	1.509	1.456	1.413	1.347
V27	16000	0.05500	9	4	2.091	2.016	1.921	1.869	1.827	1.769	1.722	1.676	1.631	1.608
V28	16000	0.05500	9	8	2.064	2.012	1.976	1.941	1.910	1.894	1.863	1.784	1.611	1.363
V29	16000	0.08875	5	4	1.652	1.625	1.605	1.587	1.574	1.539	1.504	1.498	1.361	1.311
V30	16000	0.08875	5	8	4.368	2.810	2.170	2.081	1.993	1.795	1.734	1.649	1.620	1.596
V31	16000	0.08875	9	4	1.445	1.405	1.373	1.284	1.275	1.256	1.242	1.139	1.132	1.120
V32	16000	0.08875	9	8	2.328	2.184	1.698	1.660	1.613	1.512	1.499	1.462	1.358	1.340

Table A.3 Manual threshold application – Straight flute drill: Delamination factor. Cutting variables after [2]

Test	Spindle Speed	Feed per tooth	Tool ϕ	Thickness	Delamination Factor F_d									
	rpm	mm/tooth	mm	mm	30	40	50	60	70	80	90	100	110	120
V01	12000	0.03250	5	4	2.128	1.485	1.473	1.413	1.377	1.375	1.369	1.279	1.274	1.218
V02	12000	0.03250	5	8	2.265	2.197	2.084	2.107	2.107	2.054	2.045	2.006	1.985	1.963
V03	12000	0.03250	9	4	1.349	1.322	1.314	1.306	1.289	1.205	1.184	1.180	1.151	1.149
V04	12000	0.03250	9	8	1.265	1.252	1.182	1.176	1.153	1.144	1.134	1.128	1.122	1.115
V05	18000	0.03250	5	4	1.581	1.532	1.533	1.533	1.527	1.522	1.366	1.314	1.362	1.355
V06	18000	0.03250	5	8	1.504	1.489	1.483	1.471	1.469	1.453	1.373	1.263	1.232	1.195
V07	18000	0.03250	9	4	1.463	1.328	1.325	1.297	1.188	1.159	1.150	1.138	1.129	1.125
V08	18000	0.03250	9	8	1.345	1.315	1.160	1.148	1.129	1.120	1.118	1.111	1.106	1.104
V09	12000	0.07750	5	4	1.793	1.733	1.684	1.663	1.656	1.614	1.610	1.590	1.533	1.528
V10	12000	0.07750	5	8	1.925	1.709	1.649	1.644	1.634	1.611	1.595	1.521	1.462	1.298
V11	12000	0.07750	9	4	1.419	1.413	1.393	1.325	1.320	1.311	1.259	1.216	1.217	1.211
V12	12000	0.07750	9	8	1.869	1.742	1.380	1.357	1.207	1.201	1.167	1.151	1.144	1.130
V13	18000	0.07750	5	4	1.838	1.763	1.700	1.689	1.675	1.679	1.664	1.670	1.527	1.423
V14	18000	0.07750	5	8	1.686	1.593	1.511	1.380	1.327	1.313	1.297	1.291	1.273	1.263
V15	18000	0.07750	9	4	1.459	1.404	1.404	1.278	1.185	1.178	1.172	1.165	1.158	1.152
V16	18000	0.07750	9	8	1.730	1.668	1.621	1.617	1.617	1.314	1.303	1.162	1.150	1.143
V17	8000	0.05500	5	4	1.685	1.679	1.736	1.722	1.704	1.674	1.658	1.657	1.649	1.542
V18	8000	0.05500	5	8	1.885	1.803	1.816	1.675	1.671	1.542	1.476	1.395	1.377	1.361
V19	8000	0.05500	9	4	1.365	1.373	1.368	1.329	1.317	1.309	1.302	1.159	1.157	1.113
V20	8000	0.05500	9	8	1.722	1.569	1.531	1.311	1.295	1.280	1.157	1.151	1.148	1.139
V21	8000	0.08875	5	4	1.649	1.603	1.540	1.499	1.396	1.346	1.326	1.315	1.311	1.303
V22	8000	0.08875	5	8	2.165	2.140	1.908	1.681	1.632	1.608	1.583	1.564	1.533	1.517
V23	8000	0.08875	9	4	1.263	1.256	1.243	1.212	1.209	1.206	1.140	1.136	1.132	1.129
V24	8000	0.08875	9	8	1.750	1.672	1.668	1.488	1.225	1.200	1.183	1.182	1.175	1.173
V25	16000	0.05500	5	4	1.501	1.471	1.380	1.359	1.342	1.341	1.281	1.260	1.255	1.247
V26	16000	0.05500	5	8	1.951	1.873	1.886	1.914	1.908	1.921	1.923	1.682	1.667	1.332
V27	16000	0.05500	9	4	1.460	1.399	1.366	1.329	1.325	1.258	1.255	1.246	1.245	1.174
V28	16000	0.05500	9	8	1.960	1.812	1.370	1.301	1.259	1.255	1.222	1.208	1.164	1.155
V29	16000	0.08875	5	4	1.698	1.667	1.632	1.625	1.619	1.587	1.575	1.350	1.348	1.347
V30	16000	0.08875	5	8	2.110	2.100	1.552	1.431	1.399	1.372	1.306	1.295	1.273	1.248
V31	16000	0.08875	9	4	1.313	1.269	1.193	1.180	1.177	1.147	1.140	1.136	1.136	1.691
V32	16000	0.08875	9	8	2.267	1.814	1.349	1.293	1.238	1.223	1.202	1.189	1.173	1.155

Table A.4 Manual threshold application – Straight flute drill: Adjusted delamination factor. Cutting variables after [2]

Test	Spindle Speed	Feed per tooth	Tool ϕ	Thickness	Delamination Factor F_d									
	rpm	mm/tooth	mm	mm	30	40	50	60	70	80	90	100	110	120
V01	12000	0.03250	5	4	2.564	1.764	1.720	1.632	1.574	1.551	1.530	1.419	1.402	1.333
V02	12000	0.03250	5	8	3.054	2.854	2.660	2.618	2.558	2.449	2.396	2.316	2.261	2.202
V03	12000	0.03250	9	4	1.532	1.472	1.445	1.421	1.389	1.289	1.259	1.246	1.210	1.202
V04	12000	0.03250	9	8	1.419	1.387	1.299	1.282	1.250	1.233	1.216	1.204	1.193	1.179
V05	18000	0.03250	5	4	1.931	1.836	1.811	1.788	1.760	1.736	1.549	1.480	1.518	1.497
V06	18000	0.03250	5	8	1.892	1.828	1.780	1.734	1.701	1.658	1.551	1.416	1.366	1.311
V07	18000	0.03250	9	4	1.626	1.461	1.440	1.395	1.271	1.232	1.216	1.197	1.182	1.173
V08	18000	0.03250	9	8	1.510	1.452	1.272	1.249	1.220	1.204	1.195	1.181	1.171	1.162
V09	12000	0.07750	5	4	2.298	2.163	2.038	1.977	1.938	1.859	1.833	1.790	1.704	1.681
V10	12000	0.07750	5	8	2.469	2.152	2.035	1.987	1.938	1.881	1.827	1.720	1.631	1.414
V11	12000	0.07750	9	4	1.657	1.613	1.567	1.474	1.452	1.429	1.359	1.305	1.294	1.280
V12	12000	0.07750	9	8	2.241	2.007	1.559	1.509	1.333	1.315	1.267	1.242	1.227	1.204
V13	18000	0.07750	5	4	2.321	2.184	2.064	2.003	1.953	1.925	1.880	1.860	1.678	1.554
V14	18000	0.07750	5	8	2.123	1.958	1.828	1.650	1.567	1.532	1.495	1.472	1.437	1.411
V15	18000	0.07750	9	4	1.634	1.539	1.516	1.368	1.260	1.243	1.229	1.214	1.200	1.188
V16	18000	0.07750	9	8	1.969	1.862	1.786	1.760	1.742	1.414	1.391	1.235	1.214	1.197
V17	8000	0.05500	5	4	2.059	1.995	2.012	1.971	1.931	1.882	1.849	1.830	1.809	1.685
V18	8000	0.05500	5	8	2.592	2.375	2.309	2.072	2.027	1.852	1.748	1.636	1.593	1.556
V19	8000	0.05500	9	4	1.527	1.503	1.482	1.428	1.401	1.384	1.369	1.214	1.206	1.155
V20	8000	0.05500	9	8	2.018	1.789	1.717	1.447	1.418	1.393	1.255	1.241	1.231	1.214
V21	8000	0.08875	5	4	1.963	1.868	1.766	1.698	1.571	1.501	1.468	1.445	1.430	1.411
V22	8000	0.08875	5	8	2.908	2.713	2.358	2.041	1.950	1.892	1.837	1.790	1.732	1.691
V23	8000	0.08875	9	4	1.407	1.376	1.340	1.292	1.274	1.261	1.185	1.174	1.165	1.156
V24	8000	0.08875	9	8	2.061	1.888	1.847	1.633	1.337	1.298	1.271	1.261	1.246	1.236
V25	16000	0.05500	5	4	1.828	1.743	1.618	1.573	1.536	1.520	1.442	1.406	1.384	1.366
V26	16000	0.05500	5	8	2.922	2.660	2.535	2.451	2.359	2.310	2.266	1.957	1.912	1.512
V27	16000	0.05500	9	4	1.705	1.600	1.533	1.470	1.451	1.368	1.352	1.333	1.322	1.237
V28	16000	0.05500	9	8	2.413	2.091	1.548	1.449	1.386	1.368	1.322	1.297	1.243	1.225
V29	16000	0.08875	5	4	2.040	1.973	1.909	1.879	1.851	1.792	1.760	1.507	1.492	1.480
V30	16000	0.08875	5	8	2.697	2.589	1.902	1.733	1.669	1.610	1.516	1.484	1.440	1.399
V31	16000	0.08875	9	4	1.506	1.430	1.321	1.290	1.273	1.228	1.211	1.197	1.188	1.744
V32	16000	0.08875	9	8	2.814	2.084	1.508	1.428	1.355	1.327	1.295	1.272	1.248	1.221

Table A.5 Automatic threshold application – Twist drill.

Test	**Threshold** (Otsu)	**Drill area** mm^2	**Affected Area** mm^2	F_d	$F_{d_{min}}$	**Var.** F_d	F_{da}	$F_{da_{min}}$	**Var.** F_{da}
V01	91	19.635	4.377	2.010	1.593	−20.761	2.159	1.730	−19.882
V02	84	19.635	7.066	1.473	1.323	−10.190	1.688	1.528	−9.453
V03	62	63.617	19.689	1.333	1.300	−2.445	1.510	1.475	−2.283
V04	69	63.617	41.578	1.996	1.717	−13.963	2.431	2.130	−12.383
V05	91	19.635	3.278	1.481	1.308	−11.678	1.581	1.403	−11.261
V06	76	19.635	5.678	1.454	1.313	−9.705	1.626	1.477	−9.124
V07	79	63.617	25.261	1.483	1.457	−1.748	1.720	1.693	−1.605
V08	85	63.617	42.866	1.663	1.590	−4.376	2.084	2.004	−3.833
V09	93	19.635	4.767	1.363	1.320	−3.138	1.503	1.459	−2.972
V10	73	19.635	6.179	1.362	1.289	−5.398	1.544	1.466	−5.041
V11	35	63.617	7.089	1.153	1.127	−2.224	1.213	1.186	−2.166
V12	48	63.617	31.099	1.988	1.714	−13.788	2.313	2.022	−12.564
V13	87	19.635	2.988	1.298	1.225	−5.620	1.384	1.309	−5.428
V14	73	19.635	7.916	1.558	1.403	−9.941	1.804	1.639	−9.151
V15	76	63.617	23.498	1.442	1.403	−2.766	1.661	1.618	−2.554
V16	72	63.617	27.874	1.659	1.610	−2.954	1.932	1.880	−2.696
V17	78	19.635	2.874	1.165	1.153	−0.976	1.243	1.232	−0.943
V18	74	19.635	7.981	1.611	1.504	−6.622	1.862	1.748	−6.086
V19	73	63.617	6.284	1.126	1.102	−2.139	1.179	1.154	−2.089
V20	68	63.617	19.542	1.584	1.394	−12.012	1.772	1.572	−11.269
V21	88	19.635	2.852	1.138	1.134	−0.373	1.216	1.211	−0.360
V22	74	19.635	7.838	1.383	1.321	−4.454	1.615	1.549	−4.090
V23	81	63.617	9.819	1.271	1.220	−3.986	1.357	1.305	−3.847
V24	76	63.617	17.774	1.485	1.403	−5.562	1.652	1.566	−5.234
V25	83	19.635	4.457	1.358	1.314	−3.259	1.489	1.443	−3.096
V26	68	19.635	8.928	1.400	1.373	−1.927	1.665	1.636	−1.750
V27	78	63.617	26.997	1.552	1.465	−5.598	1.810	1.717	−5.124
V28	64	63.617	26.187	1.677	1.483	−11.571	1.935	1.729	−10.650
V29	86	19.635	3.250	1.429	1.288	−9.883	1.527	1.381	−9.528
V30	61	19.635	10.568	1.710	1.608	−5.945	2.050	1.940	−5.338
V31	41	63.617	12.845	1.304	1.254	−3.895	1.419	1.366	−3.721
V32	74	63.617	20.597	1.383	1.350	−2.407	1.571	1.536	−2.242

Table A.6 Automatic threshold application – Straight flute drill.

Test	**Threshold** (Otsu)	**Drill area** mm^2	**Affected Area** mm^2	F_d	$F_{d_{min}}$	**Var.** F_d	F_{da}	$F_{da_{min}}$	**Var.** F_{da}
V01	84	19.635	5.760	1.298	1.362	−4.683	1.531	1.463	−4.391
V02	77	19.635	11.933	1.768	2.278	−22.406	2.701	2.156	−20.168
V03	76	63.617	10.377	1.209	1.292	−6.422	1.384	1.298	−6.189
V04	84	63.617	10.289	1.131	1.133	−0.119	1.218	1.217	−0.114
V05	83	19.635	6.787	1.438	1.526	−5.793	1.735	1.642	−5.382
V06	71	19.635	7.566	1.391	1.479	−5.907	1.709	1.616	−5.445
V07	77	63.617	9.003	1.163	1.192	−2.363	1.269	1.240	−2.286
V08	77	63.617	10.315	1.123	1.138	−1.345	1.225	1.209	−1.295
V09	74	19.635	8.410	1.651	1.653	−0.135	1.920	1.918	−0.123
V10	68	19.635	9.852	1.560	1.714	−8.990	2.031	1.865	−8.135
V11	73	63.617	14.267	1.295	1.323	−2.149	1.451	1.421	−2.042
V12	82	63.617	12.901	1.168	1.199	−2.601	1.310	1.277	−2.483
V13	74	19.635	8.289	1.636	1.676	−2.390	1.940	1.898	−2.188
V14	77	19.635	7.764	1.312	1.321	−0.649	1.546	1.536	−0.595
V15	63	63.617	9.664	1.200	1.206	−0.486	1.289	1.283	−0.469
V16	70	63.617	12.936	1.416	1.640	−13.635	1.766	1.535	−13.064
V17	79	19.635	6.575	1.551	1.676	−7.457	1.885	1.754	−6.953
V18	77	19.635	10.408	1.569	1.591	−1.378	1.917	1.893	−1.235
V19	73	63.617	9.089	1.234	1.255	−1.652	1.334	1.313	−1.598
V20	81	63.617	12.698	1.212	1.292	−6.132	1.404	1.322	−5.863
V21	83	19.635	5.183	1.298	1.376	−5.640	1.529	1.447	−5.322
V22	75	19.635	9.603	1.577	1.595	−1.141	1.896	1.876	−1.030
V23	56	63.617	9.978	1.227	1.265	−3.027	1.353	1.313	−2.919
V24	70	63.617	12.935	1.194	1.241	−3.794	1.354	1.305	−3.622
V25	84	19.635	5.924	1.293	1.327	−2.580	1.499	1.463	−2.413
V26	77	19.635	12.315	1.775	2.082	−14.741	2.506	2.176	−13.147
V27	71	63.617	13.866	1.262	1.457	−13.396	1.586	1.384	−12.787
V28	72	63.617	14.165	1.225	1.251	−2.068	1.375	1.348	−1.966
V29	86	19.635	6.167	1.455	1.584	−8.123	1.776	1.641	−7.601
V30	77	19.635	8.398	1.352	1.429	−5.392	1.681	1.598	−4.928
V31	63	63.617	12.479	1.173	1.223	−4.049	1.331	1.279	−3.872
V32	70	63.617	13.448	1.200	1.243	−3.430	1.360	1.315	−3.269

Table A.7 Automatic threshold application – W-shaped drill.

Test	**Threshold** (Otsu)	**Drill area** mm^2	**Affected Area** mm^2	F_d	$F_{d_{min}}$	**Var.** F_d	F_{da}	$F_{da_{min}}$	**Var.** F_{da}
V01	72	19.635	16.784	2.047	2.184	−6.256	2.770	2.622	−5.366
V02	71	19.635	19.129	1.888	2.264	−16.602	2.939	2.525	−14.107
V03	66	63.617	19.349	1.607	1.990	−19.242	2.192	1.795	−18.147
V04	81	63.617	25.425	1.500	1.524	−1.541	1.765	1.740	−1.415
V05	59	19.635	12.487	1.821	2.008	−9.293	2.432	2.232	−8.246
V06	79	19.635	20.102	1.913	2.114	−9.519	2.810	2.586	−7.973
V07	65	63.617	17.414	1.472	1.513	−2.704	1.677	1.635	−2.546
V08	82	63.617	21.492	1.373	1.382	−0.658	1.578	1.569	−0.611
V09	66	19.635	9.284	1.831	2.186	−16.228	2.510	2.137	−14.871
V10	83	19.635	19.249	2.005	2.257	−11.202	2.937	2.659	−9.473
V11	61	63.617	17.452	1.384	1.424	−2.802	1.585	1.543	−2.636
V12	73	63.617	29.524	1.589	1.669	−4.812	1.959	1.873	−4.375
V13	73	19.635	12.789	1.997	2.215	−9.824	2.663	2.431	−8.721
V14	77	19.635	16.790	1.955	2.129	−8.166	2.711	2.521	−7.006
V15	66	63.617	20.357	1.508	1.607	−6.180	1.804	1.700	−5.774
V16	79	63.617	26.315	1.404	1.474	−4.742	1.720	1.645	−4.345
V17	63	19.635	11.202	2.101	2.384	−11.881	2.786	2.487	−10.720
V18	77	19.635	22.012	2.018	2.169	−6.923	2.936	2.768	−5.713
V19	68	63.617	22.840	1.608	1.692	−4.947	1.918	1.830	−4.588
V20	73	63.617	25.803	1.394	1.419	−1.809	1.657	1.630	−1.658
V21	62	19.635	12.648	2.152	2.296	−6.269	2.745	2.592	−5.570
V22	79	19.635	15.960	2.132	2.256	−5.463	2.819	2.686	−4.720
V23	64	63.617	16.735	1.467	1.535	−4.439	1.695	1.624	−4.191
V24	73	63.617	30.792	1.559	1.626	−4.106	1.926	1.854	−3.717
V25	72	19.635	17.348	2.230	2.467	−9.608	3.096	2.840	−8.261
V26	76	19.635	17.254	2.096	2.328	−9.956	2.942	2.691	−8.548
V27	66	63.617	20.243	1.444	1.573	−8.204	1.767	1.632	−7.671
V28	78	63.617	30.008	1.565	1.631	−4.012	1.923	1.853	−3.640
V29	63	19.635	11.627	1.980	2.310	−14.312	2.724	2.373	−12.869
V30	80	19.635	12.273	1.846	2.228	−17.166	2.660	2.251	−15.360
V31	67	63.617	19.470	1.508	1.608	−6.266	1.797	1.692	−5.870
V32	77	63.617	43.887	1.536	1.588	−3.267	2.011	1.954	−2.850

Table A.8 Automatic threshold application – Twist drill pressed.

Test	**Threshold** (Otsu)	**Drill area** mm^2	**Affected Area** mm^2	F_d	$F_{d_{min}}$	**Var.** F_d	F_{da}	$F_{da_{min}}$	**Var.** F_{da}
V01	73	19.635	4.483	1.245	1.298	−4.134	1.427	1.371	−3.926
V02	57	19.635	7.727	1.520	1.827	−16.790	2.081	1.757	−15.552
V03	85	63.617	7.779	1.128	1.133	−0.372	1.198	1.193	−0.362
V04	74	63.617	19.207	1.373	1.521	−9.754	1.703	1.548	−9.150
V05	64	19.635	4.430	1.483	1.714	−13.462	1.857	1.618	−12.845
V06	59	19.635	6.941	1.283	1.286	−0.204	1.484	1.482	−0.189
V07	67	63.617	6.784	1.168	1.202	−2.851	1.260	1.225	−2.780
V08	63	63.617	18.569	1.358	1.438	−5.584	1.610	1.526	−5.241
V09	88	19.635	4.281	1.271	1.345	−5.517	1.470	1.393	−5.254
V10	65	19.635	8.189	1.471	1.699	−13.408	1.961	1.719	−12.340
V11	83	63.617	6.894	1.121	1.132	−0.923	1.189	1.179	−0.900
V12	64	63.617	33.695	1.860	2.278	−18.339	2.646	2.204	−16.680
V13	78	19.635	3.814	1.326	1.484	−10.644	1.600	1.437	−10.203
V14	63	19.635	7.818	1.376	1.429	−3.712	1.663	1.606	−3.409
V15	66	63.617	6.705	1.121	1.159	−3.296	1.216	1.177	−3.215
V16	67	63.617	21.631	1.432	1.567	−8.598	1.774	1.632	−8.005
V17	88	19.635	4.667	1.328	1.448	−8.314	1.589	1.463	−7.894
V18	70	19.635	8.064	1.378	1.470	−6.263	1.715	1.616	−5.745
V19	86	63.617	7.670	1.131	1.144	−1.144	1.208	1.195	−1.112
V20	73	63.617	26.366	1.473	1.706	−13.691	1.968	1.720	−12.608
V21	83	19.635	3.404	1.194	1.216	−1.794	1.311	1.288	−1.723
V22	65	19.635	11.306	1.722	1.919	−10.270	2.297	2.086	−9.199
V23	70	63.617	6.886	1.113	1.123	−0.914	1.180	1.170	−0.891
V24	69	63.617	17.369	1.268	1.328	−4.543	1.484	1.420	−4.276
V25	80	19.635	3.811	1.226	1.287	−4.789	1.397	1.333	−4.583
V26	64	19.635	13.012	1.929	2.142	−9.921	2.594	2.366	−8.783
V27	75	63.617	6.366	1.106	1.122	−1.358	1.175	1.159	−1.326
V28	68	63.617	20.788	1.777	1.900	−6.455	2.114	1.986	−6.037
V29	82	19.635	4.749	1.332	1.464	−9.016	1.608	1.470	−8.556
V30	67	19.635	10.239	1.592	1.802	−11.696	2.138	1.912	−10.569
V31	75	63.617	5.592	1.087	1.100	−1.152	1.146	1.133	−1.128
V32	62	63.617	15.121	1.290	1.407	−8.259	1.546	1.424	−7.841

Appendix B

Delamination results from the threshold application

B.1 Spindle Speed effect on delamination

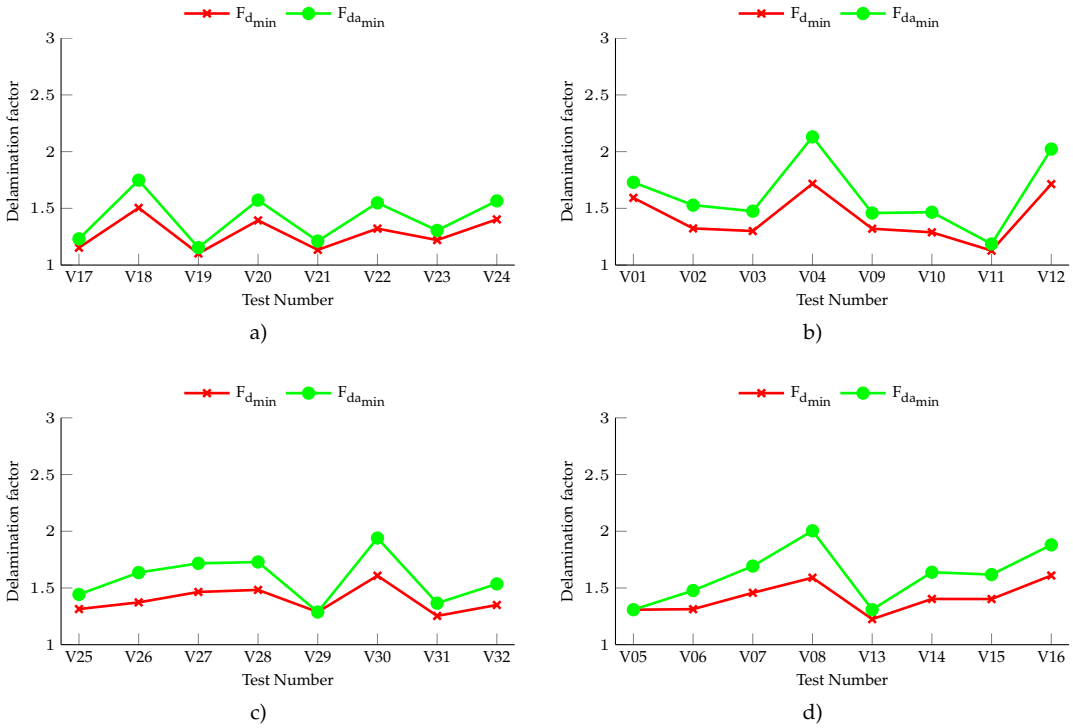

Figure B.1 Effect of spindle speed on twist drill tests: a) 8000 rpm; b) 12000 rpm; c) 16000 rpm; d) 18000 rpm.

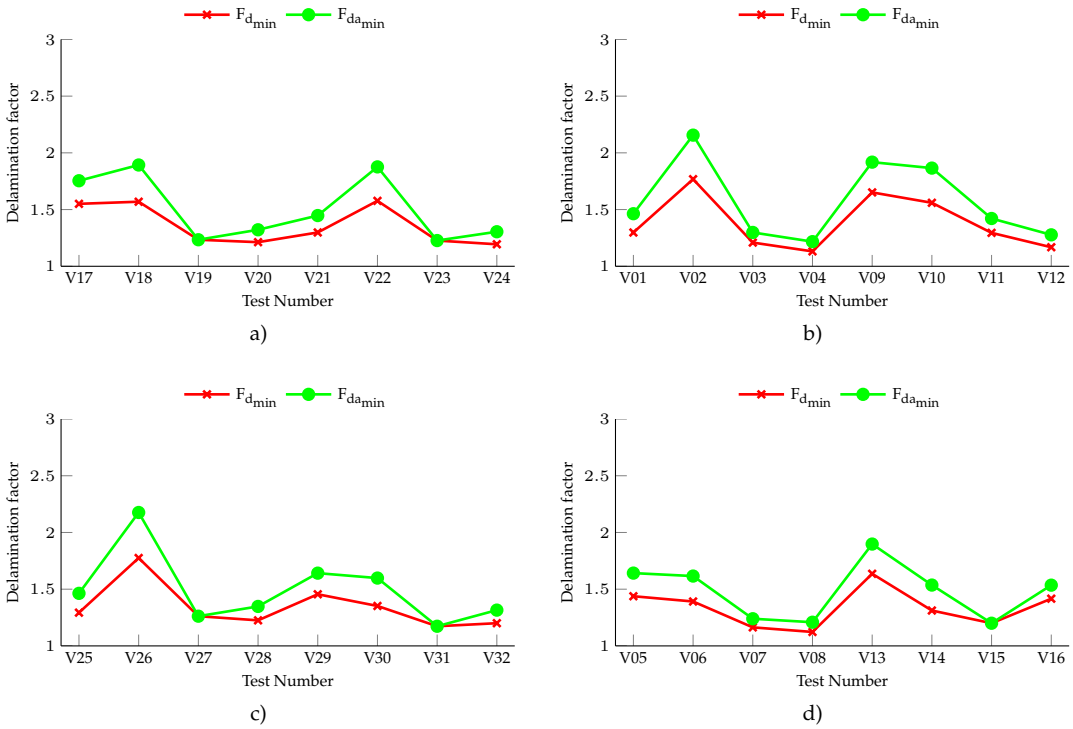

Figure B.2 Effect of spindle speed on straight flute drill tests: a) 8000 rpm; b) 12000 rpm; c) 16000 rpm; d) 18000 rpm.

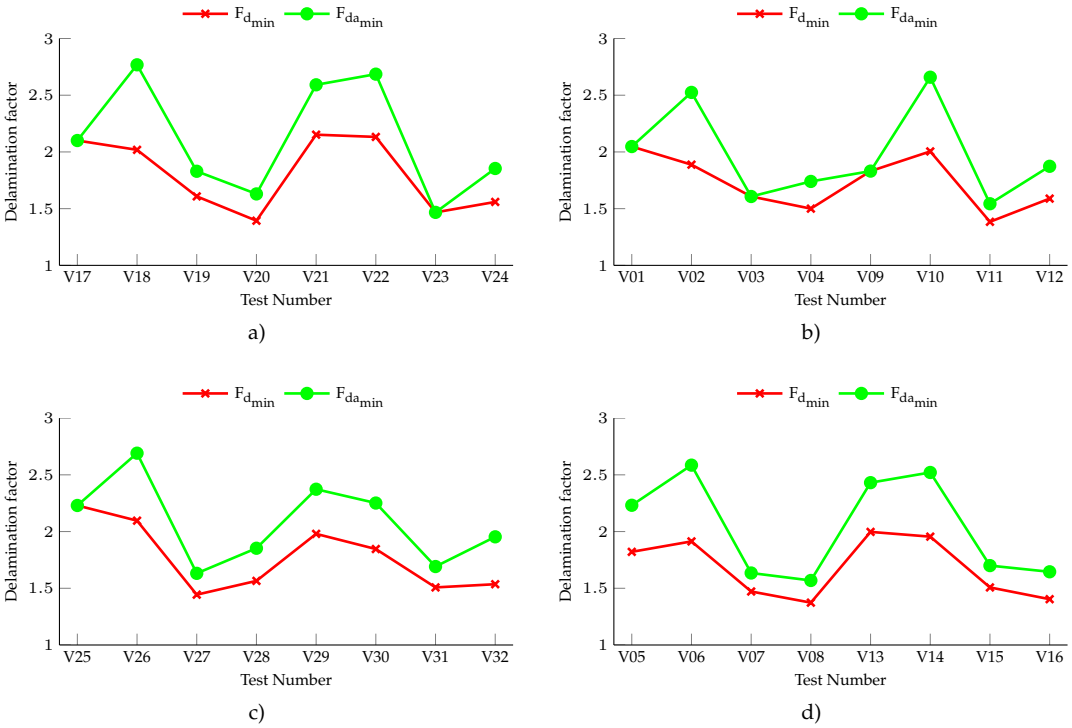

Figure B.3 Effect of spindle speed on W-shaped drill tests: a) 8000 rpm; b) 12000 rpm; c) 16000 rpm; protectd) 18000 rpm.

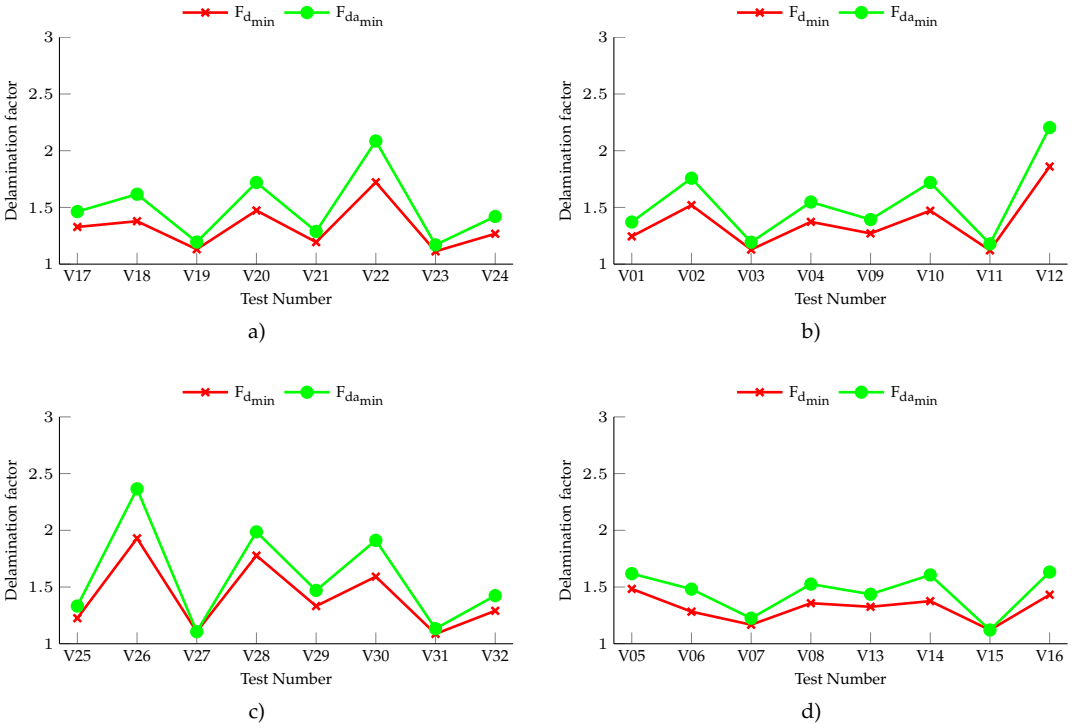

Figure B.4 Effect of spindle speed on twist drill pressed tests: a) 8000 rpm; b) 12000 rpm; c) 16000 rpm; d) 18000 rpm.

B.2 Feed per tooth effect on delamination

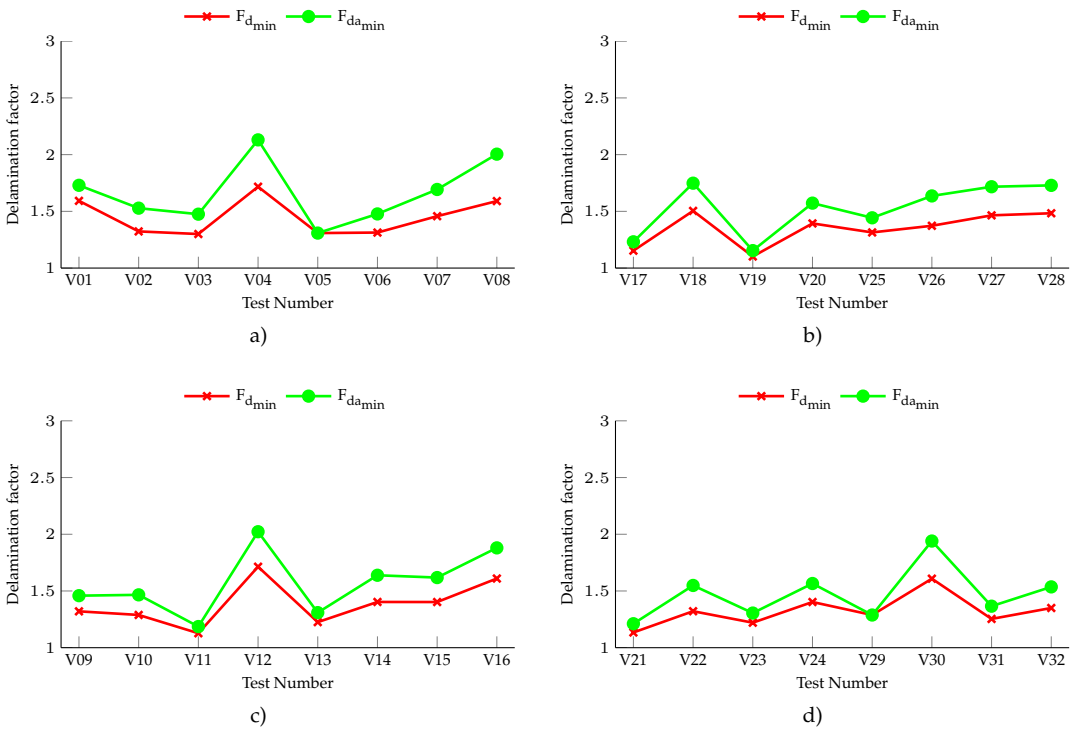

Figure B.5 Effect of feed per tooth on twist drill tests: a) 0.03250 mm/tooth; b) 0.05500 mm/tooth; c) 0.07750 mm/tooth; d) 0.08875 mm/tooth.

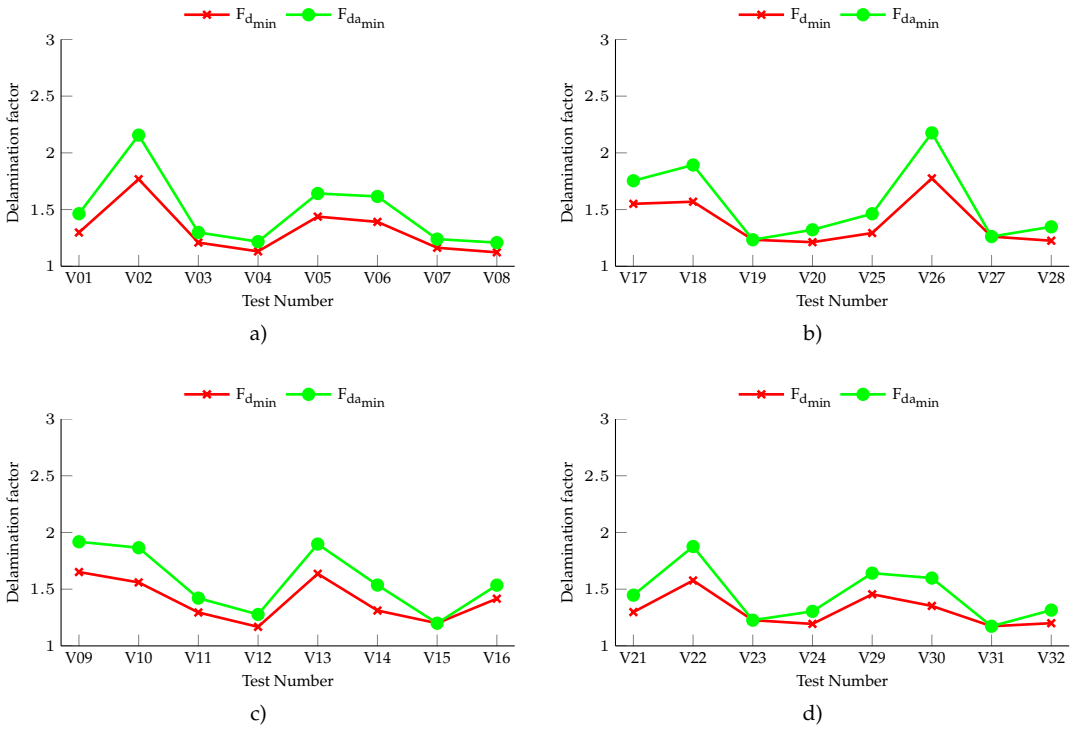

Figure B.6 Effect of feed per tooth on straight flute drill tests: a) 0.03250 mm/tooth; b) 0.05500 mm/tooth; c) 0.07750 mm/tooth; d) 0.08875 mm/tooth.

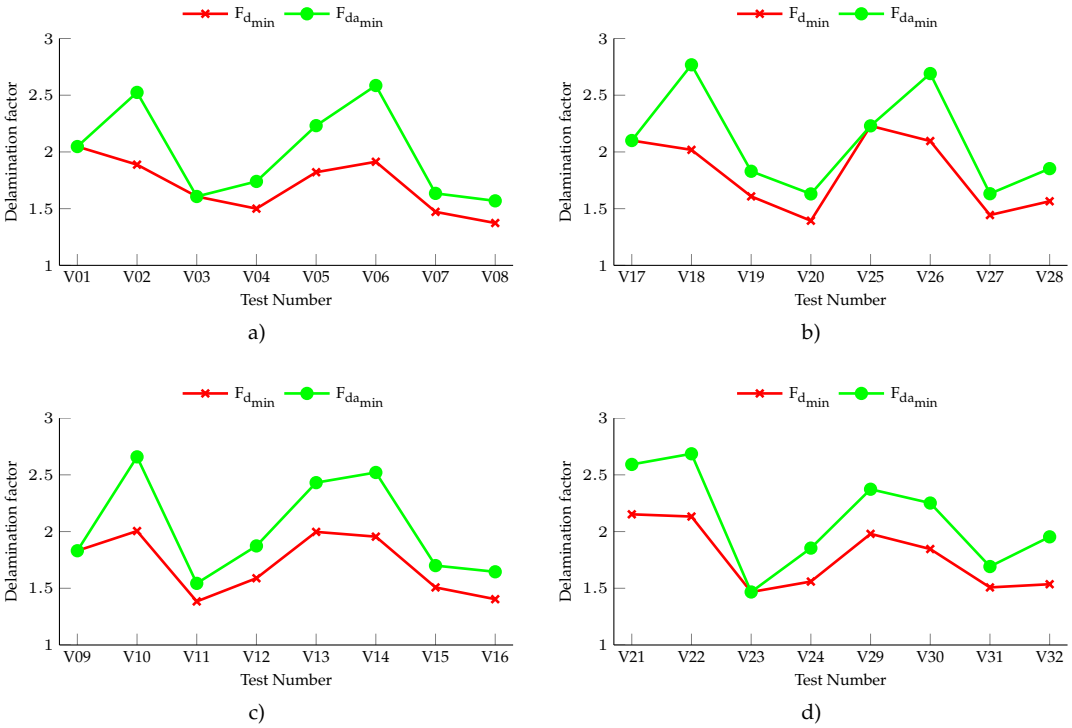

Figure B.7 Effect of feed per tooth on W-shaped drill tests: a) 0.03250 mm/tooth; b) 0.05500 mm/tooth; c) 0.07750 mm/tooth; d) 0.08875 mm/tooth.

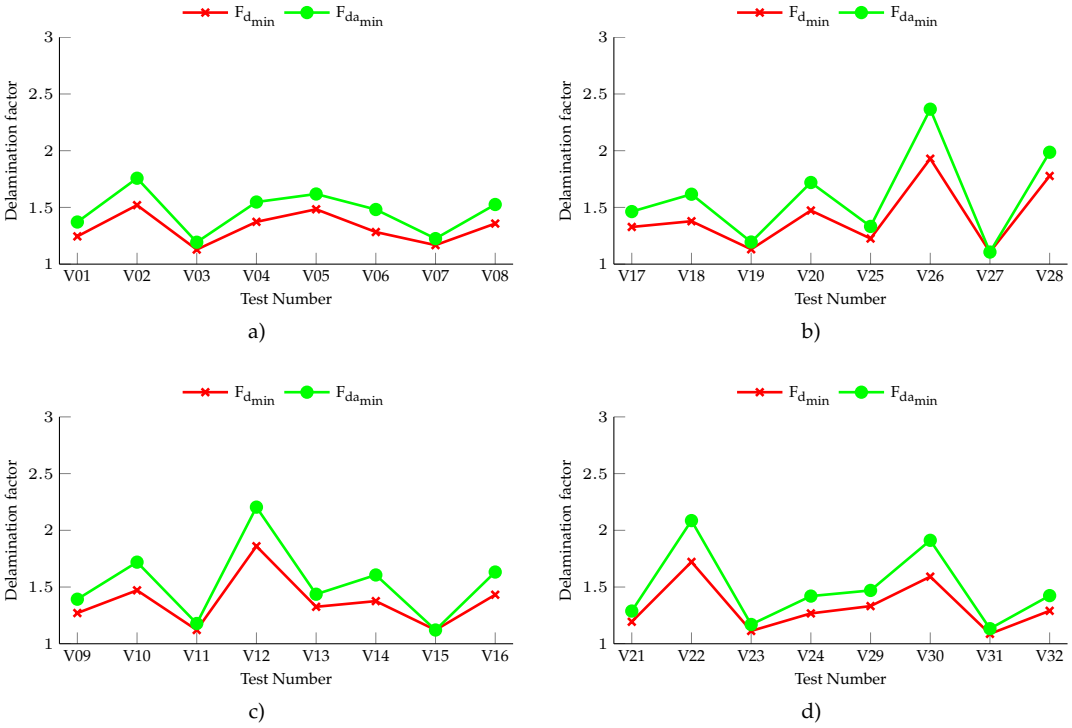

Figure B.8 Effect of feed per tooth on twist drill pressed tests: a) 0.03250 mm/tooth; b) 0.05500 mm/tooth; c) 0.07750 mm/tooth; d) 0.08875 mm/tooth.

B.3 Tool diameter effect on delamination

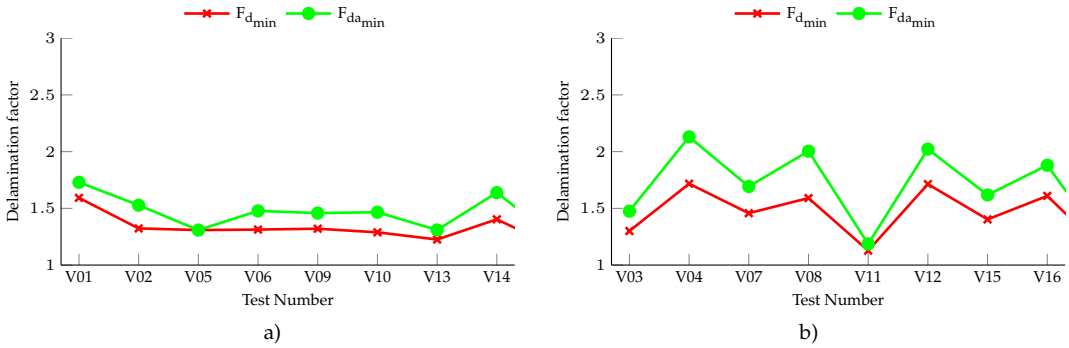

Figure B.9 Effect of tool diameter on twist drill tests: a) 5 mm; b). 9 mm

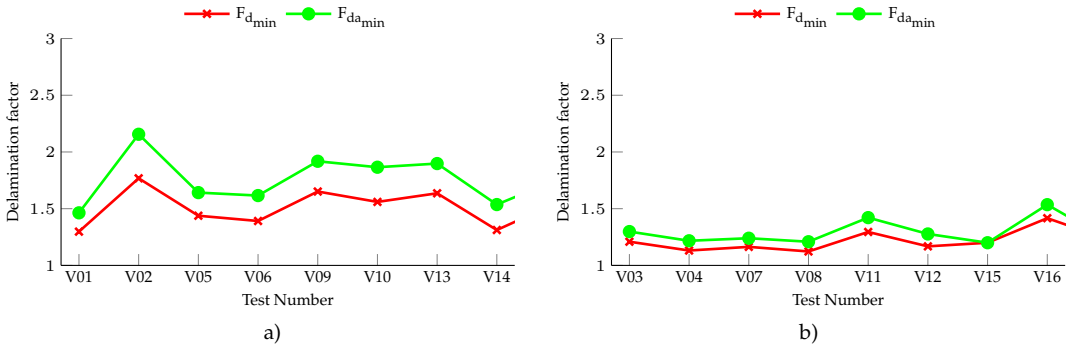

Figure B.10 Effect of tool diameter on straight flute drill tests: a) 5 mm; b). 9 mm

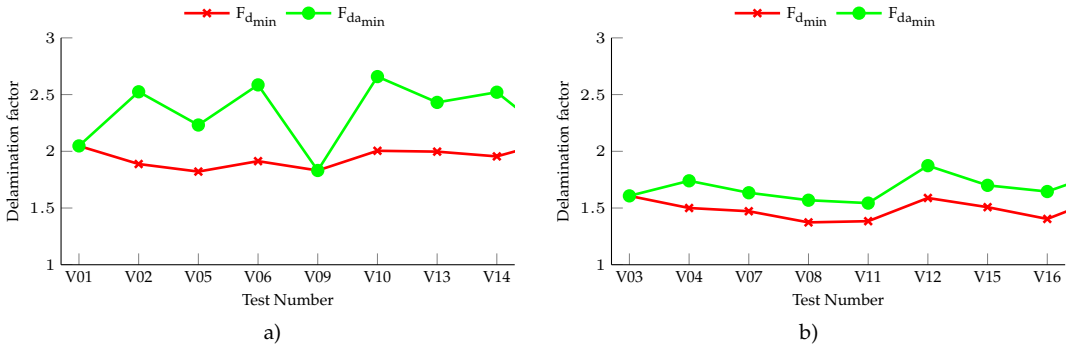

Figure B.11 Effect of tool diameter on W-shaped drill tests: a) 5 mm; b). 9 mm

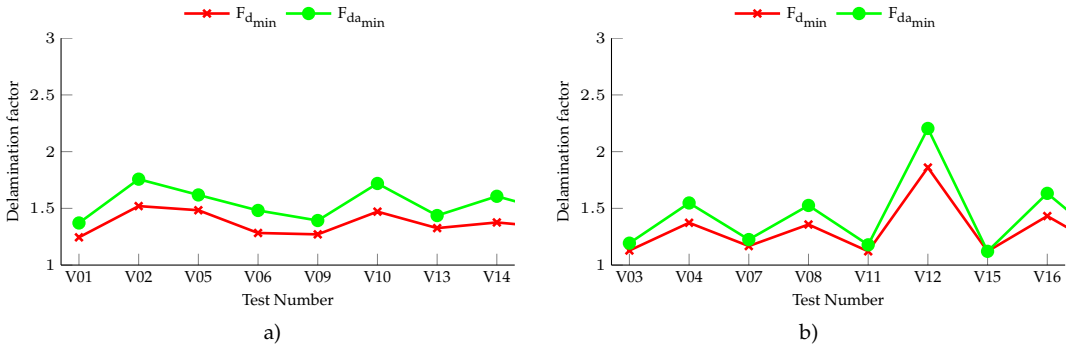

Figure B.12 Effect of tool diameter on twist drill pressed tests: a) 5 mm; b). 9 mm

B.4 Thickness effect on delamination

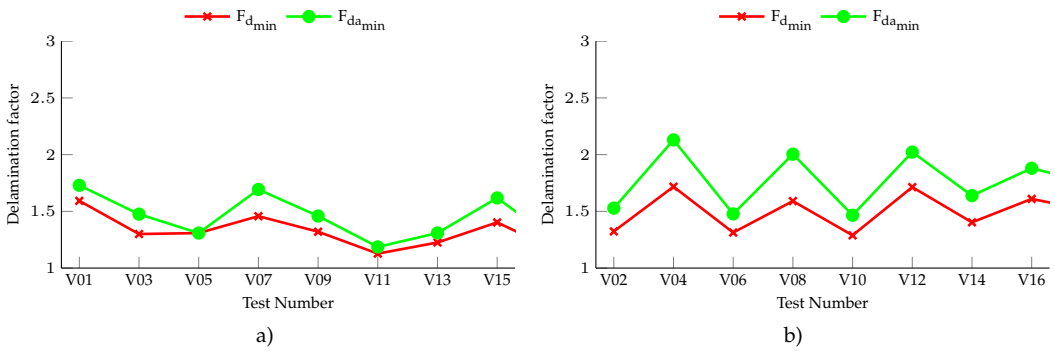

Figure B.13 Effect of workpiece thickness on twist drill tests: a) 4 mm; b) 8 mm.

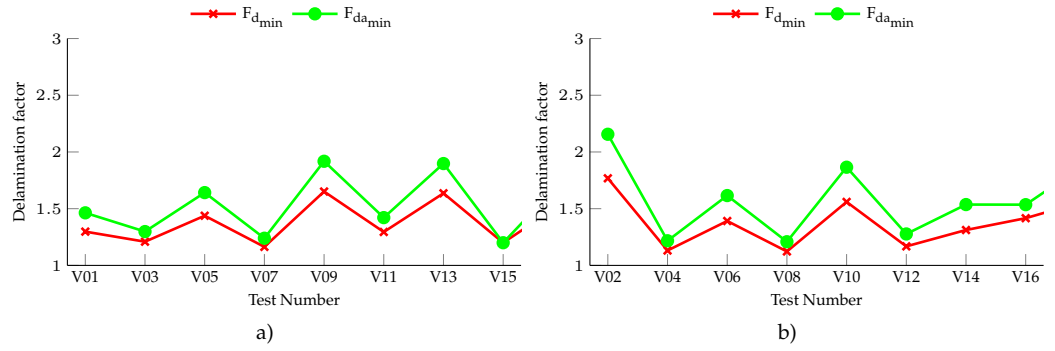

Figure B.14 Effect of workpiece thickness on straight flute drill tests: a) 4 mm; b) 8 mm.

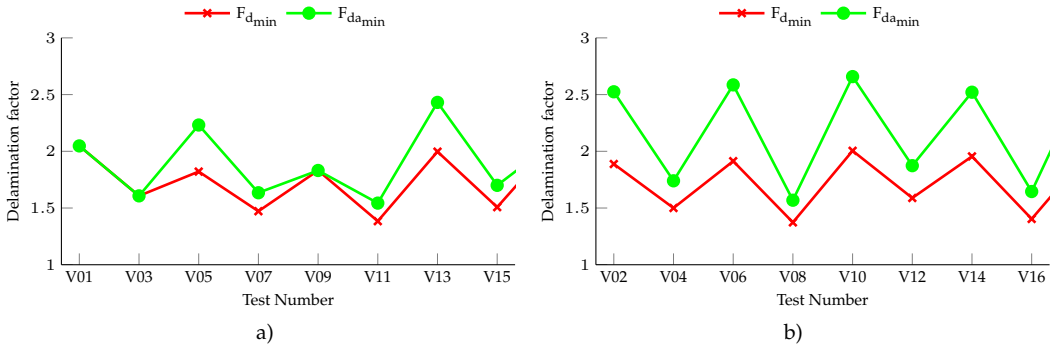

Figure B.15 Effect of workpiece thickness on W-shaped drill tests: a) 4 mm; b) 8 mm.

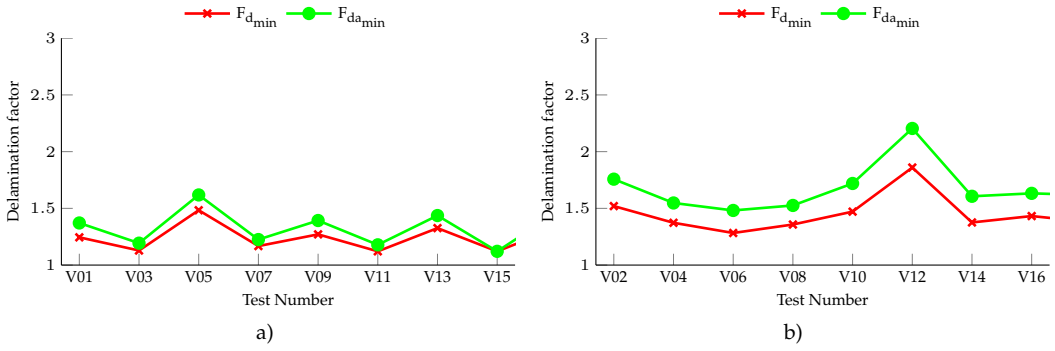

Figure B.16 Effect of workpiece thickness on twist drill pressed tests: a) 4 mm; b) 8 mm.

Appendix C

Matlab Scripts Examples

C.1 Threshold investigation

```
function []=threshold_P01_calc()

load('threshold_spade.mat');
run_dir = 'C:\Users\...\P01\';
write_dir = 'C:\Users\...\results\';

V1=[3 7 11 15 19 23 27 31 1 5 9 13 17 21 25 29];
V1S=[0 0 1 1 2 2 3 3 4 4 5 5 6 6 7 7];

constant = [0.8;0.9;0.99;0.99;0.99;0.99;0.99;0.99;0.99;0.99];
constant_h = [0.8;0.9;0.99;0.99;0.99;0.99;0.99;0.99;0.99;0.99];

threshold_255 = 30 : 10 : 120;
threshold = threshold_255 ./ 255;

for index=1:length(V1)
    for thresh_var = 1:length(threshold)
        clear BW Fd A_max
        if V1S(index)==0
            image=imread(sprintf('%sP1S_E_V%02d.tif',run_dir, V1(index)));
        else
            image=imread(sprintf('%sP1S%d_E_V%02d.tif',run_dir, V1S(index), V1
                (index)));
        end

        BW=im2uint8(im2bw(image,threshold(thresh_var)));
        [~, radius_h, affected_area, BW_clean] = threshold_sample_processing(
            BW,constant(thresh_var),constant_h(thresh_var));
```

```
27          BW_clean = im2uint8(BW_clean);
28
29          if V1S(index)==0
30              imwrite(BW_clean, sprintf('%sP01S0_E_V%02d_BW_%03d.png',write_dir,
                    V1(index),threshold_255(thresh_var)),'png')
31          else
32              imwrite(BW_clean, sprintf('%sP01S%d_E_V%02d_BW_%03d.png',write_dir
                    , V1S(index), V1(index), threshold_255(thresh_var)),'png');
33          end
34          radius_mm = radius_h * 18.5 * 1e-3;
35          threshold_spade.A0(V1(index))=(pi*(1/4).*threshold_spade.Tool_dia_mm(
                V1(index)).^2).*10^6;
36          threshold_spade.Affected_area_30_10_120(V1(index),thresh_var) =
                affected_area * 18.5^2;
37          threshold_spade.Fd_30_10_120(V1(index),thresh_var) = 2 * radius_mm ./
                threshold_spade.Tool_dia_mm(V1(index));
38          Fd=threshold_spade.Fd_30_10_120(V1(index),thresh_var);
39          A_max = (pi * radius_mm^2)*10^6;
40          threshold_spade.Fda_30_10_120(V1(index),thresh_var) = Fd + (
                threshold_spade.Affected_area_30_10_120(V1(index),thresh_var) / (
                A_max-threshold_spade.A0(V1(index)))) * (Fd^2 - Fd);
41
42      end
43
44  end
45  save('threshold_spade.mat', 'threshold_spade');
46  close
47  end
```

C.2 Otsu's threshold application

```
function [otsu_level, otsu_255]=otsu_P01_calc()

load('spade_data.mat');
run_dir='./P01\';

V1=[3 7 11 15 19 23 27 31 1 5 9 13 17 21 25 29];
V1S=[0 0 1 1 2 2 3 3 4 4 5 5 6 6 7 7];

constant = 0.99;

otsu_level = zeros(1,length(V1));
otsu_255 = zeros(1,length(V1));
for j=1:length(V1)
    if V1(j)<10 && V1S(j)==0
        str_raw = strcat(run_dir,'P1S','_E_V0',num2str(V1(j)),'.tif');
    elseif V1(j)<10 && V1S(j)~= 0
        str_raw = strcat(run_dir,'P1S',num2str(V1S(j)),'_E_V0',num2str(V1(j)),
            '.tif');
    else
        str_raw = strcat(run_dir,'P1S',num2str(V1S(j)),'_E_V',num2str(V1(j)),'
            .tif');
    end
    raw = imread(str_raw);
    otsu_level(j) = graythresh(raw);
    otsu_255(j)=otsu_level(j)*255;

    BW=im2uint8(im2bw(raw,otsu_level(j)));

    if V1(j)<10 && V1S(j)==0
        str_bw = strcat('P1S','_E_V0',num2str(V1(j)),'_BW_', num2str(round(
            otsu_255(j))),'.tif');
    elseif V1(j)<10 && V1S(j)~= 0
        str_bw = strcat('P1S',num2str(V1S(j)),'_E_V0',num2str(V1(j)),'_BW_',
            num2str(round(otsu_255(j))),'.tif');
    else
        str_bw = strcat('P1S',num2str(V1S(j)),'_E_V',num2str(V1(j)),'_BW_',
            num2str(round(otsu_255(j))),'.tif');
    end
    str_bw = strcat(run_dir,str_bw);
    imwrite(BW, str_bw,'tiff');

    index = V1(j);
    drill_fi = spade_data.Tool_dia_mm(index);
    [radius_new, radius_chen, affected_area, ~] = hough_processing(raw,str_bw,
        drill_fi,constant);

    mm_radius_new = radius_new * 18.5 * 1e-3; % convertion from pixels to
        millimetres
```

```
42      mm_radius_chen = radius_chen * 18.5 * 1e-3; % convertion from pixels to
            millimetres
43
44      affected_area = affected_area * (18.5 * 1e-3)^2;
45
46      enclosing_area_new = pi * mm_radius_new^2;
47      enclosing_area_chen = pi * mm_radius_chen^2;
48
49      enclosing_diameter_new = 2 * mm_radius_new;
50      enclosing_diameter_chen = 2 * mm_radius_chen;
51
52
53      fd_new = enclosing_diameter_new / spade_data.Tool_dia_mm(index);
54      fd_chen = enclosing_diameter_chen / spade_data.Tool_dia_mm(index);
55      fd_var = (fd_new - fd_chen)/fd_chen;
56
57      drill_area=(1/4) * pi * spade_data.Tool_dia_mm(index)^2;
58      fda_davim = fd_chen + (affected_area / (enclosing_area_chen - drill_area))
             * (fd_chen^2 - fd_chen);
59      fda_new = fd_new + (affected_area / (enclosing_area_new - drill_area)) * (
            fd_new^2 - fd_new);
60      fda_var = (fda_new - fda_davim)/fda_davim;
61
62      spade_data.ref(index,1) = {str_bw};
63      spade_data.threshold(index,1) = otsu_255(j);
64      spade_data.drill_area(index,1) = drill_area;
65      spade_data.affected_area(index,1) = affected_area;
66      spade_data.enclosing_area_new(index,1) = enclosing_area_new;
67      spade_data.enclosing_area_chen(index,1) = enclosing_area_chen;
68      spade_data.enclosing_diameter_new(index,1) = enclosing_diameter_new;
69      spade_data.enclosing_diameter_chen(index,1) = enclosing_diameter_chen;
70      spade_data.fd_new(index,1) = fd_new;
71      spade_data.fd_chen(index,1) = fd_chen;
72      spade_data.fd_var(index,1) = fd_var * 100;
73      spade_data.fda_davim(index,1) = fda_davim;
74      spade_data.fda_new(index,1) = fda_new;
75      spade_data.fda_var(index,1) = fda_var * 100;
76
77      save('spade_data.mat', 'spade_data');
78  end
79  end
```

C.3 Automatic image processing

```
function [radius, radius2drill_centre, affected_area, drill_radius] = hough_processing(raw,pic,drill_fi,constant)
%% MINIMUM DELAMINATION METHODOLOGY
% DAMAGED CENTRE: DETERMINATION THROUGH THE BOUNDARIES OF THE AFFECTED AREA (Copyright Duarte Silva  FCT-UNL 2013)
addpath('MinBoundSuite');

img_orig = imread(pic);
img_orig_tag = bwlabel(img_orig);                          % Blob tagging
img_orig_props = regionprops(img_orig_tag, 'Area');        % Blob properties determination
var2filter = [img_orig_props.Area];                        % Blob properties extraction
[px_filter,~] = pixel_filter(var2filter,constant);         % Blob filter determination
img = bwareaopen(img_orig, px_filter);                     % Blob filter application

img_tag = bwlabel(img);
img_props = regionprops(img_tag, 'Area', 'ConvexHull');
imshow(img_tag,'InitialMagnification','fit')

if numel(img_props) == 1
    affected_area = img_props(1).Area;
    [Y,X] = find(img == 1,1,'first');
    img_contour = bwtraceboundary(img,[Y, X], 'W', 8);
    boundary_X = img_contour(:,2);
    boundary_Y = img_contour(:,1);
    edge_points = img_props.ConvexHull;
    xx = edge_points(:,1);
    yy = edge_points(:,2);
    [c,radius] = minboundcircle(xx,yy);
    centre_X = c(1);
    centre_Y = c(2);

else    % More than one shape
    warning('Multiple␣shapes␣identified␣--␣Center␣was␣estimated.␣Make␣sure␣all␣shapes␣represent␣interesting␣areas');
    affected_area = 0;
    boundaries = cell2mat(bwboundaries(img_tag,'noholes'));
    for looper = 1:numel(img_props)
        affected_area = affected_area + img_props(looper).Area;
        edge_points = img_props(looper).ConvexHull;
        if exist('xx') && exist('yy')
            xx = [xx; edge_points(:,1)];
            yy = [yy; edge_points(:,2)];
        else
            xx = edge_points(:,1);
```

```
42              yy = edge_points(:,2);
43          end
44      end
45      [c,radius] = minboundcircle(xx,yy);
46      centre_X = c(1);
47      centre_Y = c(2);
48  end
49
50  %% CLASSIC DELAMINATION METHODOLOGY
51  % DRILL CENTRE: DETERMINATION THROUGH THE HOUGH TRANSFORM
52  % Chen's Delamination Factor and Davim's Adjusted Delamination Factor
53  addpath('CircularHough_Grd');
54  if drill_fi == 5
55      radrange = round([2.30, 2.70] .* (1/18.5e-3));    % Target fi = 5mm
56  elseif drill_fi == 9
57      radrange = round([4.40, 5.60] .* (1/18.5e-3));    % Target fi = 9mm
58  end
59  raw_img = rgb2gray(raw);
60
61  [accum, circen, cirrad] = CircularHough_Grd(raw_img, radrange, 10, 70);
62
63  drill_centre_X = circen(1,1);
64  drill_centre_Y = circen(1,2);
65  drill_radius = cirrad;    % Experimental drill radius
66
67  if numel(img_props) == 1
68      dist2drill_centre = zeros(length(img_contour),1);
69      for i = 1:length(img_contour)
70          dist2drill_centre(i) = hypot((drill_centre_X-boundary_X(i)),(
                drill_centre_Y-boundary_Y(i)));
71      end
72      radius2drill_centre = max(dist2drill_centre);
73  else
74      dist2drill_centre = zeros(length(boundaries), 1);
75      for i=1:length(boundaries)
76          dist2drill_centre(i) = hypot((drill_centre_X - boundaries(i,2)),(
                drill_centre_Y - boundaries(i,1)));
77      end
78      radius2drill_centre = max(dist2drill_centre);
79  end
80
81  %% HOUGH TRANSFORM PLOTS
82  % FIGURE 1 - Accumulation Array
83  % FIGURE 2 - Raw Image with Circles Detected
84  % FIGURE 3 - 3-D View of the Accumulation Array
85
86  % figure; imagesc(accum); axis image;
87  % title('Accumulation Array from Circular Hough Transform');
88  % figure; imagesc(rawimg); colormap('gray'); axis image;
89  % hold on;
```

```
% plot(circen(:,1), circen(:,2), 'r+');
% for k = 1 : size(circen, 1),
%     DrawCircle(circen(k,1), circen(k,2), cirrad(k), 32, 'b-');
% end
% hold off;
% title(['Raw Image with Circles Detected ', ...
%     '(center positions and radii marked)']);
% figure; surf(accum, 'EdgeColor', 'none'); axis ij;
% title('3-D View of the Accumulation Array');

% display(circen);
% display(cirrad);

%% PLOTTING OF THE DELAMINATION ENCLOSING AREAS
addpath('results');
enc_areas = figure(1);
imshow(img,'InitialMagnification',50);
theta = [linspace(0,2*pi) 0];
% MINIMUM DELAMINATION AREA
hold on
centre_min = plot(centre_X,centre_Y,'color',[1 .6 0],'Marker','*');
% plot(xx,yy,'g*');
radius_min = plot(cos(theta)*radius+centre_X,sin(theta)*radius+centre_Y,...
    'Color',[1 .6 0],'LineWidth', 2);

% CLASSIC DELAMINATION AREA
% hold on
centre_classic = plot(drill_centre_X,drill_centre_Y,'color',[.4 .8 0],'Marker'
    ,'*');
radius_classic = plot(cos(theta)*radius2drill_centre+drill_centre_X,...
    sin(theta)*radius2drill_centre+drill_centre_Y,'Color',[.4 .8 0],...
    'LineWidth', 2);
plot_lg = legend([radius_min radius_classic],'Minimum','Classical',...
    'Location','NorthEast');
if size(raw) == 600
    font_size = 6;
elseif size(raw) == 800
    font_size = 8;
else
    font_size = 9;
end
set(plot_lg,'Box','off','Color', [0 0 0],'TextColor',[1 1 1],'FontSize',
    font_size);

% EXPORT FIGURE
pic_name = textscan(pic,'%*s␣%*s␣%s','delimiter',['.' '\\']);
str=char(pic_name{1});
format=strcat('./results\fd_plot_',str,'.png');
export_fig(format, '-native');
```

```
138 % imwrite(enc_areas,strcat('./results\fd_plot_',char(pic_name{1}),'.png'),'png
        ');
139
140 close(enc_areas);
141 end
```

C.4 Drilling induced damage isolation

```
function [px_filter, index] = pixel_filter(areas,constant)
clear area
area = sort(areas,'descend');
area = area.^2; % squaring areas maximizes differences
sum_area_i = 0;
index = 1;
% Maybe have the constant brought in from each sample m.file
% constant=0.8;     % for images with plenty of noise P04
% constant=0.99;      % for images almost noiseless P01
while sum_area_i < constant * sum(area)
    sum_area_i = sum_area_i + area(index);
    index = index + 1;
end
if numel(area) == 1 || numel(area) == 2
    px_filter = sqrt(area(1)) - 1;
else
    px_filter = sqrt(area(index)) + 1;
end
end

% for index = 1:16
% image=imread(pic(index,:));
% L = bwlabel(image);
% s = regionprops(L, 'Area');
% var=[s.Area];
% [px_filter(index),index_mat(index)] = pixel_filter_sq(var);
% end
% for ix=1:16
% I=imread(pic(ix,:));figure(1);imshow(I)
% J=bwareaopen(I, px_filter(ix));figure(2);imshow(J)
% pause
% end
```